NASA TM X-517

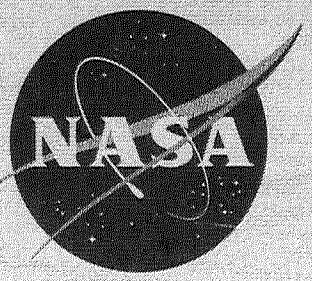

TECHNICAL MEMORANDUM

X-517

AFTERBODY TEMPERATURES, PRESSURES, AND AERODYNAMIC CHARACTERISTICS RESULTING FROM EXTENSION OF SPEED-BRAKE CONFIGURATIONS INTO THE EXHAUST JETS OF A TWIN-ENGINE ATTACK-TYPE-AIRPLANE MODEL

By Charles E. Mercer, Leland B. Salters, Jr.,
and Francis J. Capone

Langley Research Center
Langley Field, Va.

NATIONAL AERONAUTICS AND SPACE ADMINISTRATION
WASHINGTON
August 1961

NATIONAL AERONAUTICS AND SPACE ADMINISTRATION

TECHNICAL MEMORANDUM X-517

AFTERBODY TEMPERATURES, PRESSURES, AND AERODYNAMIC CHARACTERISTICS RESULTING FROM EXTENSION OF SPEED-BRAKE CONFIGURATIONS INTO THE EXHAUST JETS OF A TWIN-ENGINE ATTACK-TYPE-AIRPLANE MODEL*

By Charles E. Mercer, Leland B. Salters, Jr.,
and Francis J. Capone

SUMMARY

An investigation of the effects of twin hot jets on the afterbody surface temperatures, pressures, and aerodynamic characteristics of an attack-type airplane model equipped with speed brakes used as thrust spoilers has been conducted in the Langley 16-foot transonic tunnel. The model was tested at Mach numbers of 0.60 to 0.90 over an angle-of-attack range of -4° to 8°. The jet total-pressure ratio was varied from 1.0 (jet off) to about 4.7. Nine speed-brake configurations were tested. Hydrogen peroxide turbojet-engine simulators were used to supply the hot-jet exhaust.

The slotted-brake and the perforated-brake configurations provided the best protection to the fuselage from the heating effects of the jets. By relocating the jets further outboard, the temperature problem was solved, but apparently the brake retracted drag was increased slightly.

INTRODUCTION

Interference effects between turbojet exhausts and the airplane fuselage have been a problem in aircraft design for years and have been the subject of considerable research efforts as indicated in references 1, 2, and 3. In this connection interest has been shown in the heating effects of hot-jet exhausts on afterbody surface temperatures as evidenced in references 4 and 5. The present investigation is

*Title, Unclassified.

concerned primarily with one aspect of the heating problem, namely, the heating of the downstream fuselage surfaces by hot-jet exhausts impinging upon thrust spoilers which extend into the jet exhaust stream. The initial part of the investigation was the test of the basic model configuration with and without speed brakes used as thrust spoilers as reported in reference 6. The basic configuration consisted of a twin-jet, attack-type-airplane model with canted tailpipes exhausting hot jets along the sides of the fuselage.

In order to reduce excessive temperatures which are produced on surfaces adjacent to the speed brakes and which occurred on the basic configuration, a series of modifications were made to the speed brake. Provision was also made for relocating the jets laterally to increase the clearance between jets and afterbody. The results of these modifications on the temperatures, pressures, and aerodynamic forces and moments are reported as the second phase of the investigation.

The investigation was conducted at free-stream Mach numbers from 0.60 to 0.90, jet total-pressure ratios from 1.0 (jet off) to 4.7, angles of attack from -4° to 8°, angles of sideslip of 0° and 5°, and horizontal-tail deflections of 0° and -5°. The Reynolds number, based on the mean aerodynamic chord of 1.10 feet, was approximately 5×10^6.

SYMBOLS

C_D fuselage-tail drag coefficient, $\frac{D}{q_\infty S}$

$\Delta C_{D,B}$ incremental drag coefficient due to extending speed brakes, $C_{D,\text{brakes extended}} - C_{D,\text{basic}}$

$\Delta C_{D,j}$ incremental drag coefficient due to jet operation, $C_{D,\text{jets on}} - C_{D,\text{jets off}}$

C_L fuselage-tail lift coefficient, $\frac{L}{q_\infty S}$

$\Delta C_{L,B}$ incremental lift coefficient due to extending speed brakes, $C_{L,\text{brakes extended}} - C_{L,\text{basic}}$

$\Delta C_{L,j}$ incremental lift coefficient due to jet operation, $C_{L,\text{jets on}} - C_{L,\text{jets off}}$

C_m fuselage-tail pitching-moment coefficient, $\frac{M_Y}{q_\infty S \bar{c}}$

$\Delta C_{m,B}$	incremental pitching-moment coefficient due to extending speed brakes, $C_{m,\text{brakes extended}} - C_{m,\text{basic}}$
$\Delta C_{m,j}$	incremental pitching-moment coefficient due to jet operation, $C_{m,\text{jets on}} - C_{m,\text{jets off}}$
$\Delta C_{m,\delta}$	incremental pitching-moment coefficient due to horizontal-tail deflection, $C_{m,\delta_{h=-5^\circ}} - C_{m,\delta_{h=0^\circ}}$
C_p	pressure coefficient, $\frac{p_l - p_\infty}{q_\infty}$
$\bar{c}$	mean aerodynamic chord of basic wing, 13.22 in.
D	fuselage-tail drag, lb
d_j	diameter of jet exit, 1.81 in.
L	fuselage-tail lift, lb
M_∞	free-stream Mach number
M_Y	fuselage-tail pitching moment about $0.2265\bar{c}$, in-lb
p_l	local static pressure, lb/sq ft
p_∞	free-stream static pressure, lb/sq ft
$p_{t,j}$	jet total pressure, lb/sq ft
$\bar{p}_{t,j}$	average jet total pressure, lb/sq ft
q_∞	free-stream dynamic pressure, lb/sq ft
r	radial distance from base of rake, in.
S	basic wing area, 5.2 sq ft
T_j	jet total temperature, $^\circ F$
T_∞	free-stream total temperature, $^\circ F$

t	measured model surface temperature, ^{o}F
x	longitudinal distance from jet-exit center (station 36.50), positive rearward, in.
y	lateral distance from model plane of symmetry, positive to right looking forward, in.
z	vertical distance from wing chord plane, positive upward, in.
α	angle of attack of fuselage reference line, deg
β	angle of sideslip of plane of symmetry, deg
δ_h	horizontal-tail deflection from fuselage reference line, deg
τ	brake deflection angle, deg

APPARATUS

Wind Tunnel

This investigation was conducted in the Langley 16-foot transonic tunnel which is a single-return atmospheric wind tunnel with an octagonal, slotted test section. It has a speed range from Mach number 0.20 to about 1.10 and the Mach number is varied over this range by variation of tunnel drive power.

Model and Support System

The model, which was constructed of steel except for the plastic forebody, was supported at the wing tips by means of a bifurcate sting as shown in figures 1, 2, and 3. This method of model suspension was chosen instead of the usual tail-support method in order to prevent interference between the jet exhausts and the sting. The wing was fixed rigidly to the support booms and was, therefore, part of the support system. In order to permit the fuselage-tail component to deflect the six-component strain-gage balance, a clearance gap, filled with flexible rubber seal, was maintained between the body and wing as shown in figure 2. The model body was attached to the wing through a six-component strain-gage balance. Hydrogen peroxide turbojet simulators were used to furnish the hot-jet exhausts at a temperature of approximately 1,360° F as described in reference 7. The turbojet simulators were attached directly to the wing; therefore, the direct jet thrust

was not measured but only the jet-interference effects on the fuselage-tail forces and moments were measured. The jet nozzles were canted outward and down as shown in figure 4. The nine speed-brake configurations tested are shown in figures 5 and 6. Speed-brake wells were simulated by recessing the fuselage just downstream of the hinge line. The horizontal tail was designed for variable incidence.

TESTS

L
1
3
2
8

In this investigation, nine speed-brake configurations were tested at 60° deflection and the perforated brake was tested at the additional deflections of 0° and 30°. The tests included two lateral locations of the jets, a Mach number range from 0.60 to 0.90, angles of attack from -4° to 8°, jet total-pressure ratio from 1.0 (jet off) to 4.7, angles of sideslip of 0° and 5°, and horizontal-tail deflections of 0° and -5° and with the horizontal tail removed. The Reynolds number, based on the wing mean aerodynamic chord of 1.10 feet, was approximately 5×10^6.

INSTRUMENTATION

Forces and moments on the fuselage-tail combination were measured by a six-component strain-gage balance as shown in figure 3. Total pressures and temperatures were measured inside both jets at locations indicated in figure 4. This figure also shows the location of the single orifice installed in each exit to measure engine base pressures. Static-pressure orifices were located on the external surfaces of the right side of the model and thermocouples were located on the left side at places indicated in figure 7 and tables I and II. Most of the thermocouples were located on a 0.031-inch-thick steel panel designed for rapid temperature response. Thermocouples were also installed on rakes as indicated in figure 7(b).

Pressures were transmitted to fast response electrical pressure transducers by means of tubing routed through the support system. The electrical signals from the pressure transducers, thermocouples, and strain-gage balance were transmitted to recording oscillographs.

DATA REDUCTION AND ACCURACIES

The oscillograph records were read manually and the data were converted to punch cards for reduction to standard coefficient form by

machine computation. Based on the accuracy of the instruments, calibrations, and readout procedures, the data presented are estimated to be accurate to within the following limits:

M_∞	±0.005
α, deg	±0.10
C_p	±0.02
$p_{t,j}/p_\infty$	±0.10
t, °F	±5
C_D	±0.0010
C_L	±0.0050
C_m	±0.0010

At a given data point a slight variation in jet pressure ratio occurred between the right and left simulator. Therefore, pressure ratios of the left jet were used for the temperature data and those of the right jet for the pressure data. The average pressure ratio of both jets was used for all force data.

The effect of the support-system interference is not known but is believed to be small. Restraint due to the rubber seals was accounted for in the model calibration. These factors should have even less influence on the incremental data which are the information of primary interest.

RESULTS AND DISCUSSION

Effect of Various Speed-Brake Configurations on Body Surface Temperatures

The variation in fuselage surface temperatures with jet pressure ratio at Mach numbers 0.60 and 0.90 for various speed-brake configurations is shown in figure 8. Fuselage surface temperatures while the jet was not operating $(p_{t,j}/p_\infty = 1)$ are included in the figures as a basis for comparison with the temperatures while the jet was operating at various pressure ratios; the difference in the temperatures was the effects of the jet on fuselage surface temperatures. It may be noted that the jet-off temperatures are higher for $M = 0.90$ than for $M = 0.60$ by some 30° to 40°. This is caused by the differences in free-stream stagnation temperatures between Mach number 0.60 and 0.90. The duration of the data points was made of sufficient length to insure reasonable temperature stabilization and, as previously pointed out,

the model skin was made extremely thin on those parts where the temperatures were measured in order to decrease time lag caused by heat sink. The geometry of the various speed-brake configurations is shown in figures 5 and 6.

Solid brakes.- Fuselage surface temperatures obtained with the basic speed-brake configuration (the solid brakes, basic nozzle position, 60° brake deflection, 0° angle of attack, 0° sideslip, and 0° tail deflection) are shown in figure 8(a).

L 1328

The second thermocouple of row 10 located immediately downstream of the hinge line indicated the highest temperatures for all Mach numbers and pressure ratios and attained a maximum temperature of about 360° above free-stream stagnation temperature. It should be noted here that this temperature was much lower than that for the solid brake as reported in reference 6 which indicated temperatures from 600° to 700° above free-stream stagnation temperatures. The configurations were identical except for the speed-brake wells which were simulated only on the present configuration. The simulation of the speed-brake well, therefore, altered the flow pattern in such a way that body surface temperatures were reduced.

Jet deflectors.- The effect of the addition of the jet deflectors on the surface temperatures is shown in figure 8(b). The jet deflectors illustrated in figures 5(b) and 6(b) consist of a 30° wedge placed at each jet exit to deflect the jet away from the body. The jet deflectors were very effective in lowering body temperatures at Mach number 0.60 but less effective at Mach number 0.90. A detrimental side effect which was not indicated on the curves was the rapid rise in internal temperatures of the model when jet deflectors were used. This was caused by the deflection of some of the hot gases of the jet back up into the model through the clearance gap between the nozzle and fairing.

Solid brakes with scoop.- The effect of the addition of the scoop to the solid brake is shown in figure 8(c). In general, the scoop lowered the body temperatures on the order of 50°. The scoop tended to redirect some of the exhaust gases away from the body and acted as a partial shield to the surfaces behind the scoop.

Slotted brake.- Of all the configurations investigated, the slotted brake (fig. 8(d)) was the most effective in protecting the body surfaces from the influence of the hot jet. For all practical purposes, the heating of the body was negligible in this case.

Perforated brake.- The influence of the perforated brake on body temperatures is shown in figure 8(e). As compared to the solid brake, the perforated brake shows considerable improvement both in general

temperature decrease of all thermocouples and a decided decrease in those which were highest for the solid brake such as those near the brake-fuselage juncture. This configuration is probably second to the slotted brake in overall effectiveness in protecting the afterbody from the heating effects of the jets.

Vent fillers.- The solid vent filler of figure 8(f), the perforated vent filler of figure 8(g), and the trapezoidal vent filler of figure 8(h) produced detrimental effects when added to the original perforated brake in that they increased body surface temperatures. Each of them produced temperature increases of approximately 200° F near the brake-fuselage juncture.

Perforated brake with hinged flap.- The addition of the hinged flap to the perforated brake did not change the temperature pattern of the body significantly as is shown by a comparison of figures 8(e) and 8(i). The slight temperature decrease noted on some of the curves in figure 8(i) was partially caused by the differences in free-stream stagnation temperatures. These temperature differences were from 6° F to 18° F.

Influence of Various Speed-Brake Configurations on the Stagnation Temperatures in the Brake Well

Since a knowledge of the environmental temperature distribution of the brake actuator mechanism is important to the airplane designer, rake stagnation temperatures behind the various speed brakes are shown in figure 9 for Mach numbers 0.60 and 0.90. The thermocouple rake (rake 2) was attached to the model at the approximate center of the brake well so that measured temperatures represented those to which the brake actuator mechanism would be exposed. The reference plane of the rake $\left(r/d_j = 0\right)$ was at the intersection of the rake and the inside surface of the well. A partial view of the rake may be seen in figure 6(c). A sketch of the rake installation is shown in figure 7(b). It may be noted in figure 9 that the slotted brake afforded the greatest protection from the heat of the jet out to $r/d_j = 1.2$ but the least protection of any brake outboard of $r/d_j = 1.2$. Evidently, its action was to deflect the whole jet outward from the body which exposed the outboard parts to the full blast of the jet while protecting inboard parts from the direct action of the jet. This also seemed to be the case for all the perforated brakes. The only brakes which offered any measure of protection to the outboard parts are the solid-brake configurations and they offered only partial protection. The effect of Mach number on the temperature distribution was small.

Body Pressure Distributions

The pressure distribution on the body for various speed-brake configurations with and without jet operation is shown in figure 10. The locations of the static-pressure orifices are indicated in figure 7 and table I.

The pressure distribution on the jet shroud, forward of the jet exit, was not greatly affected by the speed-brake configuration but was increased slightly in a positive direction by an increase in Mach number and also by jet-on operation as compared to jet-off operation. Some indication of the pressure drop across the brake may be obtained from a comparison of the pressures of the two orifices of row 2, one located immediately upstream and the other immediately downstream of the brake. The magnitude of the pressure differences and the close proximity of the orifice locations relative to one another indicate a quite sudden and usually a large pressure drop.

Although the magnitude of the pressures varied with brake configuration, Mach number, and jet operating conditions, the pressures in the brake well (rows 4 and 5) maintained the same general distribution pattern. The orifice on the rear wall of the brake well (row 4) always indicated a considerably greater pressure (in the positive direction) than the other orifices. The difference in the pressures acting on the forward and rearward facing walls of the brake well provides an indication of the magnitude of the pressure drag produced by the brake well. Apparently, a significant part of the total drag of the brake configuration occurs in the brake well itself.

The orifices on the body aft of the brake well maintained pressures close to free-stream static pressure except those near the edge of the brake well. The close proximity of these orifices to the sharp edge of the brake well probably was the cause of their constantly indicating pressures more negative than the others.

Jet-Induced Incremental Aerodynamic Coefficients

The effect of average pressure ratio on the jet-induced incremental aerodynamic coefficients is shown in figure 11 for Mach number 0.60 and 0.90. The incremental drag coefficients increased fairly uniformly with pressure ratio. The jet-induced drag of the slotted brakes was noticeably lower than that of the other configurations which produced nearly identical drag increments with increasing pressure ratio.

The incremental pitching-moment coefficients generally increased rather consistently for all configurations with an increase in pressure ratio while the incremental lift-coefficient variation changed considerably

with a change in configuration. An increase in Mach number decreased the pitching-moment coefficient and increased the lift coefficient fairly consistently for all configurations.

Extended Investigation of Perforated Brake

Although the slotted brakes provided the greatest protection to the fuselage surfaces from the heating effects of the hot jets, the perforated brakes were considered more practical from the structural viewpoint. Therefore, additional information was obtained with the perforated speed brakes to determine the effects of angle of attack, brake deflection angle, and model sideslip angle on the surface temperatures and aerodynamic characteristics. Surface temperatures at various angles of attack are shown in figure 12 for maximum jet-pressure-ratio conditions and the effect of pressure ratio is shown in figure 13 for an angle of attack of 8°. Basic temperature data for the speed brakes retracted are presented in figure 14 which can be compared with $\beta = 0°$ results for the brakes extended 30° and 60° in figure 15. With the brakes retracted (fig. 14), temperatures of over 300° F were obtained on the rear portion of the fuselage, whereas deflecting the brakes 30° reduced most of the surface temperatures to near ambient and a further extension to 60° resulted in the high (over 400° F) local temperatures previously noted near the fuselage-brake extension. Changing the model sideslip angle from 0° to 5° produced temperature increases of up to 50° on the downstream side of the fuselage for both the 30° and 60° brake deflections. (See fig. 15.)

The effects of the perforated-brake deflection on the body-tail aerodynamic characteristics with power off is shown in figure 16. The effectiveness of the perforated brake as a speed brake is indicated by the drag increase of 0.025 to 0.030. The pitching-moment coefficient was increased up to 0.018 in the positive direction but the lift coefficient was not changed significantly.

Some indication of the effectiveness of the perforated brake as a thrust spoiler is shown in figure 17 with the jet operating. Jet impingement on the brakes increased the drag coefficient from 100 to 200 percent of the jet-off incremental value of figure 16. Horizontal-tail-control effectiveness decreased with increase in jet total-pressure ratios as indicated in figure 18 with losses up to 15 percent of the jet-off values.

Effects of Relocating Jet Exits in a More Outboard Position

Moving the jet exits outboard 0.22-jet diameters reduced the fuselage surface temperatures markedly for the solid brakes retracted as

indicated by a comparison of figures 14 and 19. In fact, the temperatures of figure 19 do not vary from ambient temperatures significantly, except towards the aft portion of the fuselage (aft of about $x/d_j = 6$). There was also a marked reduction in body surface temperatures for extended speed brakes as shown by a comparison of figures 8 and 20. It may be stated that moving the jets outboard essentially eliminated the fuselage-skin-temperature problem for all practical purposes.

Repositioning the nozzles did not influence the power-off aerodynamic characteristics greatly (fig. 21) although the drag appeared to increase slightly. With outboard nozzles and solid brakes retracted drag is reduced by jet operation as indicated in figure 22. Jet-induced incremental drag of the perforated brake was not significantly affected by nozzle position as indicated by a comparison of $M = 0.90$ data of figures 17(a) and 23.

CONCLUSIONS

An investigation of afterbody temperatures, pressures, and aerodynamic characteristics resulting from extension of speed brakes into the exhaust jets of a twin-engine attack-type aircraft model indicate the following conclusions:

1. The slotted brakes provided the greatest protection to the fuselage surfaces from the heating effects of the hot jets.

2. The solid brake series offered more protection to the brake-actuator mechanism than the perforated-brake series.

3. With speed brakes extended, the simulation of the brake well decreased body surface temperatures.

4. Reducing the perforated-brake deflection angle from 60° to 30° eliminated the body-surface-temperature problem.

5. Relocating the jets in a more outboard position essentially eliminated the body-heating problem but apparently the brake retracted drag was increased slightly.

Langley Research Center,
National Aeronautics and Space Administration,
Langley Field, Va., January 20, 1961.

REFERENCES

1. Küchemann, Dietrich, and Weber, Johanna: Aerodynamics of Propulsion. McGraw-Hill Book Co., Inc., 1953.

2. Cornette, Elden S., and Ward, Donald H.: Transonic Wind-Tunnel Investigation of the Effects of a Heated Propulsive Jet on the Pressure Distributions Along a Fuselage Overhang. NACA RM L56A27, 1956.

3. Foss, Willard E., Jr., Runckel, Jack F., and Lee, Edwin E., Jr.: Effects of Boattail Area Contouring and Simulated Turbojet Exhaust on the Loading and Fuselage-Tail Component Drag of a Twin-Engine Fighter-Type Airplane Model. NACA RM L58C04, 1958.

4. Lee, Edwin E., Jr., Foss, Willard E., Jr., and Runckel, Jack F.: Jet Effects on the Base, Afterbody, and Tail Regions of a Twin-Engine Airplane Model with High and Low Horizontal-Tail Locations. NASA TM X-2, 1959.

5. Lee, Edwin E., Jr., and Salters, Leland B., Jr.: Effects of Afterbody Shape and Hot Jet Exhausts on Pressures, Temperatures, and Drag of a Twin-Engine Fighter-Airplane Model Having an Overhanging Fuselage. NACA MEMO 12-29-58L, 1959.

6. Lee, Edwin E., Jr., and Mercer, Charles E.: Jet Interference Effects on a Twin-Engine Attack-Type-Airplane Model With Large Speed-Brake Thrust-Spoiler Surfaces. NASA TM X-454, 1961.

7. Runckel, Jack F., and Swihart, John M.: A Hydrogen Peroxide Hot-Jet Simulator For Wind-Tunnel Tests of Turbojet-Exit Models. NASA MEMO 1-10-59L, 1959.

TABLE I.- COORDINATES OF PRESSURE-ORIFICE LOCATION

Row	Model station, in.	y, in.	z, in.	x/d_j
		Base		
	36.65	-2.70	-1.40	0.08
	36.65	2.70	-1.40	.08
		Exit fairing - basic nozzle position		
A	34.20	5.45	-0.50	-1.27
	34.90	5.35	-.55	-.88
	35.60	5.25	-.65	-.50
B	35.60	3.30	-.25	-.50
	36.50	3.25	-.65	0
C	35.60	2.90	-2.15	-.50
	36.50	2.95	-1.85	0
D	35.60	4.20	-2.60	-.50
		Exit fairings - outboard nozzle position		
A	34.20	5.75	-0.60	-1.25
	34.90	5.70	-.60	-.88
	35.60	5.60	-.65	-.50
B	35.60	3.45	-.30	-.50
	36.50	3.45	-.65	0
C	35.60	3.05	-2.10	-.50
	36.50	3.05	-1.75	0
D	35.60	4.60	-2.60	-.50
		Fuselage		
1	45.30	2.45	0	4.86
	49.20	2.15	.20	7.02
	52.50	1.75	.20	8.84
2	38.30	2.75	-1.20	.99
	39.70	2.65	-1.15	1.77
	45.30	2.25	-.80	4.86
	48.00	2.05	-.55	6.35
	50.70	1.75	-.30	7.85
	52.50	1.50	-.10	8.84
3	39.70	1.70	-2.10	1.77
	45.30	1.35	-1.45	4.86
	48.00	1.20	-1.10	6.35
	50.70	1.00	-.70	7.85
	52.50	.80	-.40	8.84
		Brake well		
4	40.13	2.35	-0.40	2.01
	41.25	1.90	-.40	2.62
	45.15	2.25	-.40	4.86
5	41.25	1.65	-1.40	2.62

TABLE II.- COORDINATES OF THERMOCOUPLE LOCATION

Row	Model station, in.	y, in.	z, in.	x/d_j
		Rake 1		
	38.20	-2.95	-1.00	0.94
	38.20	-3.30	-1.15	.94
	38.20	-3.60	-1.30	.94
		Rake 2		
	41.81	-2.45	-0.60	2.93
	41.81	-2.85	-.85	2.93
	41.81	-3.30	-1.05	2.93
	41.81	-3.70	-1.30	2.93
	41.51	-4.30	-1.60	2.77
	41.05	-4.80	-1.90	2.49
		Rake 3		
	48.00	-2.50	-0.10	6.35
	48.00	-2.85	-.20	6.35
	48.00	-3.25	-.30	6.35
	48.00	-3.70	-.45	6.35
		Fuselage		
6	39.70	-1.50	-2.10	1.77
7	38.66	-2.20	-1.75	1.19
	39.70	-2.15	-1.65	1.77
	46.00	-1.75	-1.15	5.25
	48.00	-1.60	-.90	6.35
8	38.20	-2.75	-1.00	.94
	39.70	-2.65	-.95	1.77
	46.00	-2.20	-.65	5.25
	48.00	-2.00	-.45	6.35
	50.00	-1.80	-.35	7.46
	52.00	-1.50	-.15	8.56
9	46.00	-2.35	-.20	5.25
	48.00	-2.15	-.10	6.35
	50.00	-1.95	.05	7.46
	52.00	-1.70	.25	8.56
10	38.66	-2.95	.10	1.19
	39.70	-2.85	.05	1.77
	48.00	-2.25	.45	6.35
	50.00	-2.10	.55	7.46
	52.00	-1.80	.75	8.56
11	39.30	-2.95	1.05	1.55
	42.40	-2.75	1.25	3.26
		Brake well		
12	42.75	-2.45	0.70	3.45
13	41.25	-1.95	.20	2.62
	40.13	-2.40	-.10	2.01
	45.15	-2.35	-.25	4.78
14	40.13	-2.05	-1.10	2.01
	41.25	-1.65	-1.20	2.62
	42.75	-1.65	-1.10	3.45
	44.20	-1.65	-.90	4.25
	45.15	-1.80	-.65	4.78

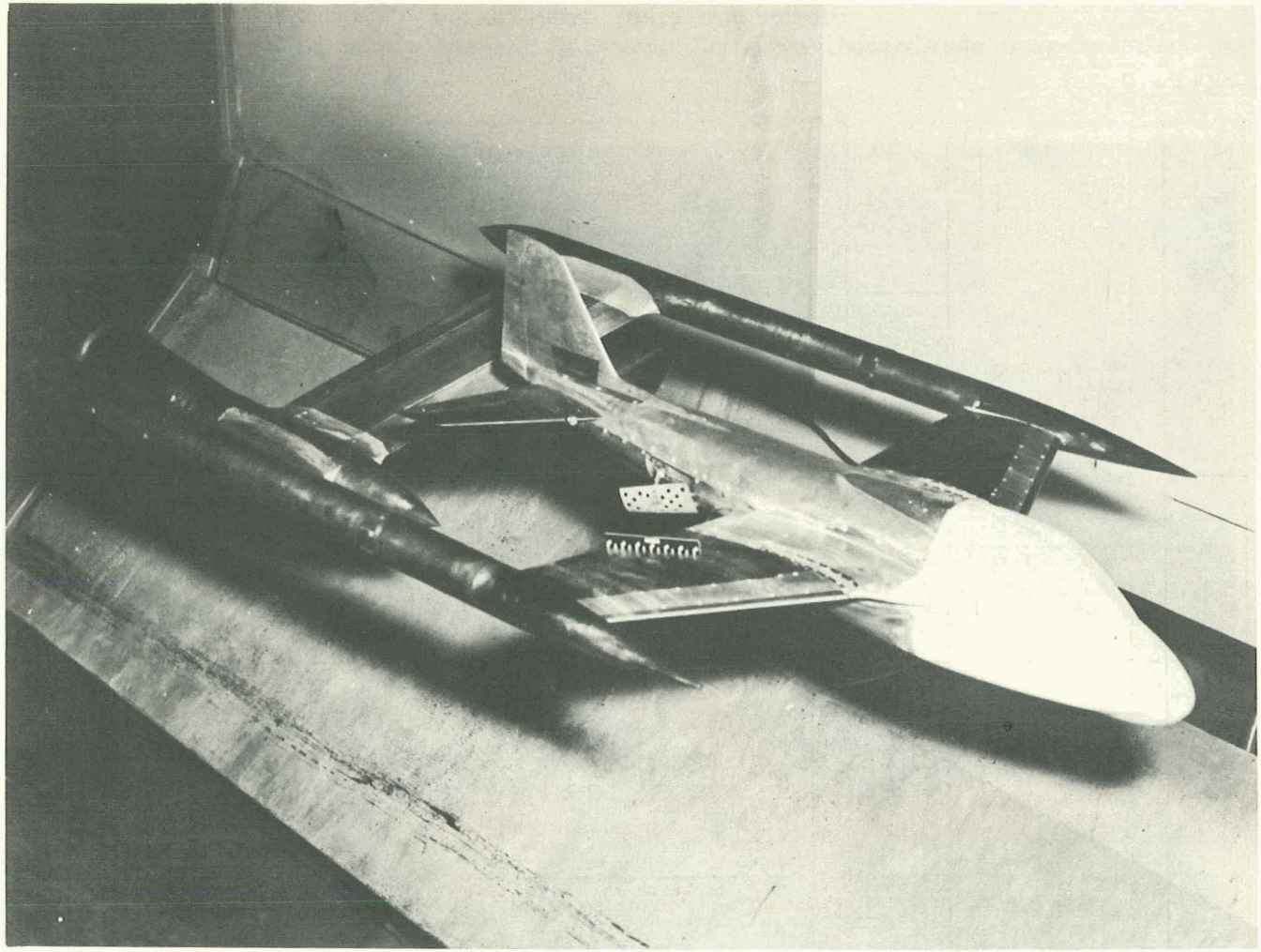

L-59-6338

Figure 1.- Model and bifurcate-sting system in the Langley 16-foot transonic tunnel.

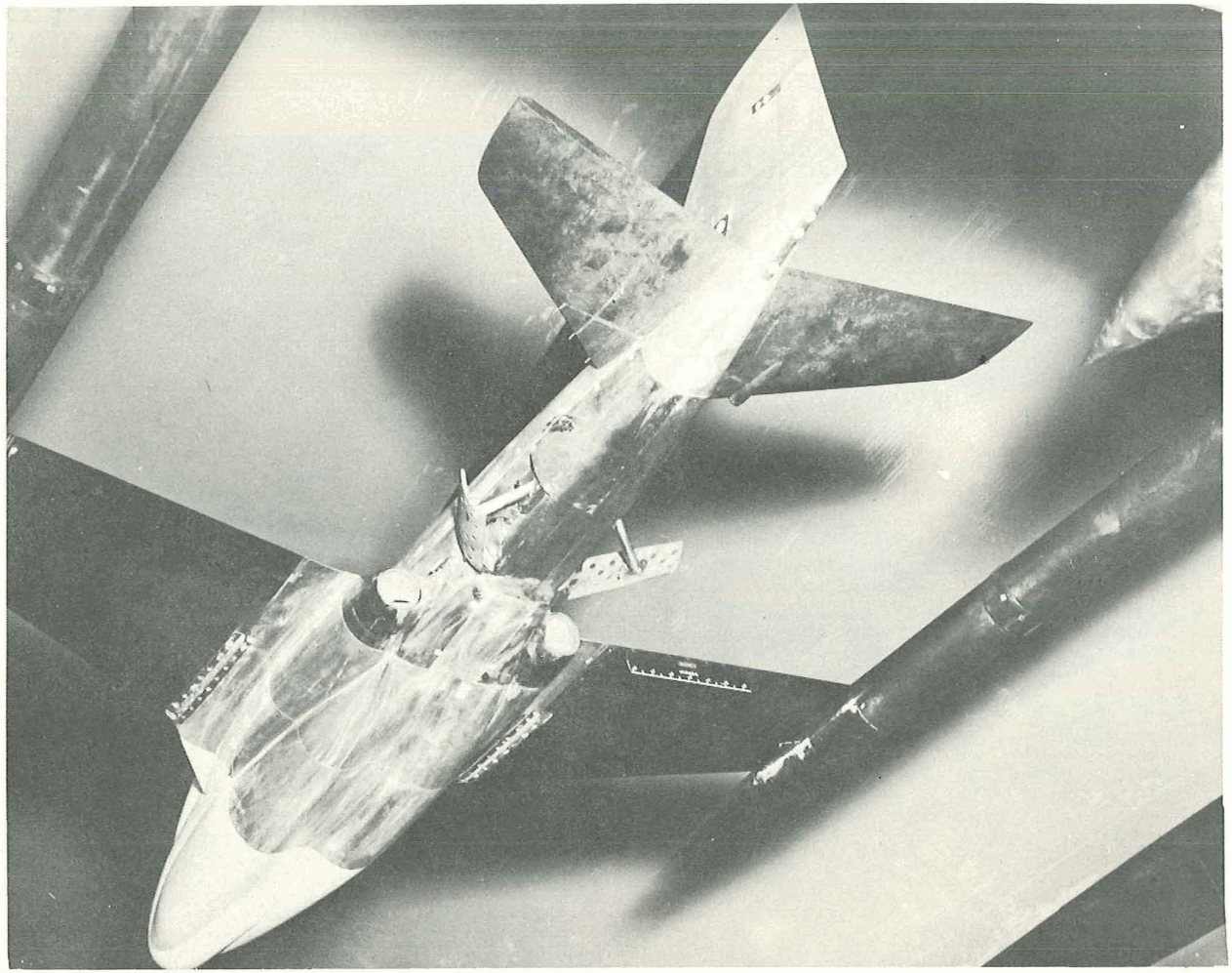

L-59-6340

Figure 2.- Bottom view of model showing jet-exit fairings, perforated brakes, brake well, and survey-rake instrumentation.

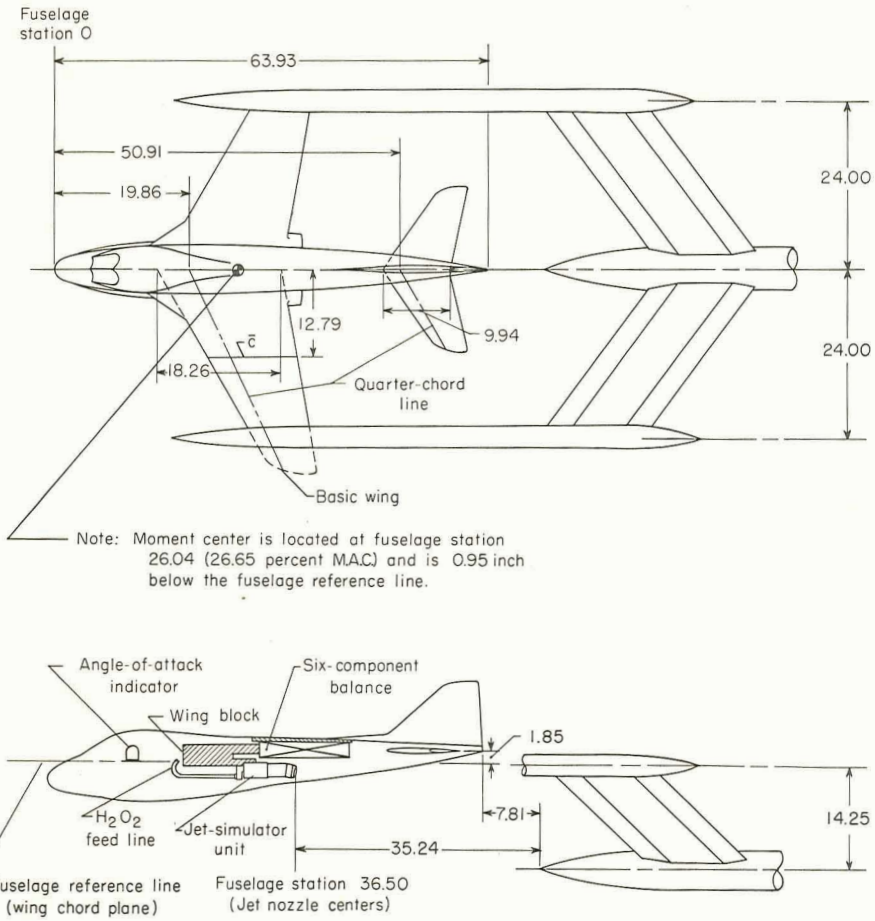

Item	Wing, Basic (Shown By Dashed Lines)	Horizontal Tail	Vertical Tail
Area, sq ft	5.20	1.20	0.75[1]
Span, ft	5.10	2.07	.87
Aspect ratio	5.00	3.57	1.02
Mean aerodynamic chord, ft	1.10	.62	.90[1]
Taper ratio	.34	.40	.37
Incidence angle, deg	0.00	0.00	0.00
Dihedral angle, deg	0.00	0.00	
Sweepback at quarter chord, deg	25.00	30.00	30.00
Root airfoil section	NACA 0009 Mod.	64A008	64A009
Tip airfoil section	NACA 64A006 Mod.	64A008	64A006

[1] Excludes dorsal fin.

Figure 3.- Geometrical details of the model and support system. All dimensions are in inches unless otherwise noted.

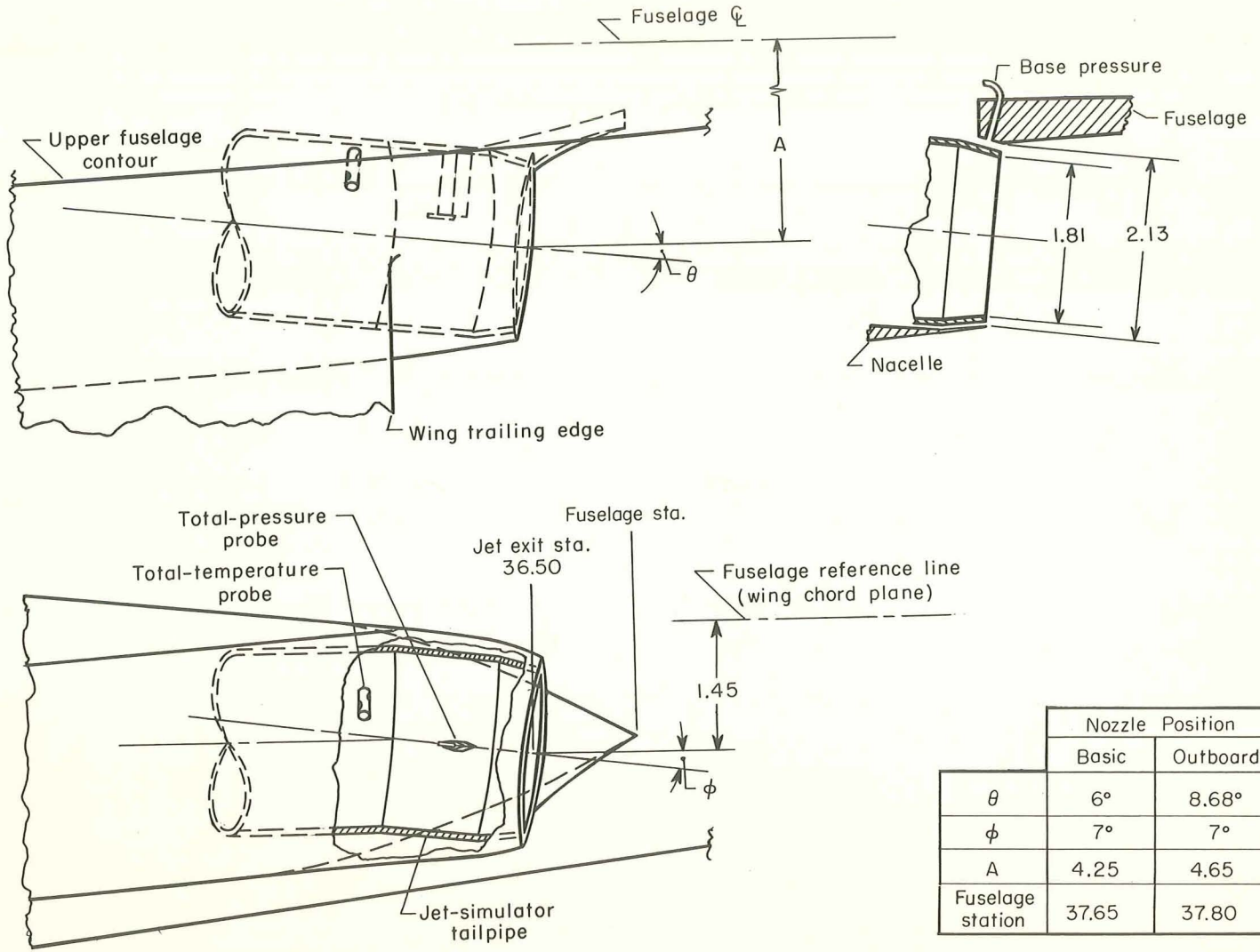

	Nozzle Position	
	Basic	Outboard
θ	6°	8.68°
ϕ	7°	7°
A	4.25	4.65
Fuselage station	37.65	37.80

Figure 4.- Sketch showing the location of nozzles and details of the jet exits. All dimensions are in inches unless otherwise noted.

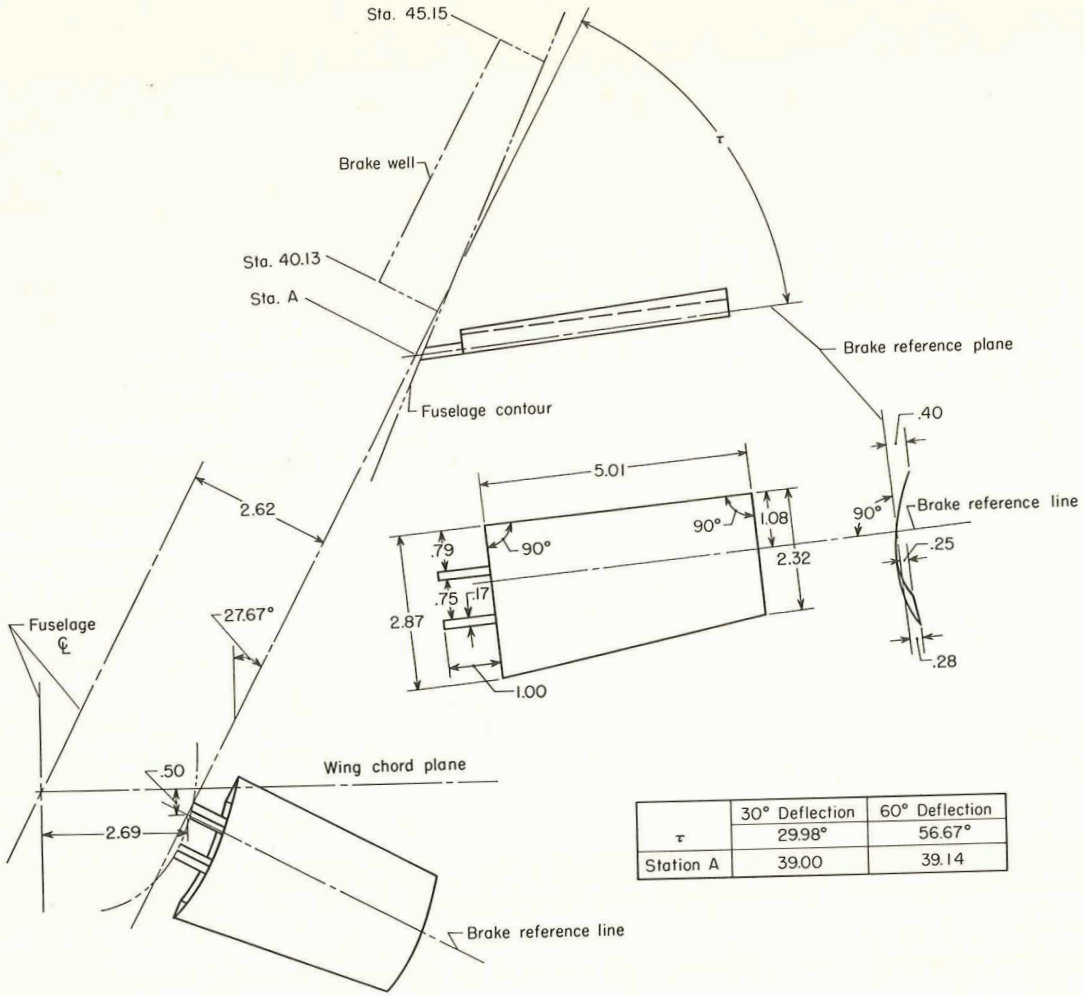

τ	30° Deflection	60° Deflection
	29.98°	56.67°
Station A	39.00	39.14

(a) Basic solid speed brake.

Figure 5.- Dimensional details of the speed brakes. All dimensions are in inches unless otherwise noted.

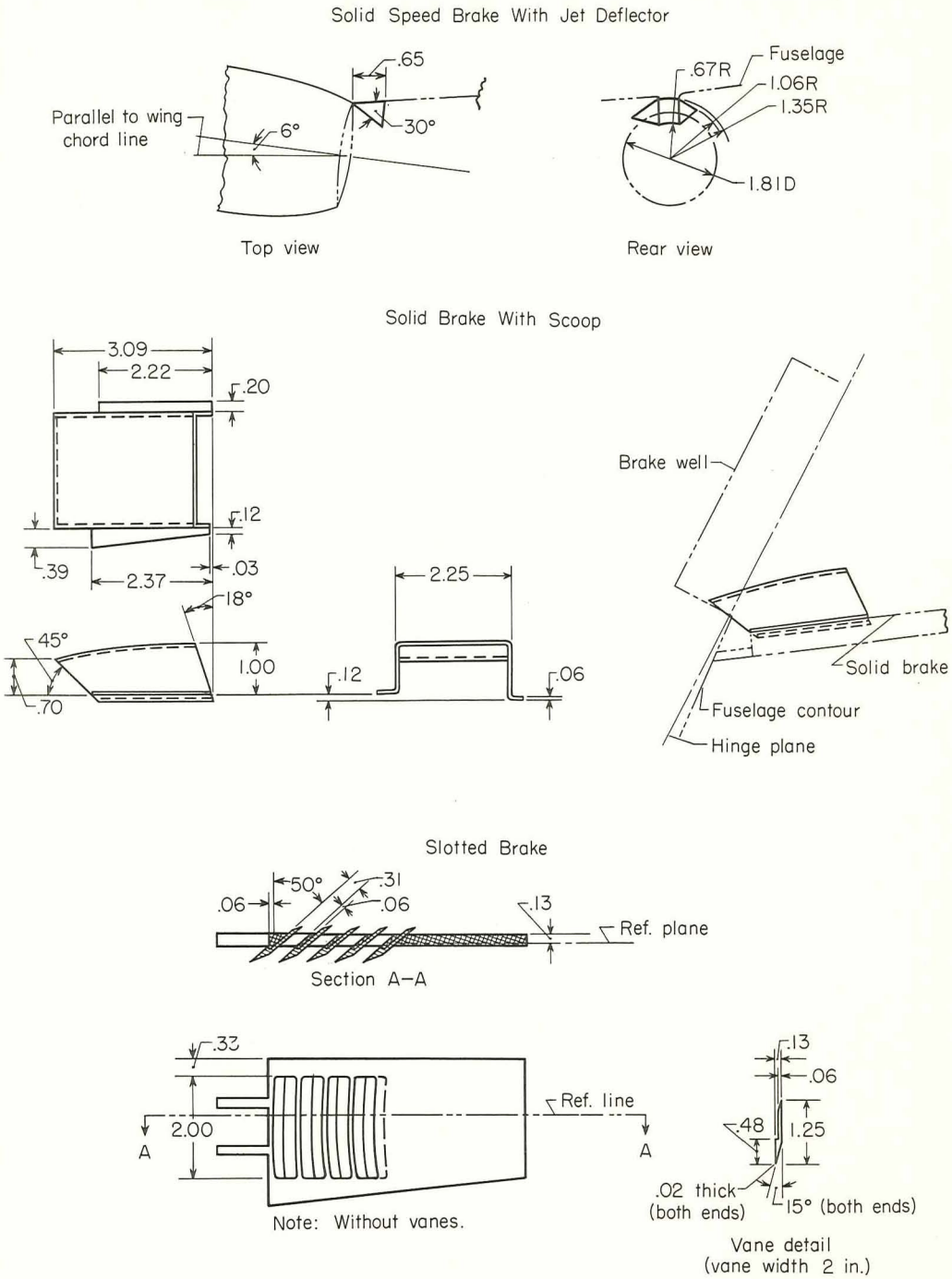

(b) Modifications to basic solid brake.

Figure 5.- Continued.

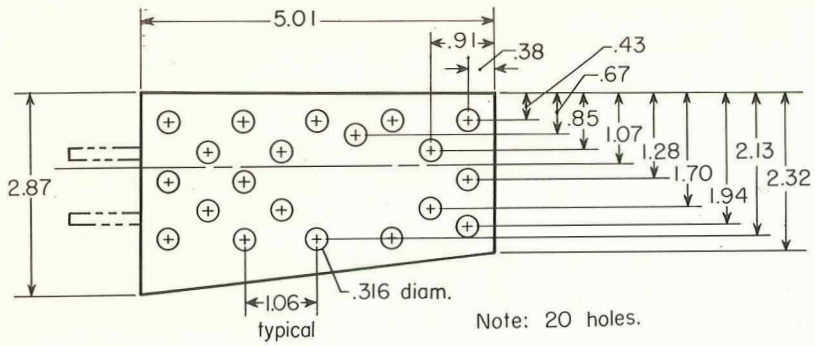

Perforated Brake

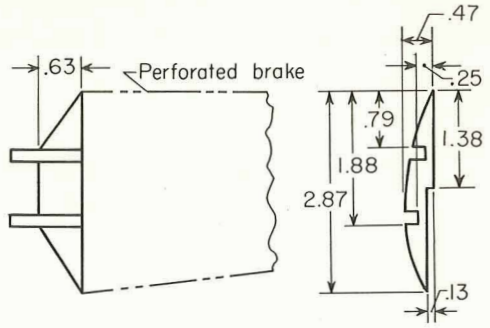

Perforated Brake With
Trapezoidal Vent Filler

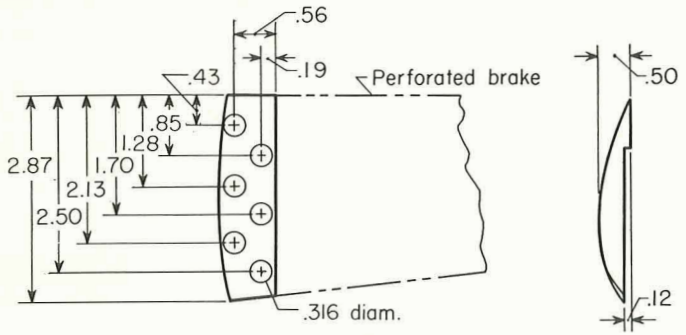

Perforated Brake With Perforated Vent Filler
(Solid Vent Filler Same Except No Holes)

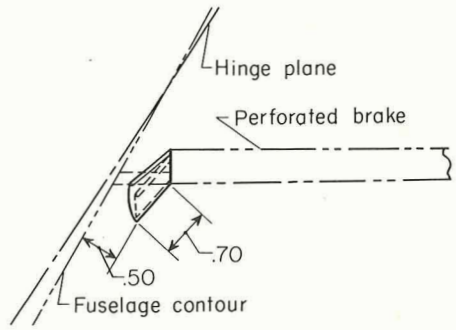

Perforated Brake With Hinged Flap

(c) Perforated speed brake and modifications to perforated speed brake.

Figure 5.- Concluded.

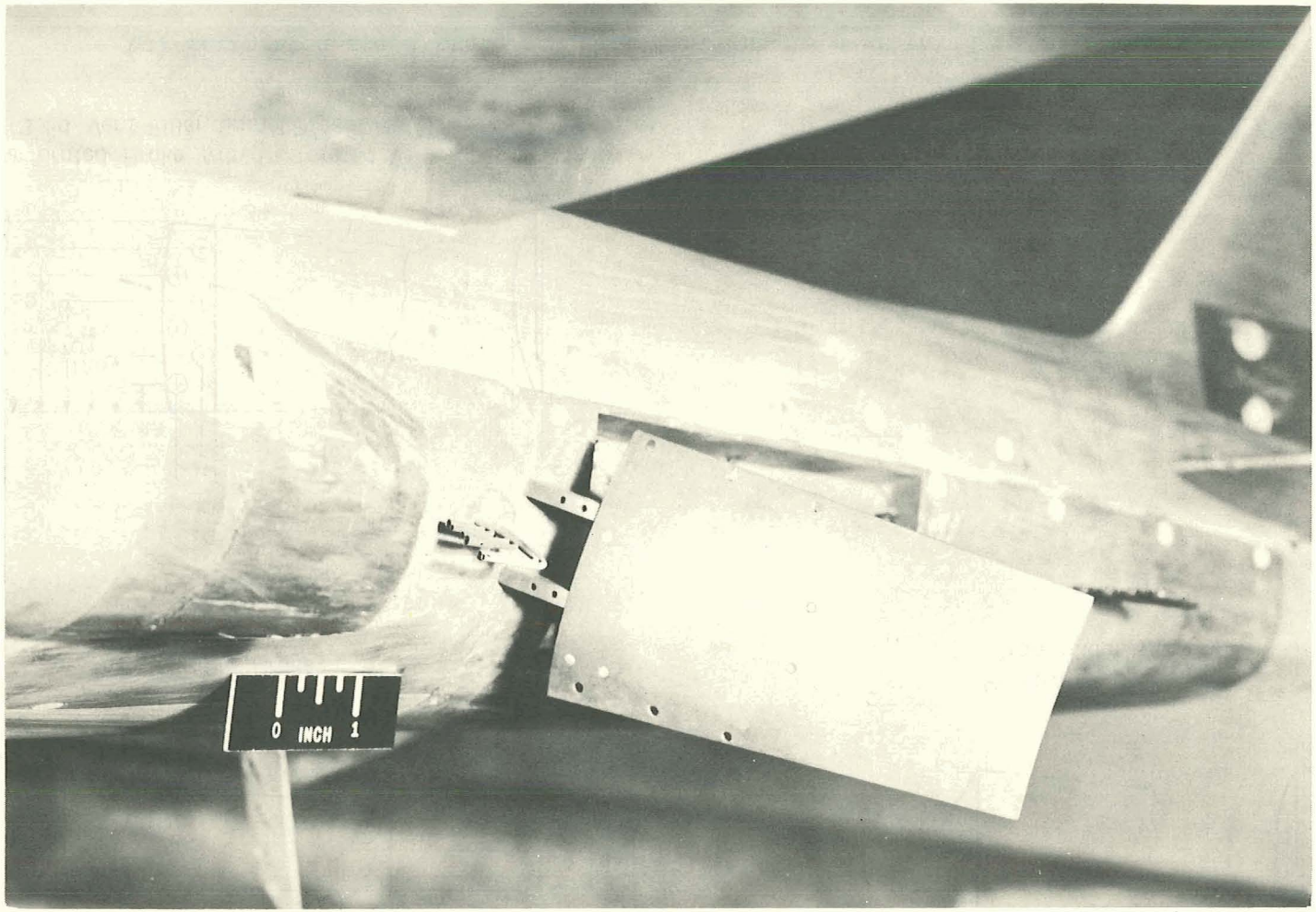

(a) Basic solid speed brake. L-59-6585

Figure 6.- Closeup view of the various speed brakes.

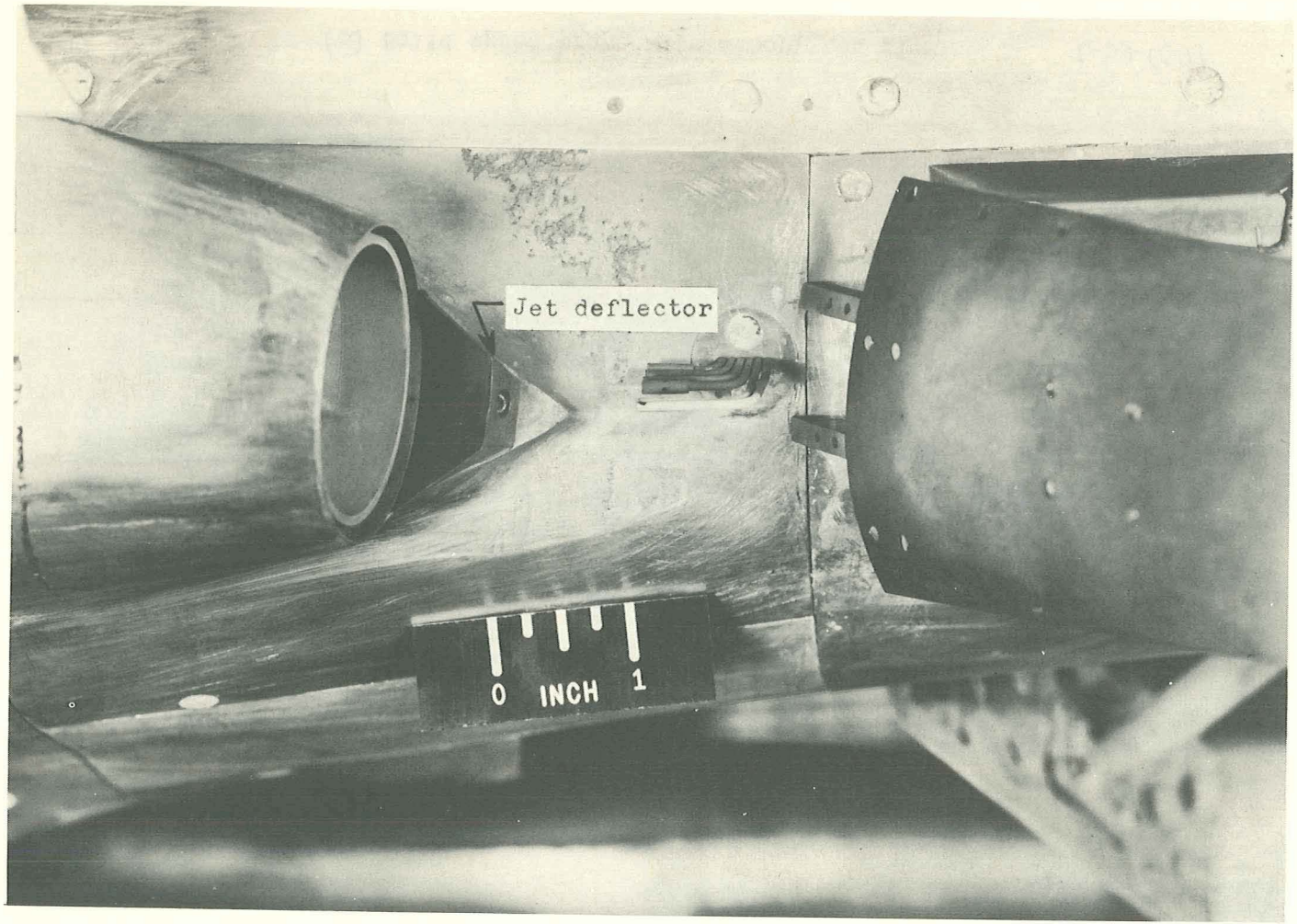

(b) Solid speed brake with jet deflector. L-59-6591.1

Figure 6.- Continued.

(c) Solid speed brake with scoop, top view. L-59-6597

Figure 6.- Continued.

L-1328

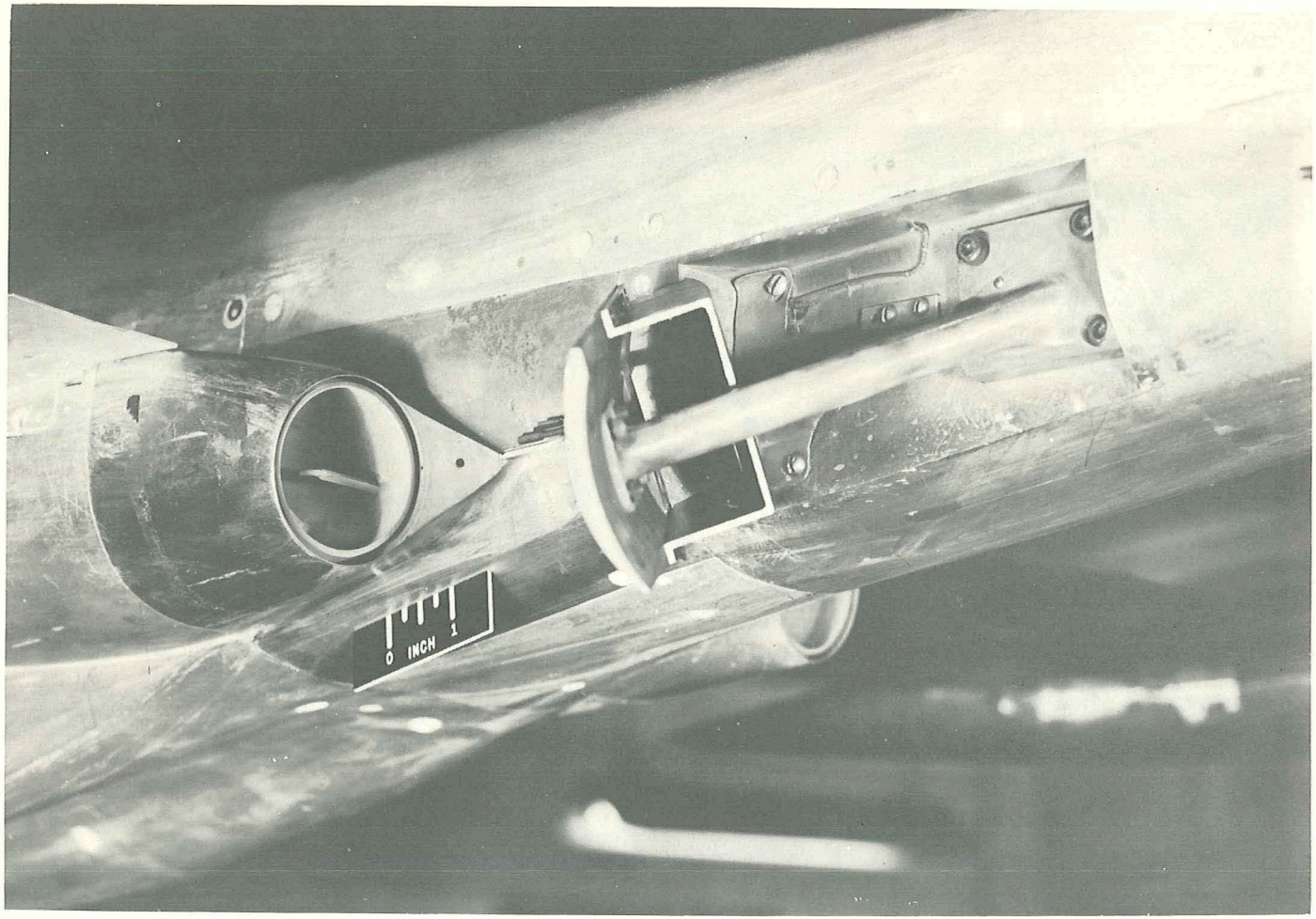

(c) Solid speed brake with scoop, end view. Concluded. L-59-6593

Figure 6.- Continued.

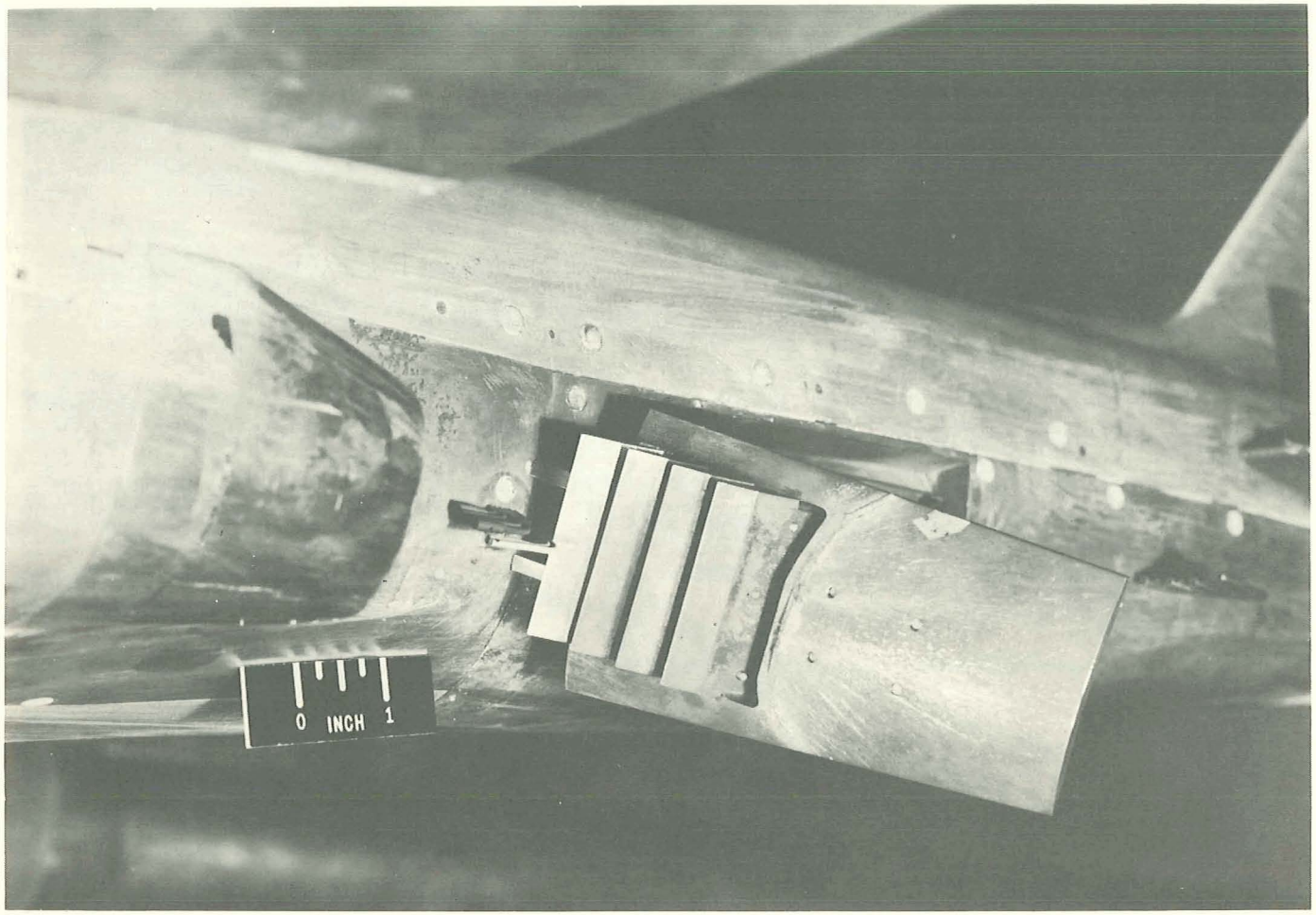

(d) Slotted brake, side view. L-59-6594

Figure 6.- Continued.

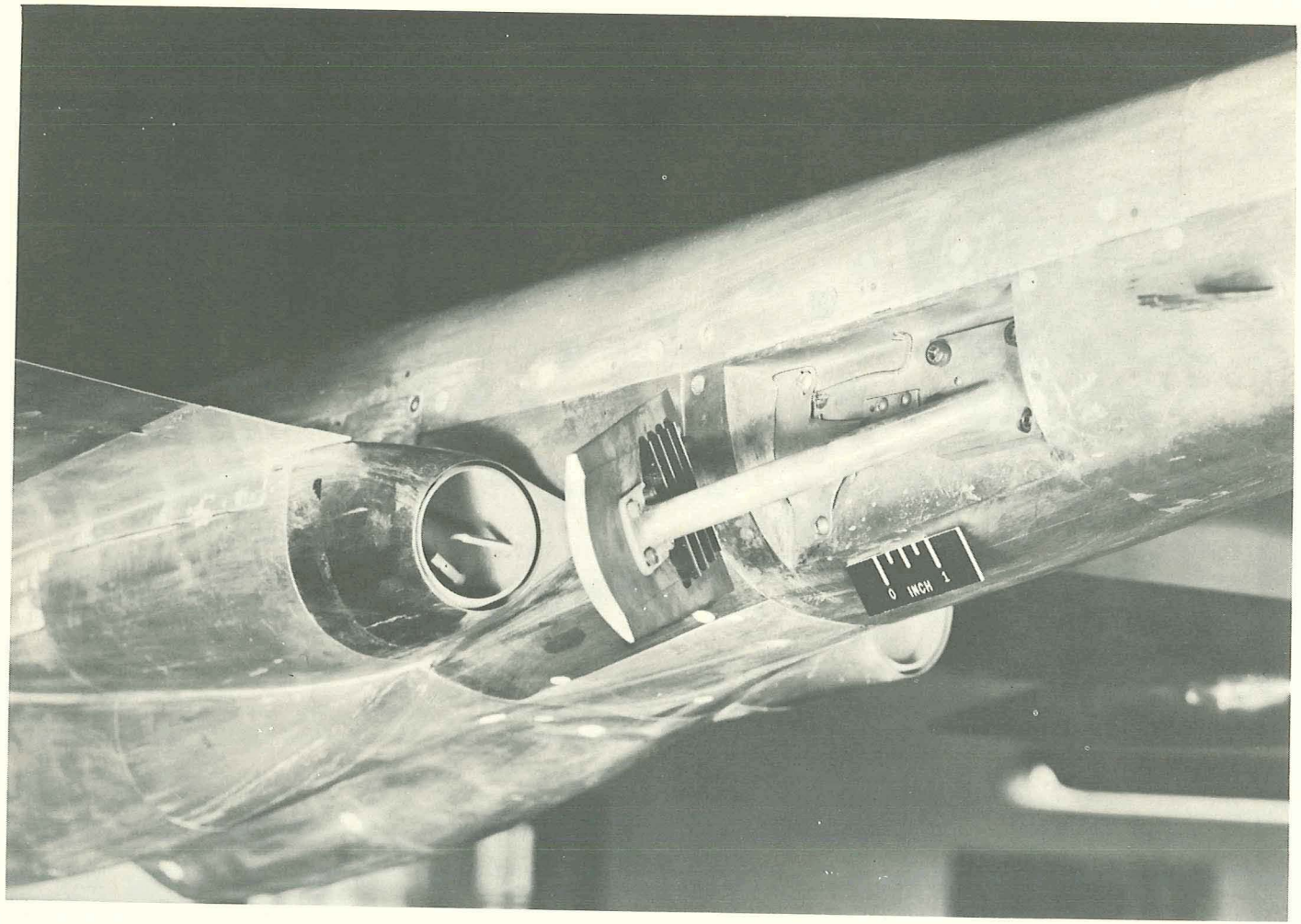

(d) Slotted brake, end view. Concluded. L-59-6595

Figure 6.- Continued.

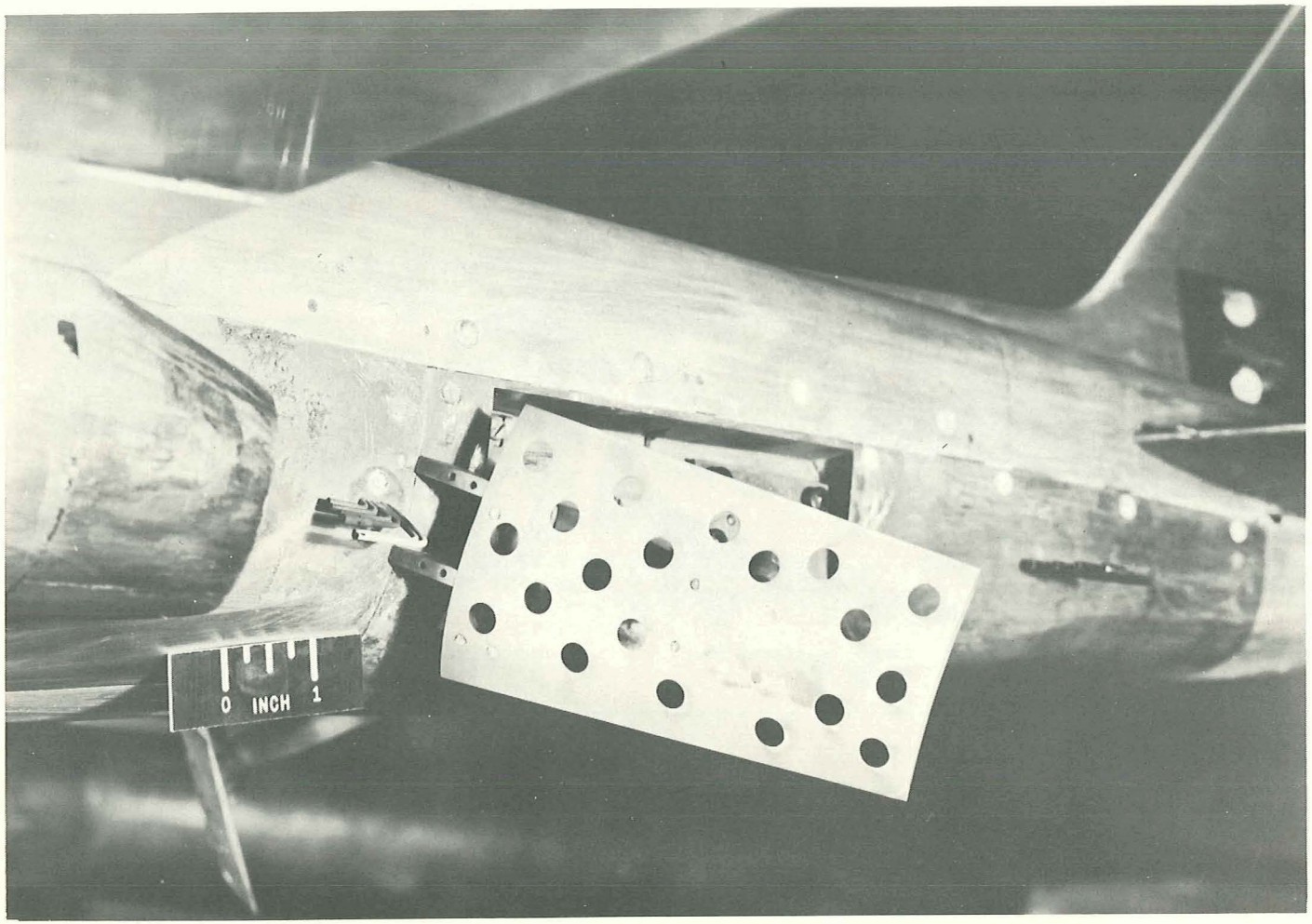

(e) Perforated brake. L-59-6587

Figure 6.- Continued.

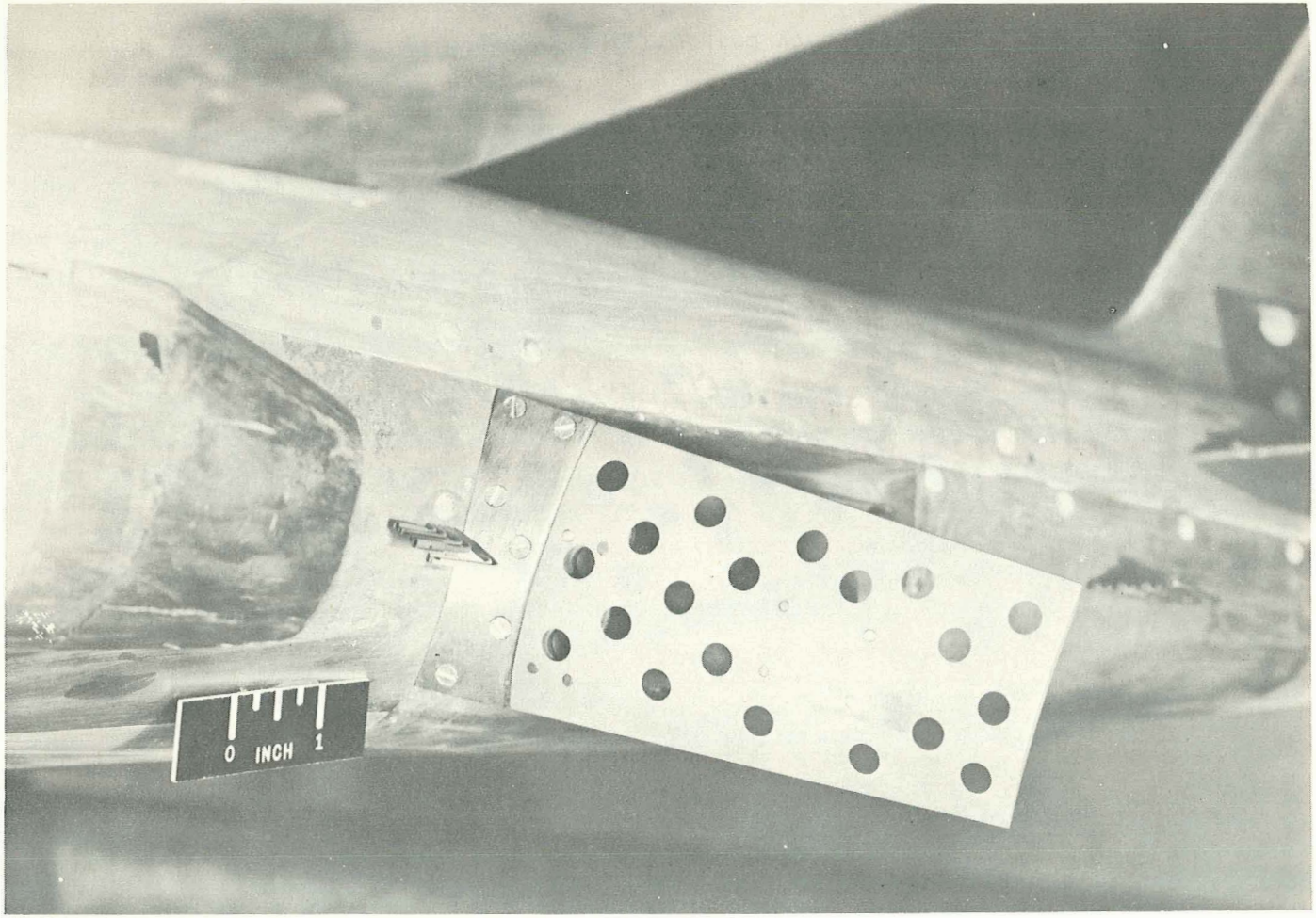

(f) Perforated brake with solid vent filler. L-59-6583

Figure 6.- Continued.

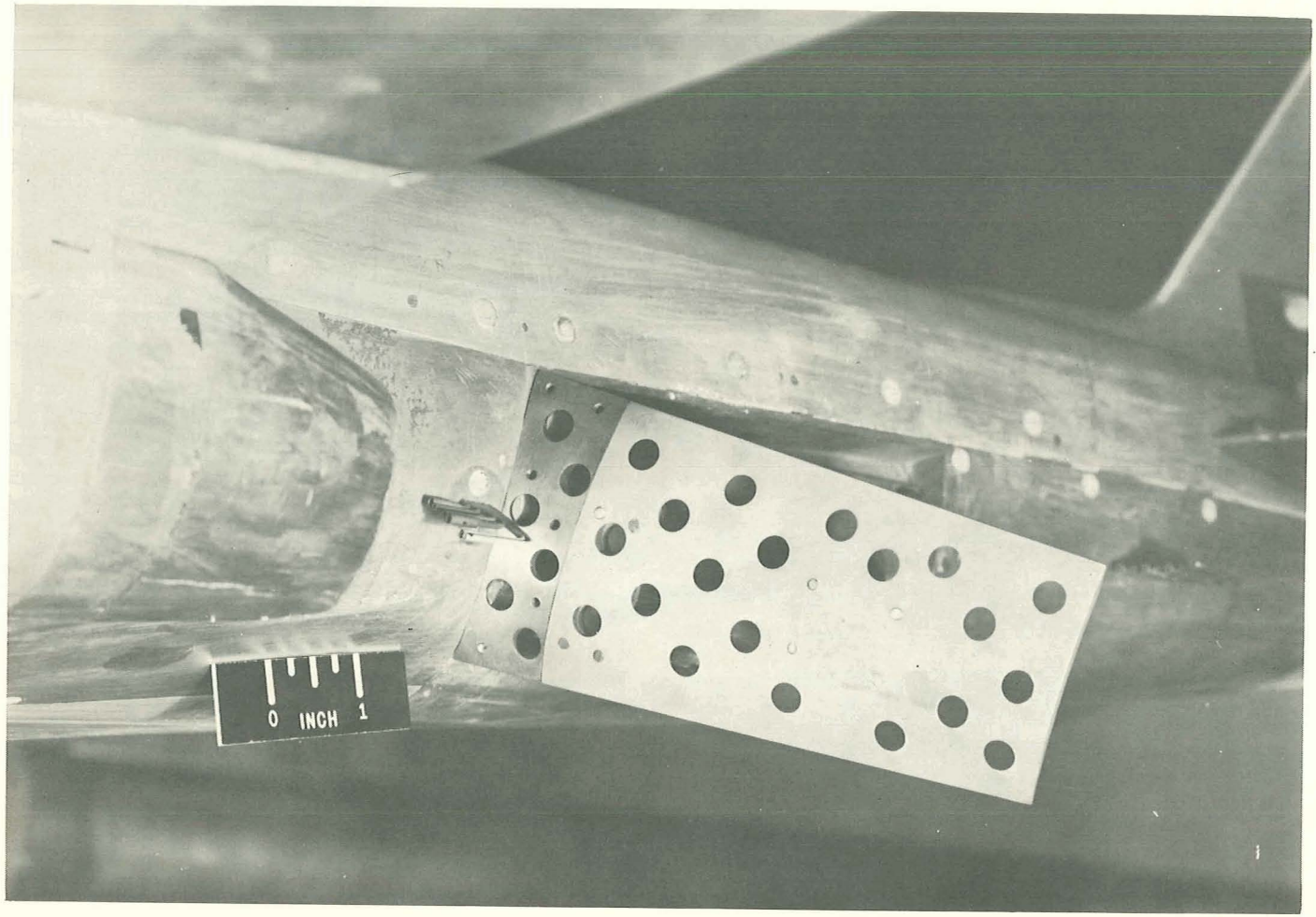

(g) Perforated brake with perforated vent filler. L-59-6584

Figure 6.- Continued.

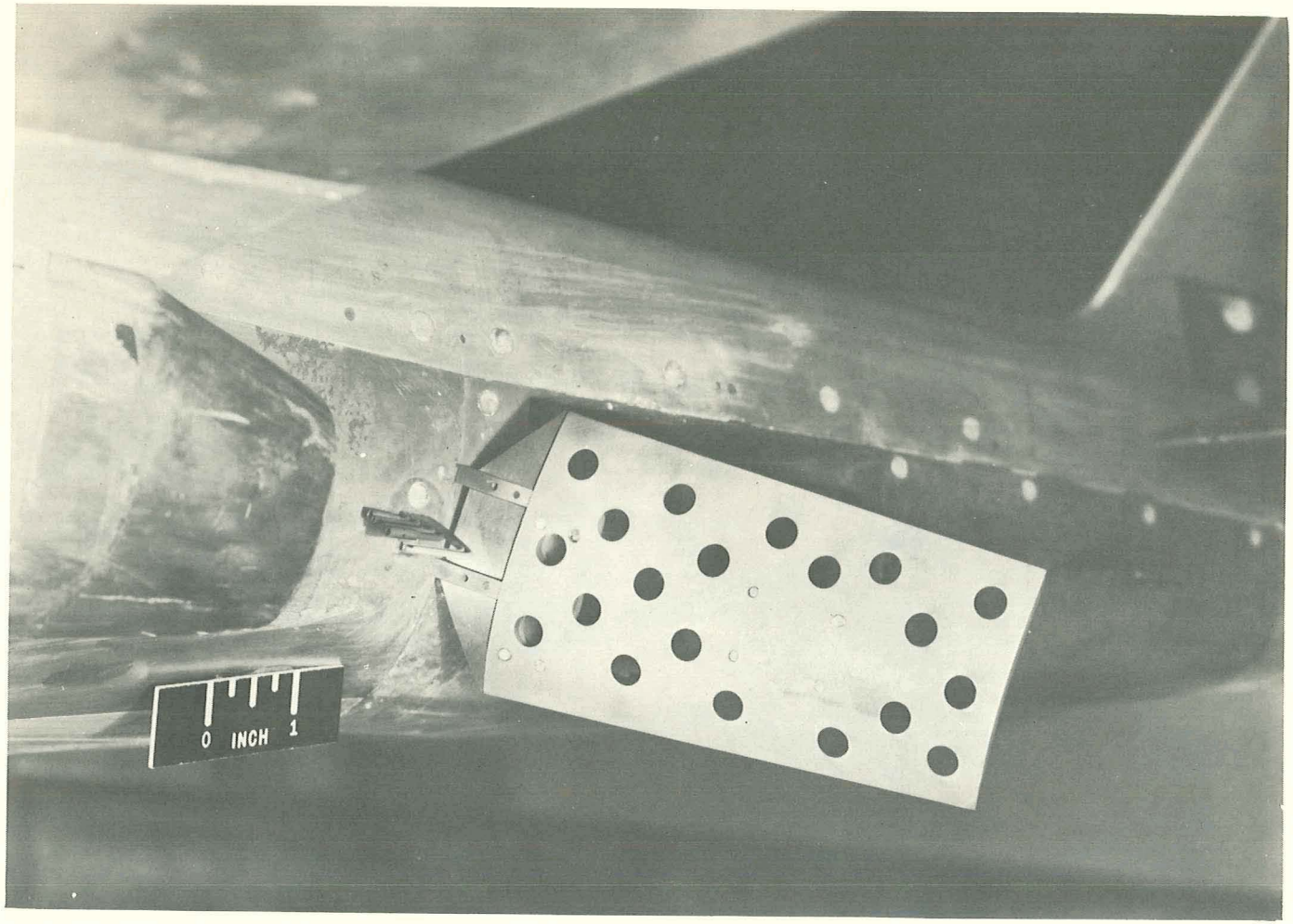

(h) Perforated brake with trapezoidal vent filler. L-59-6581

Figure 6.- Continued.

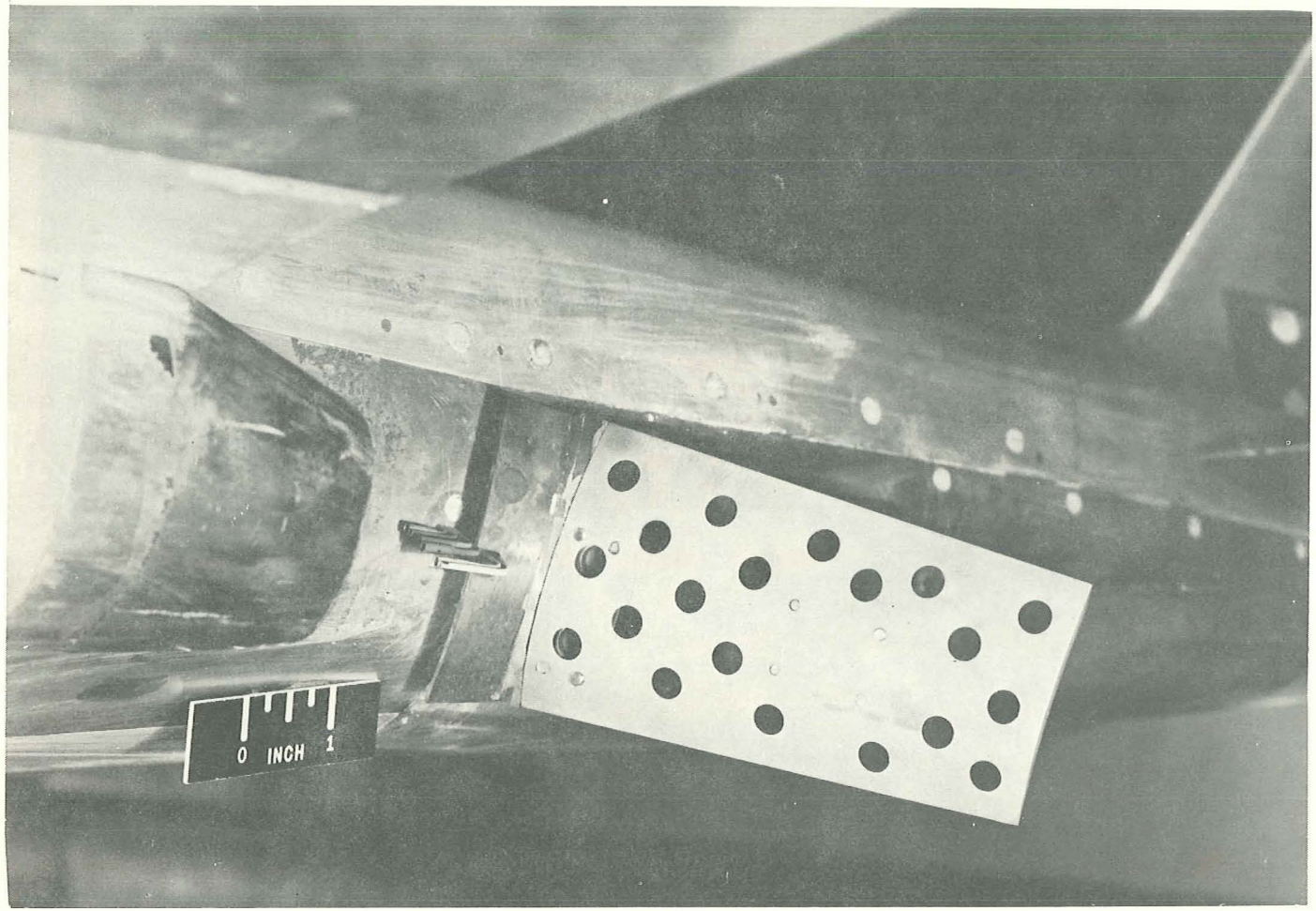

(i) Perforated brake with hinged flap. L-59-6582

Figure 6.- Concluded.

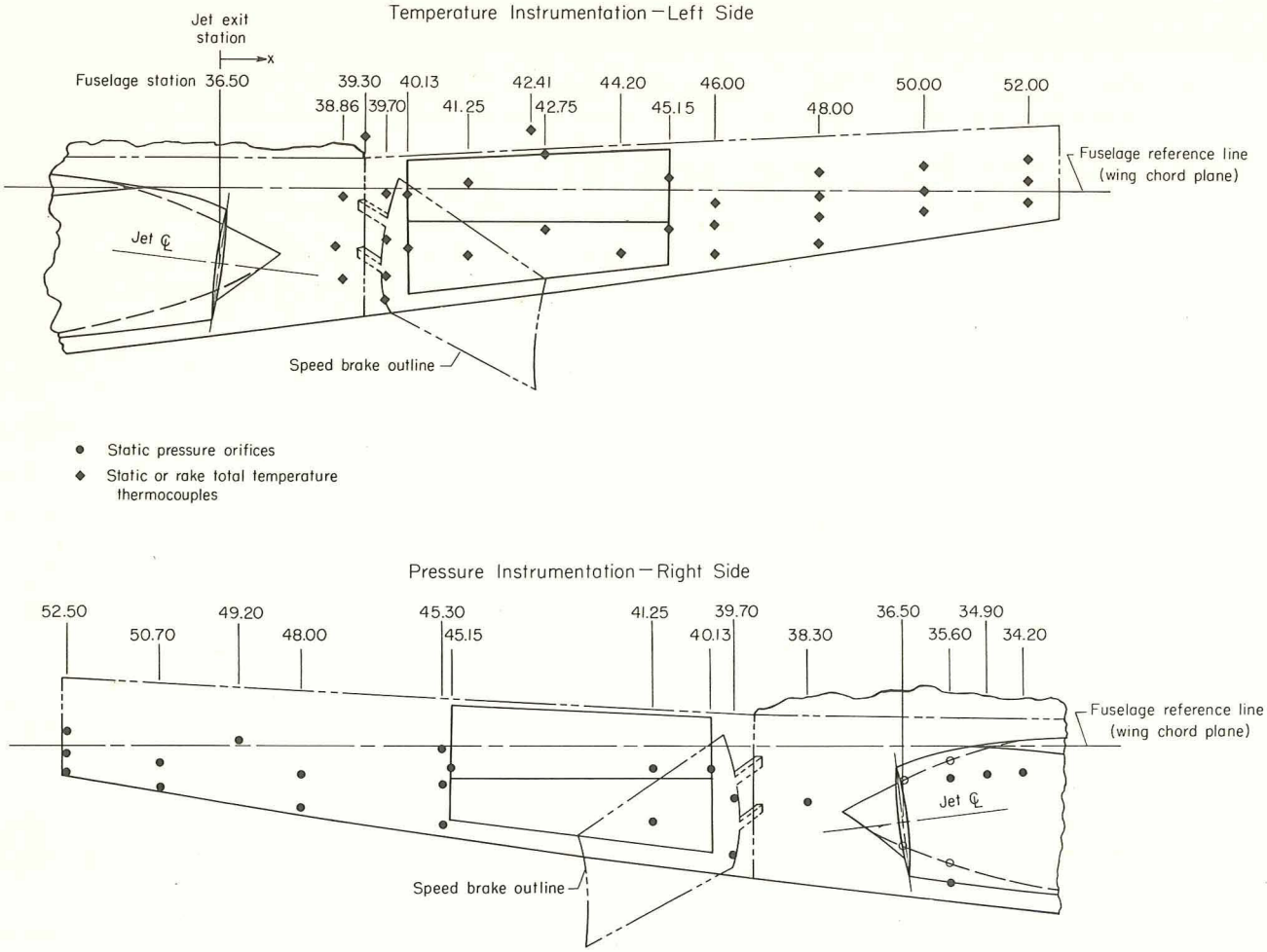

(a) Side veiw.

Figure 7.- Location of model temperature and pressure instrumentation. Open circular symbols indicate orifices hidden from view. All dimensions are in inches unless otherwise noted.

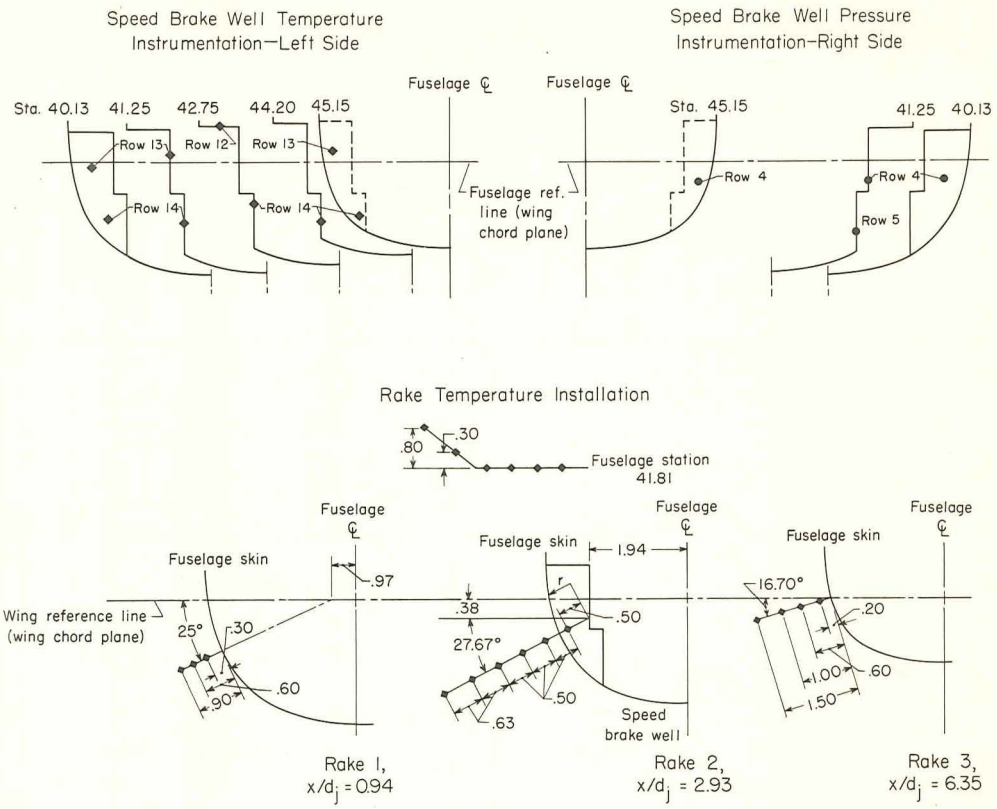

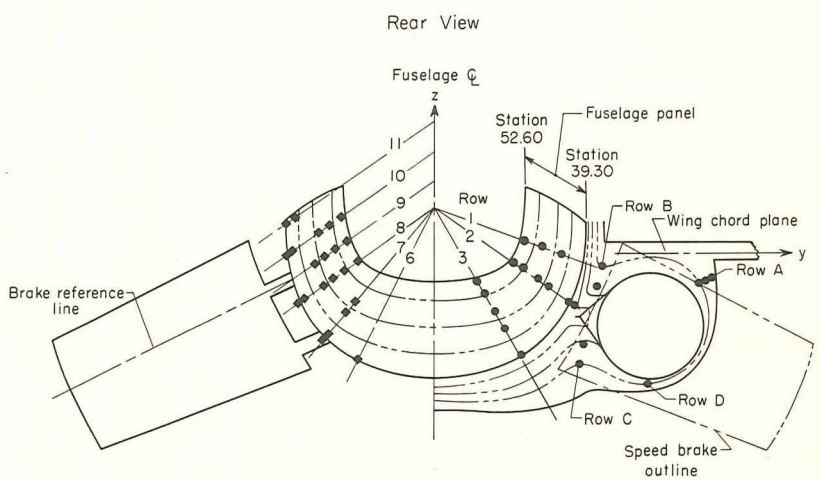

(b) Brake well and rake instrumentation locations.

Figure 7.- Concluded.

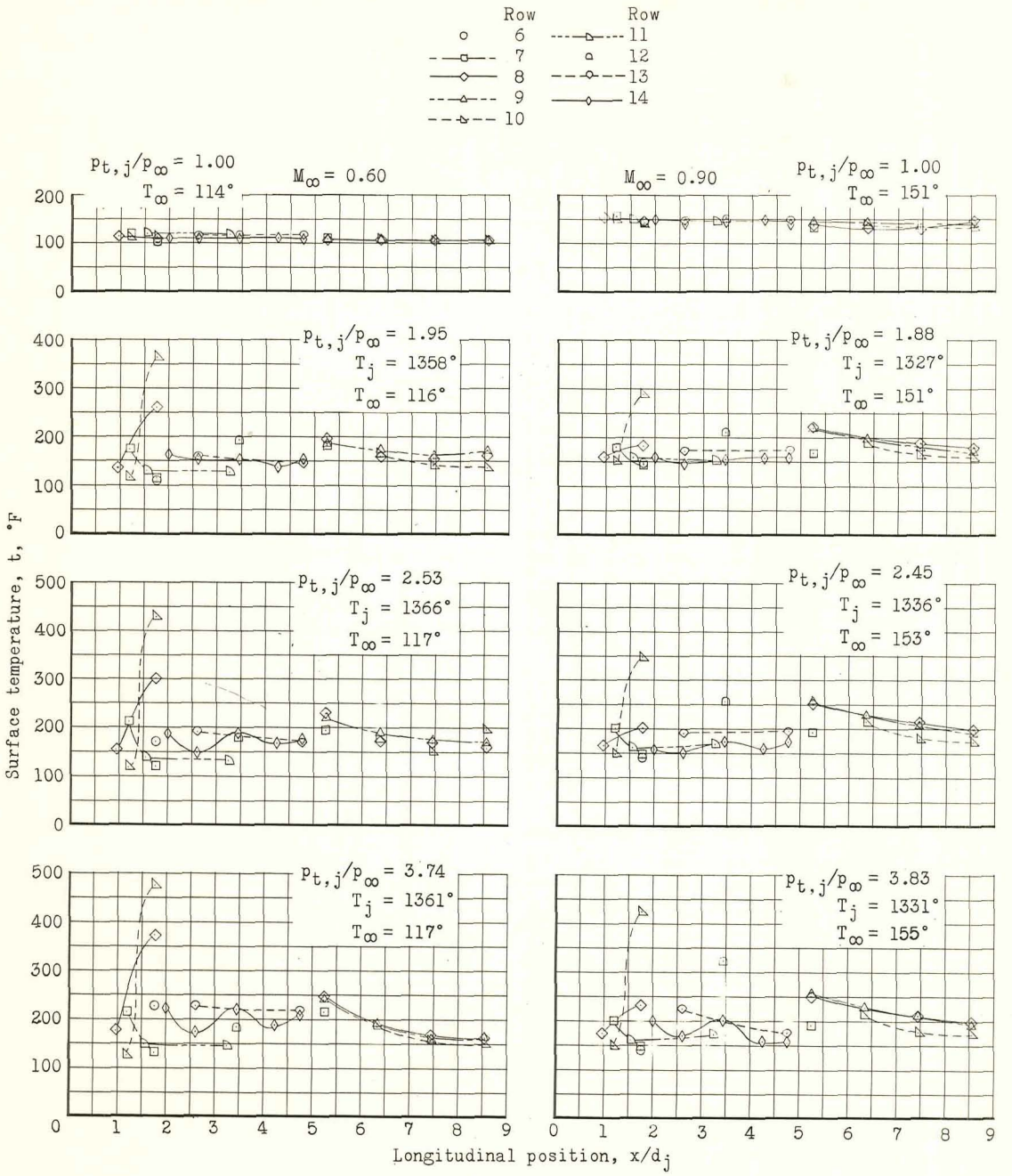

(a) Solid brakes.

Figure 8.- Variation of fuselage surface temperatures with jet pressure ratio for various speed-brake configurations. All brakes deflected 60°; basic nozzle position; $\alpha = 0°$; $\beta = 0°$; $\delta_h = 0°$.

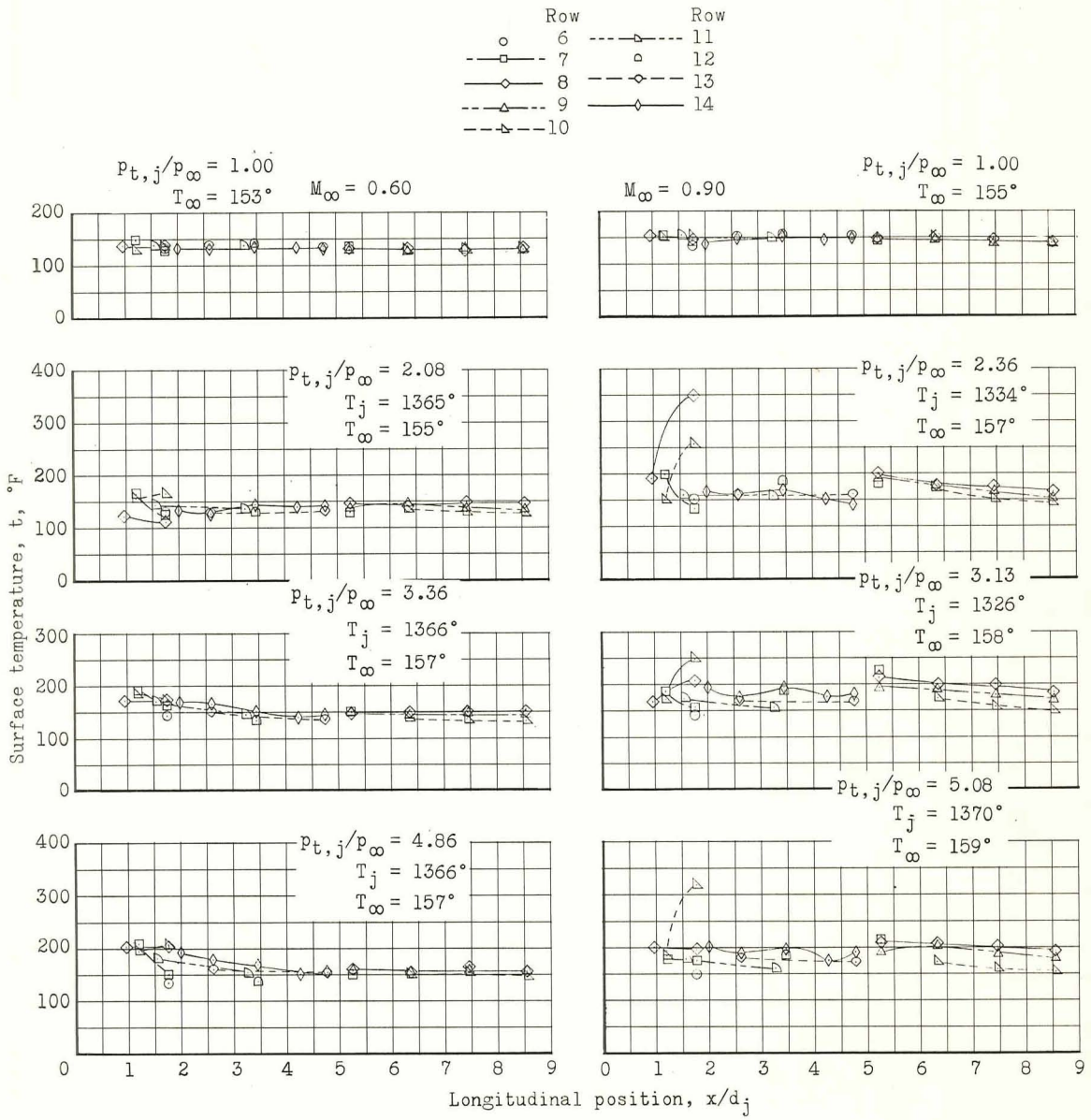

(b) Solid brakes with jet deflector.

Figure 8.- Continued.

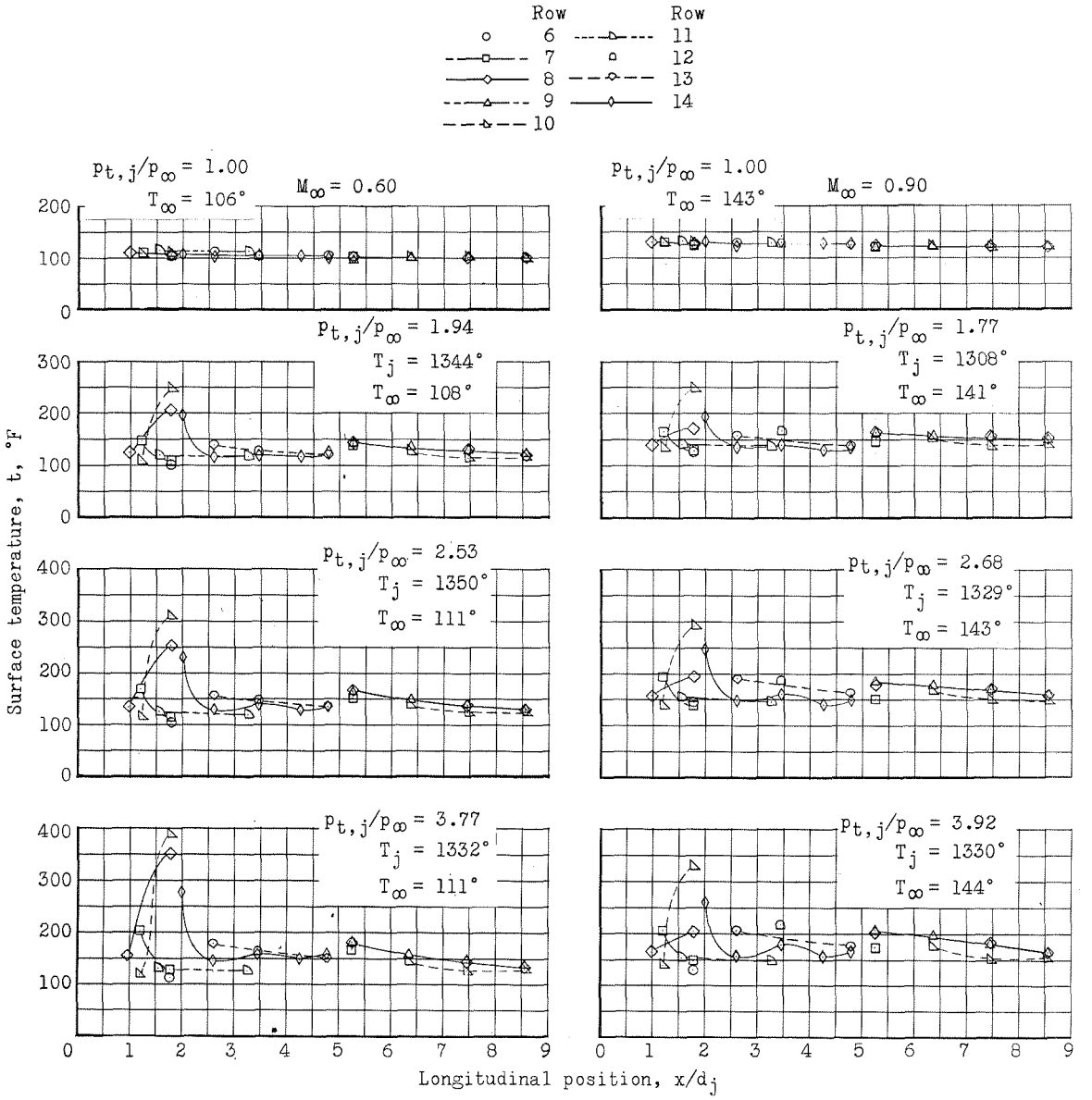

(c) Solid brakes with scoop.

Figure 8.- Continued.

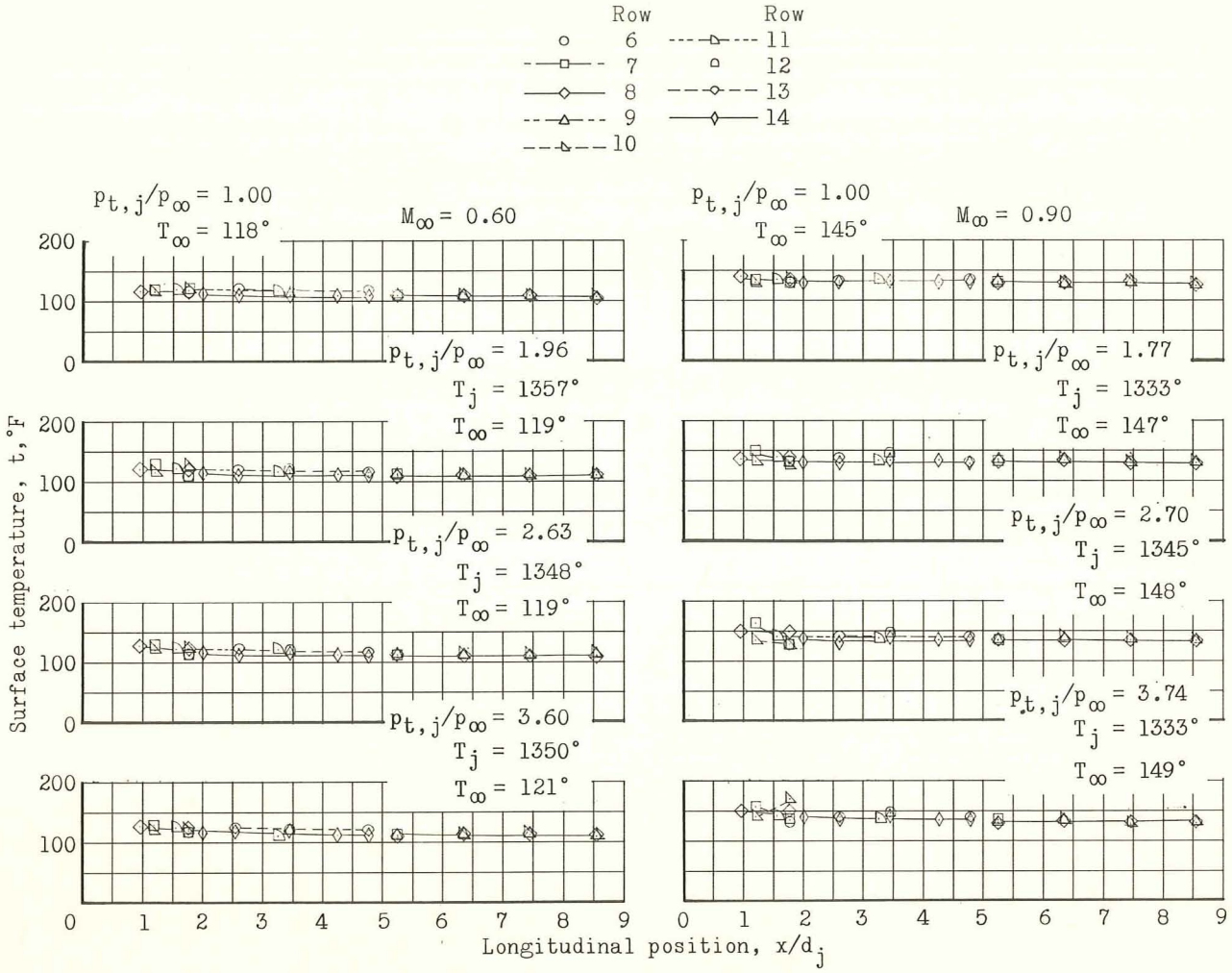

(d) Slotted brake.

Figure 8.- Continued.

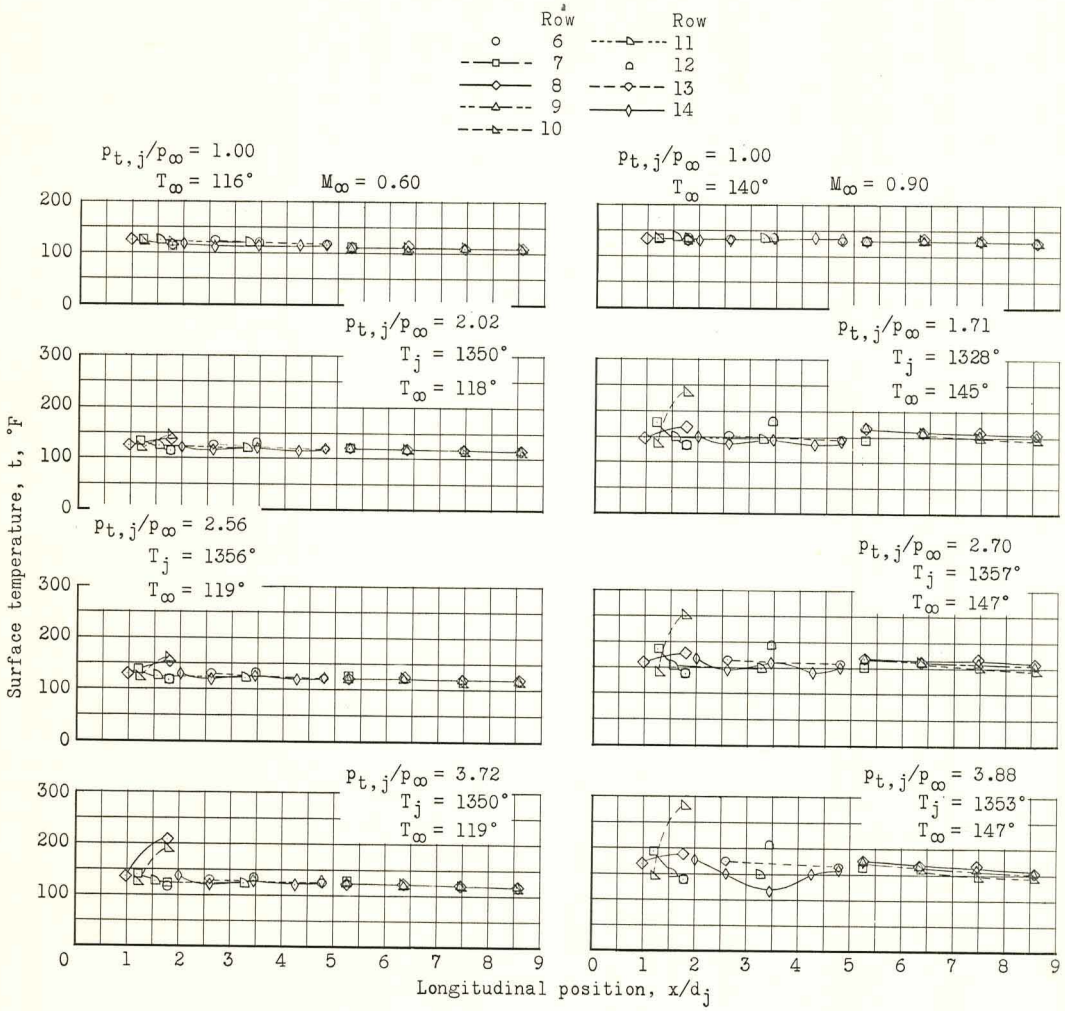

(e) Perforated brake.

Figure 8.- Continued.

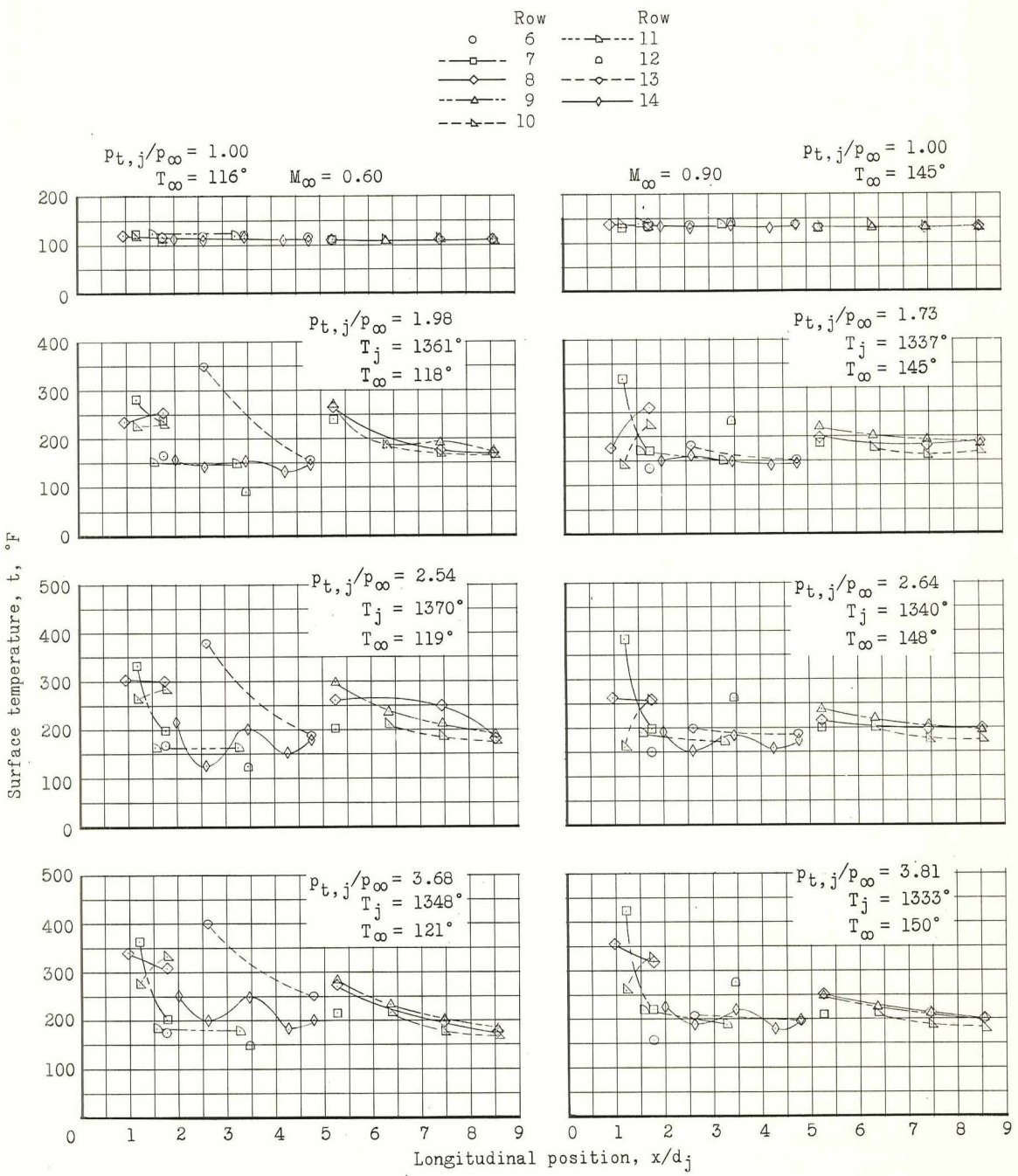

(f) Perforated brake with solid vent filler.

Figure 8.- Continued.

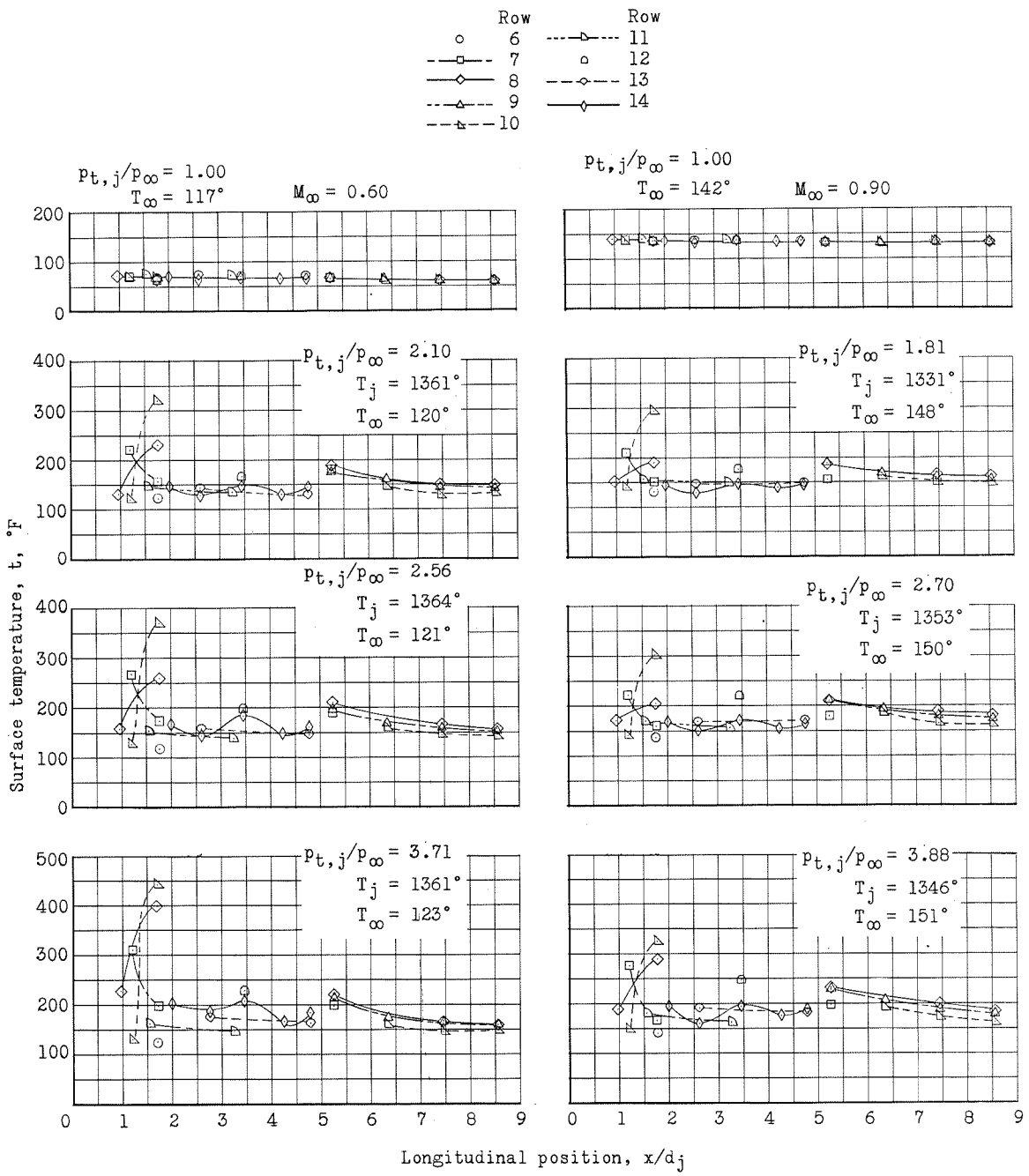

(g) Perforated brake with perforated vent filler.

Figure 8.- Continued.

L-1328

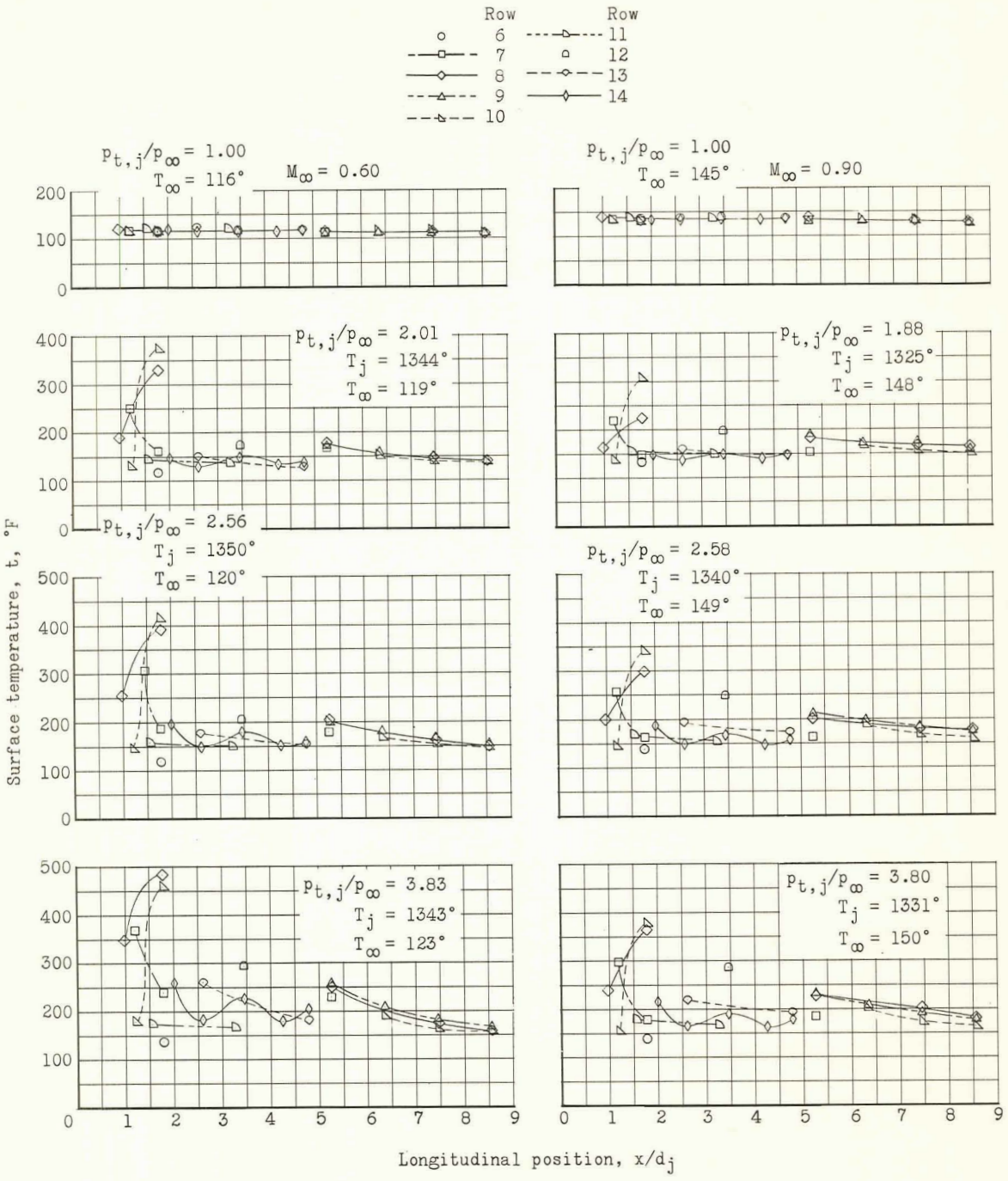

(h) Perforated brake with trapezoidal vent filler.

Figure 8.- Continued.

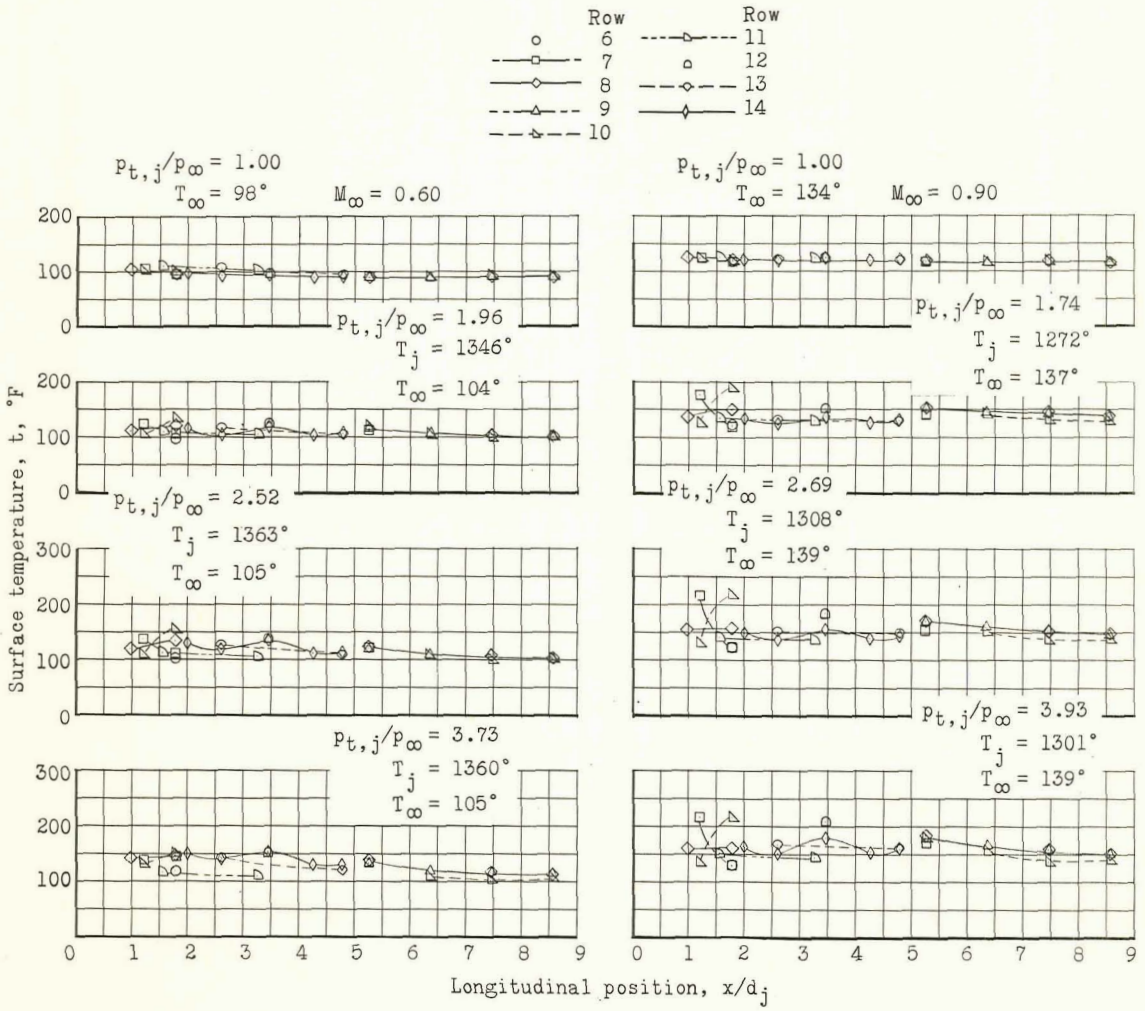

(i) Perforated brake with hinged flap.

Figure 8.- Concluded.

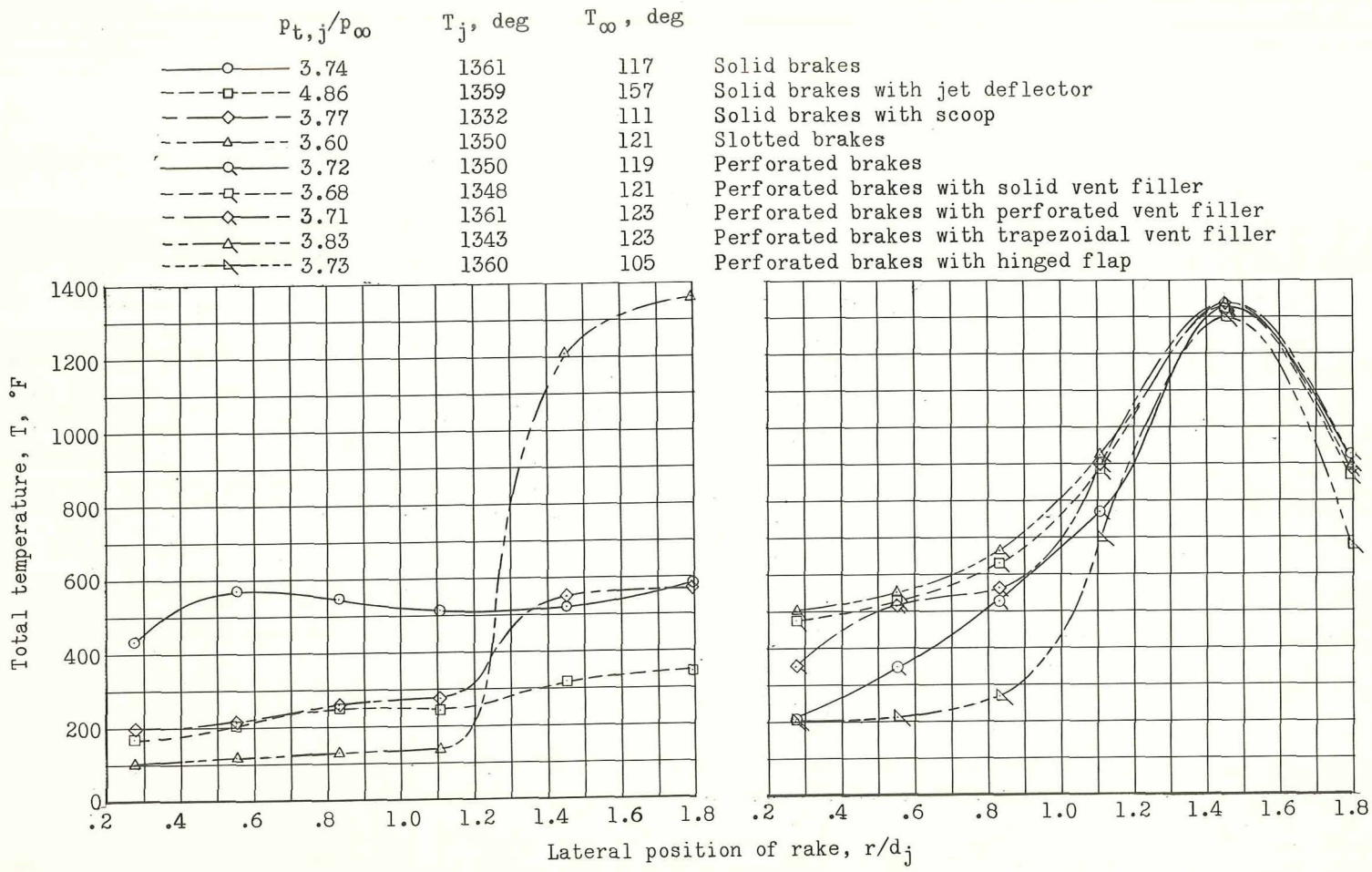

(a) $M_\infty = 0.60$.

Figure 9.- Rake stagnation temperatures behind the different speed brakes. All brakes deflected 60°; basic nozzle position; $\alpha = 0^\circ$; $\beta = 0^\circ$; $\delta_h = 0^\circ$.

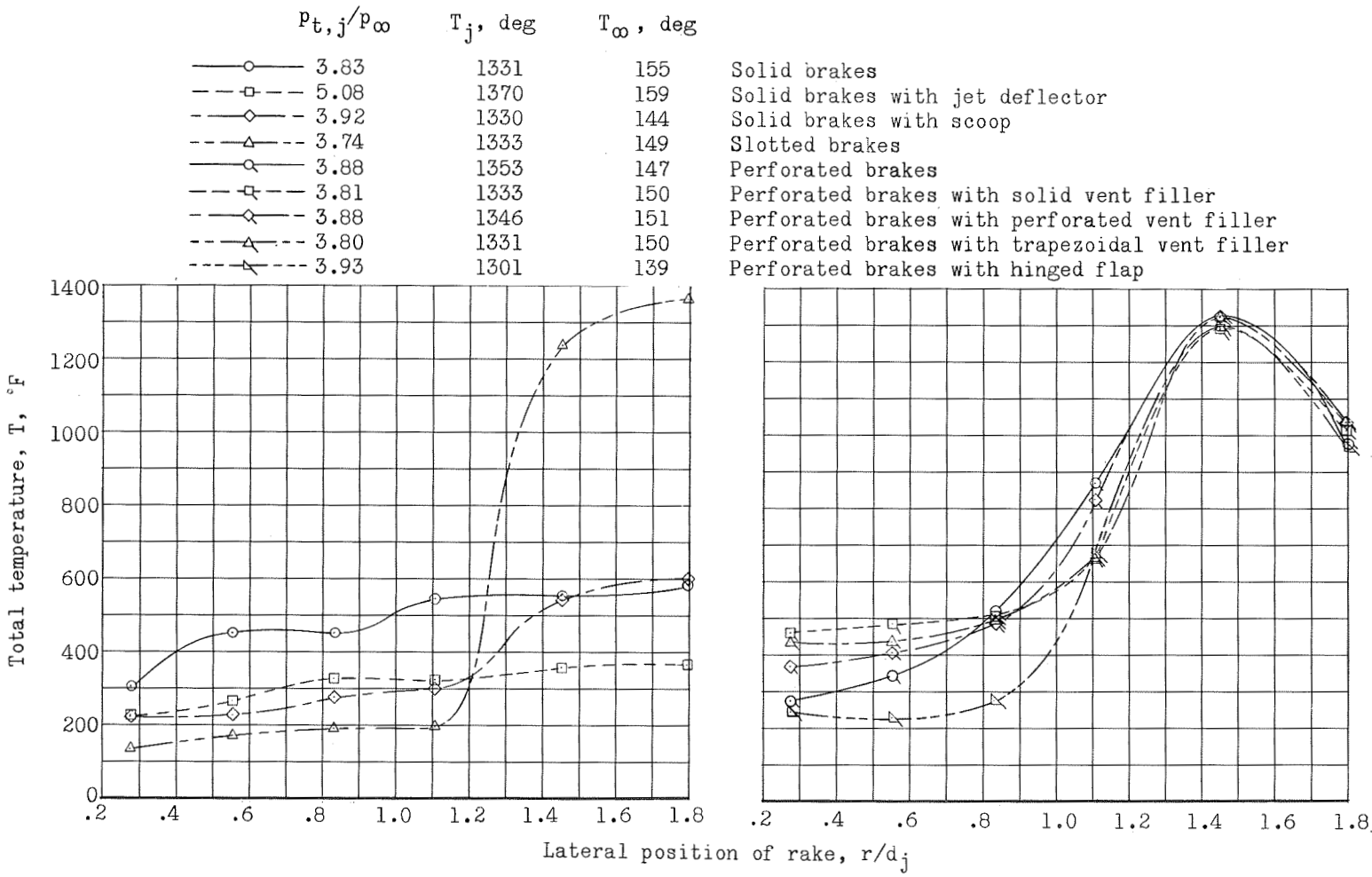

(b) $M_\infty = 0.90$.

Figure 9.- Concluded.

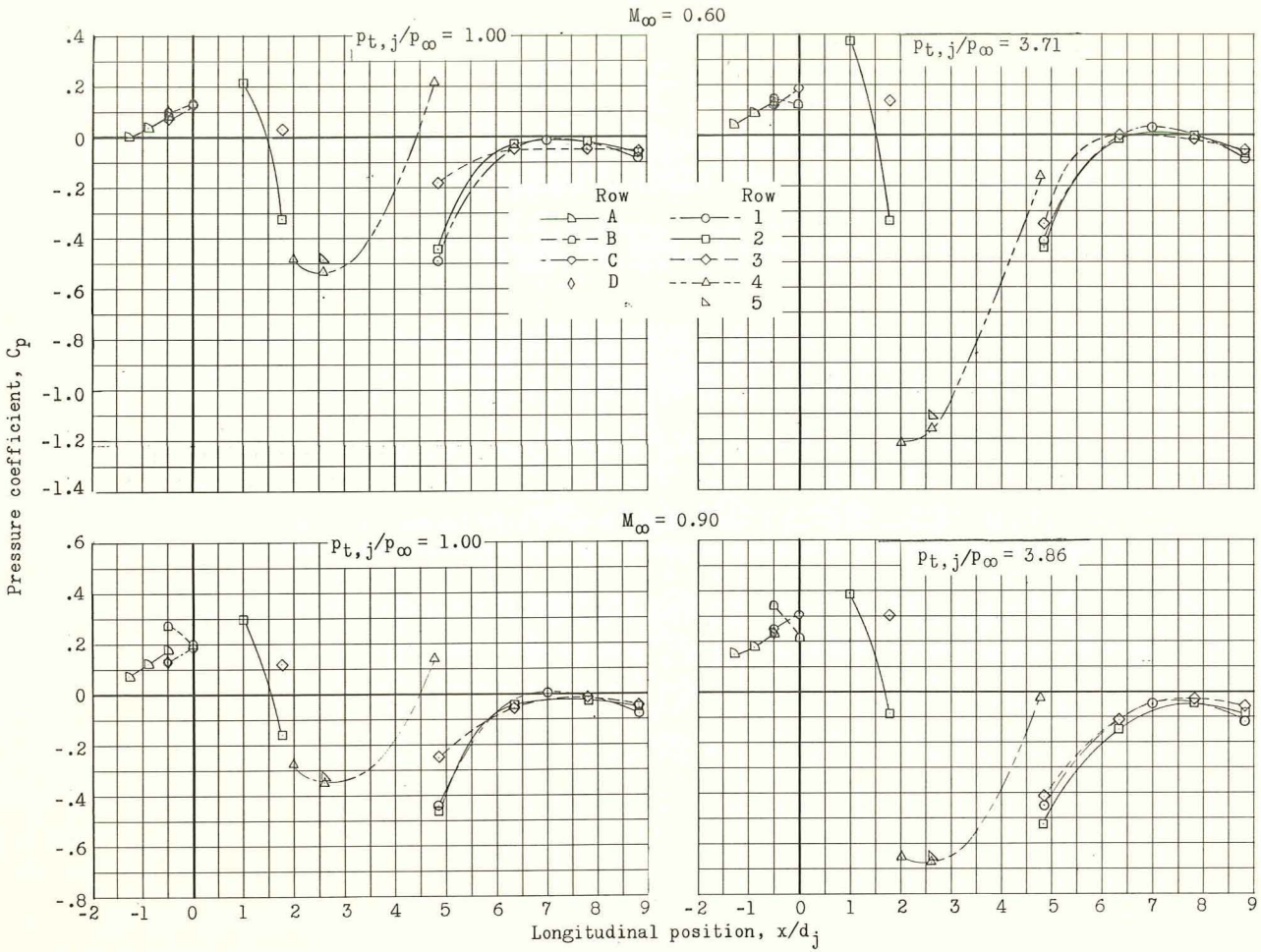

(a) Solid brake.

Figure 10.- Influence of speed-brake geometry on fuselage pressure distributions with and without jet operation. All brakes deflected 60°; basic nozzle position; $\alpha = 0°$; $\beta = 0°$; $\delta_h = 0°$.

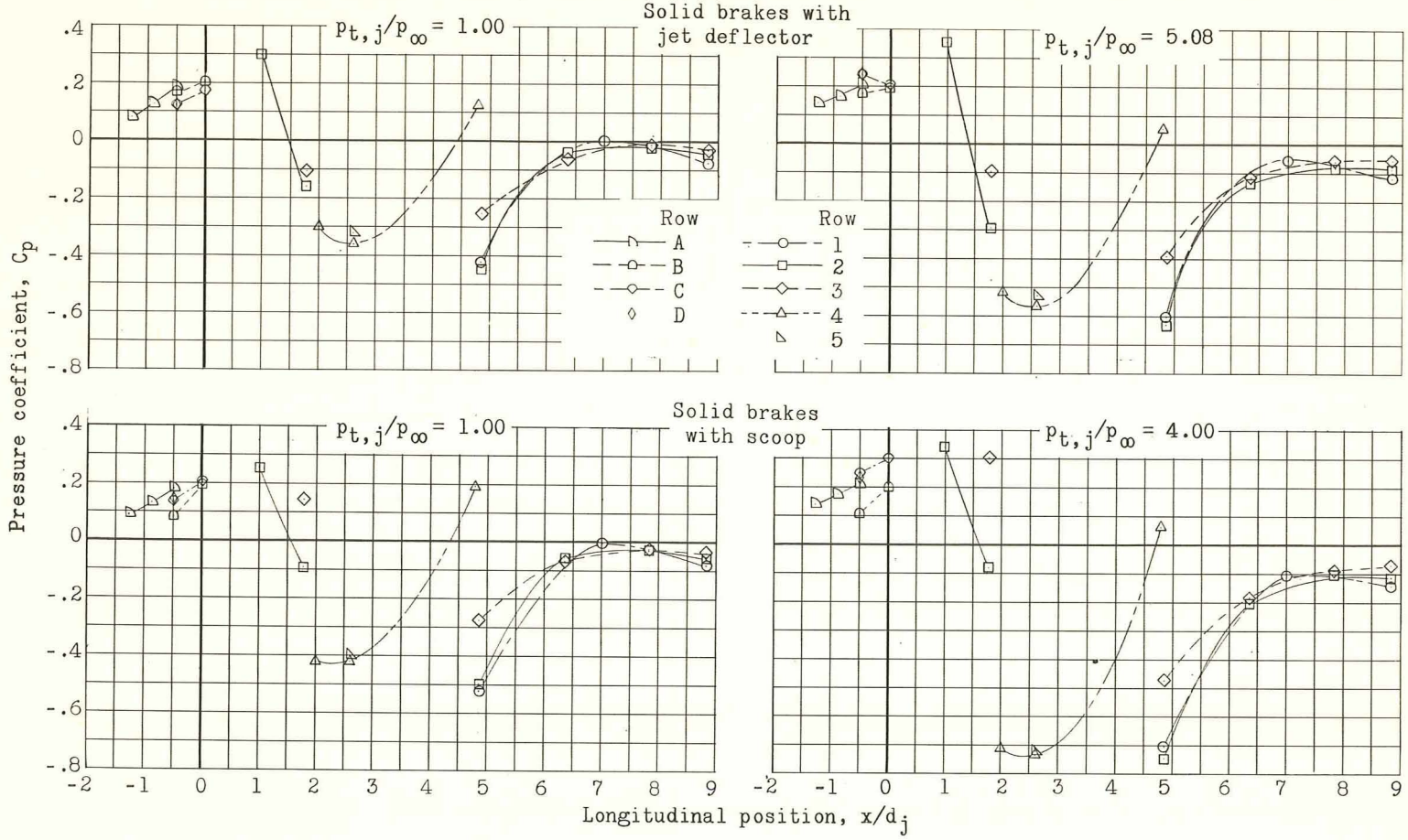

(b) Solid brake with jet deflector and with scoop; M_∞ = 0.90.

Figure 10.- Continued.

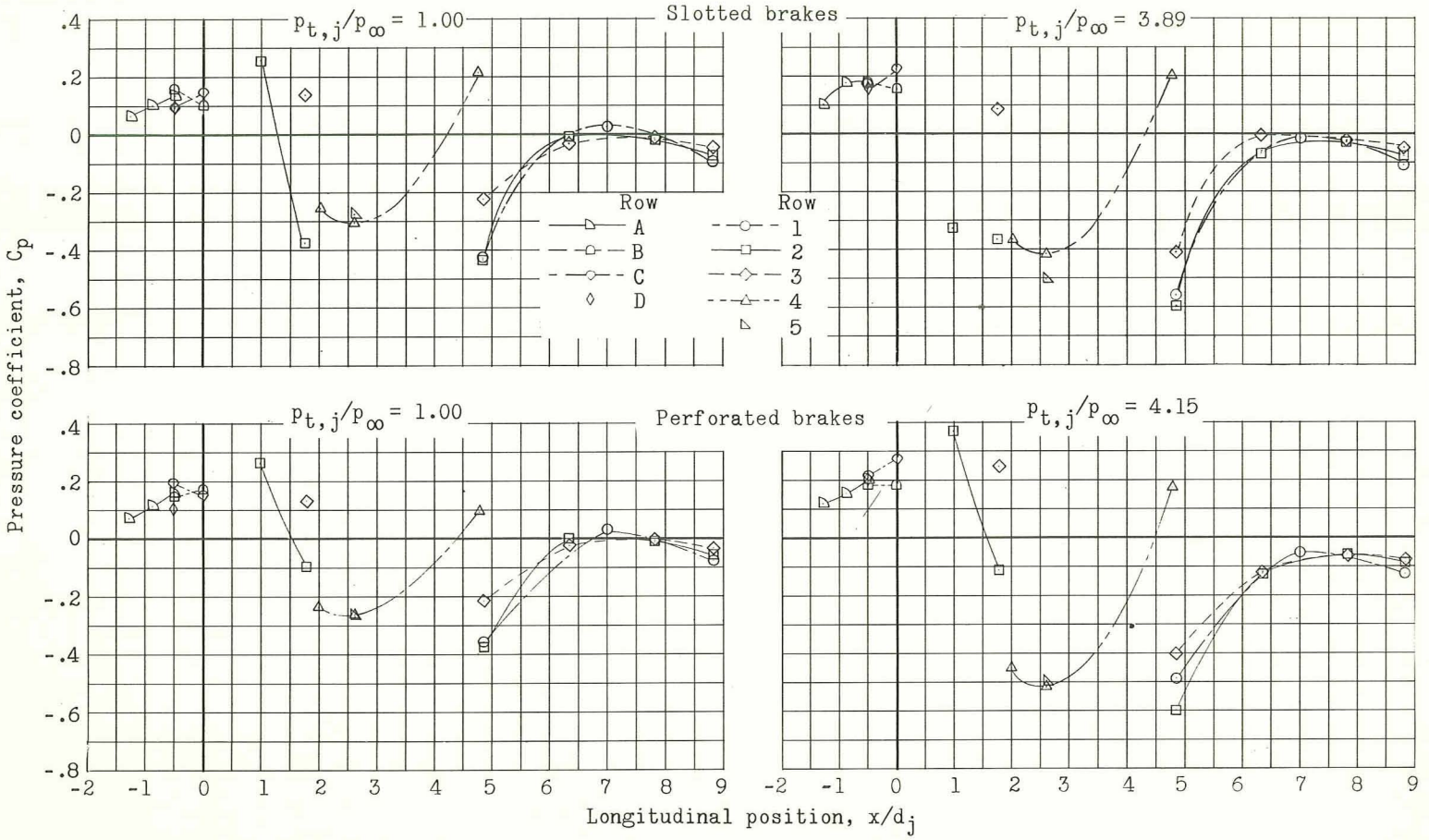

(c) Slotted brake and perforated brake; M_∞ = 0.90.

Figure 10.- Continued.

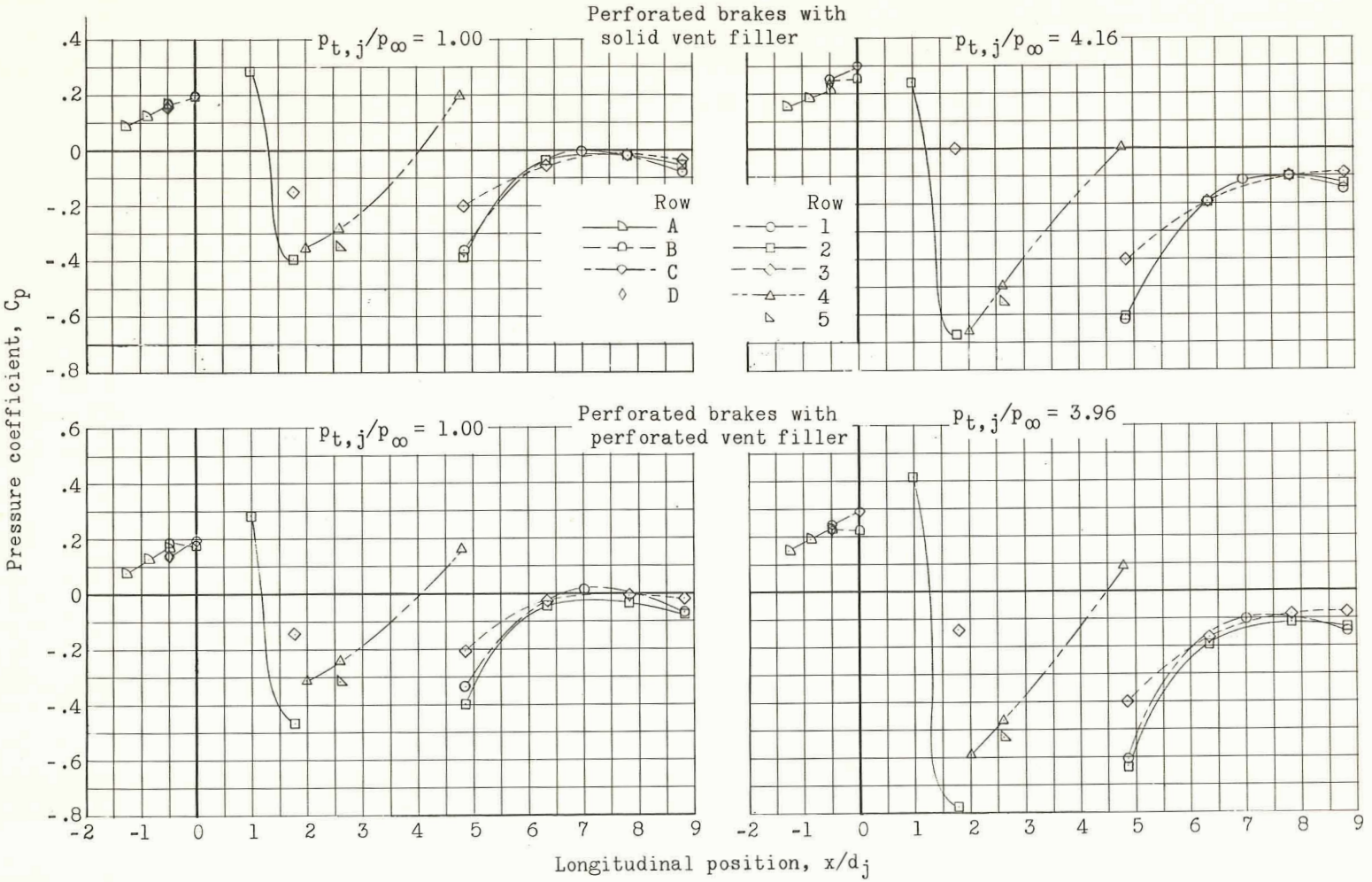

(d) Perforated brake with solid vent filler and with perforated vent filler; M_∞ = 0.90.

Figure 10.- Continued.

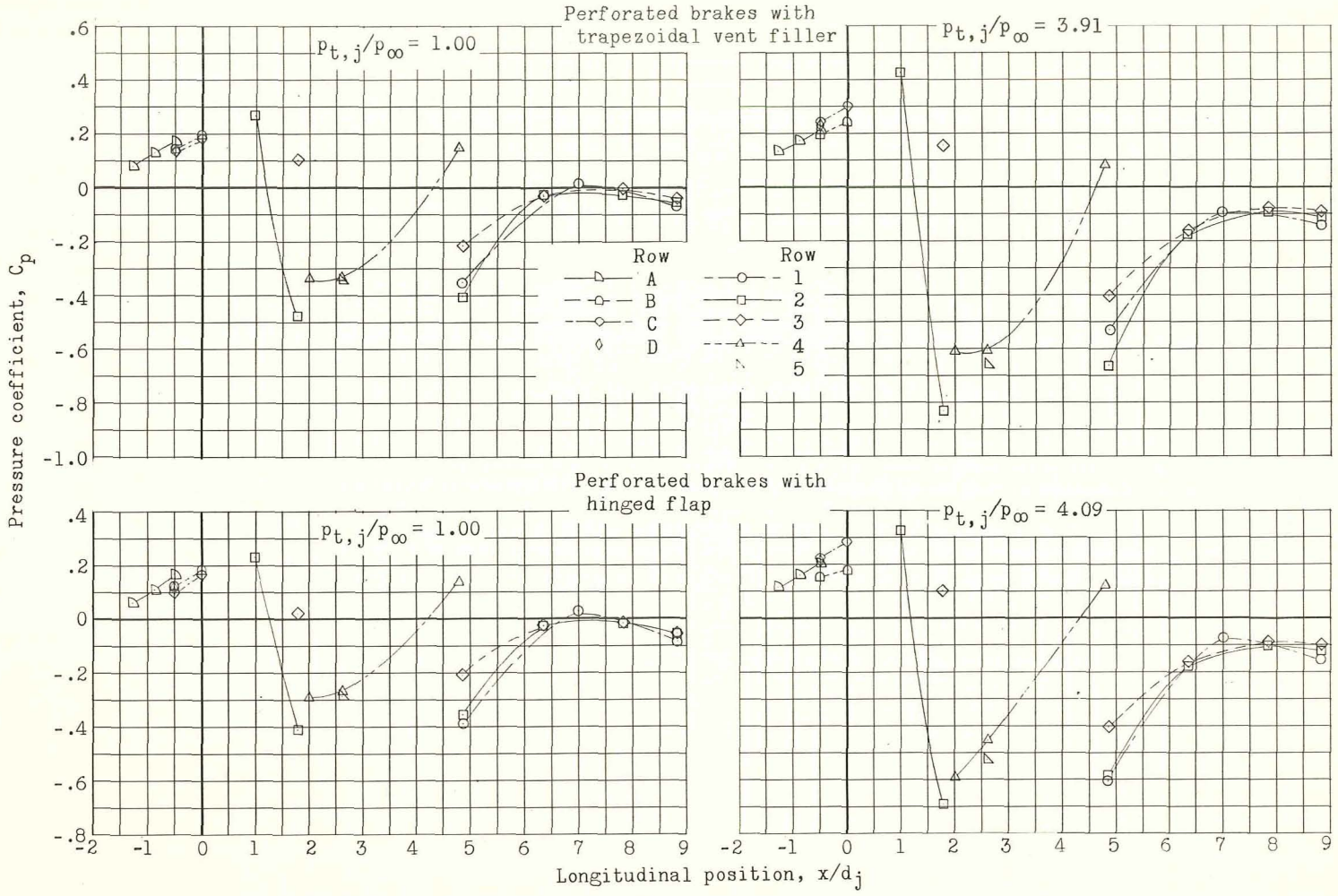

(e) Perforated brake with trapezoidal vent filler and with hinged flap; M_∞ = 0.90.

Figure 10.- Concluded.

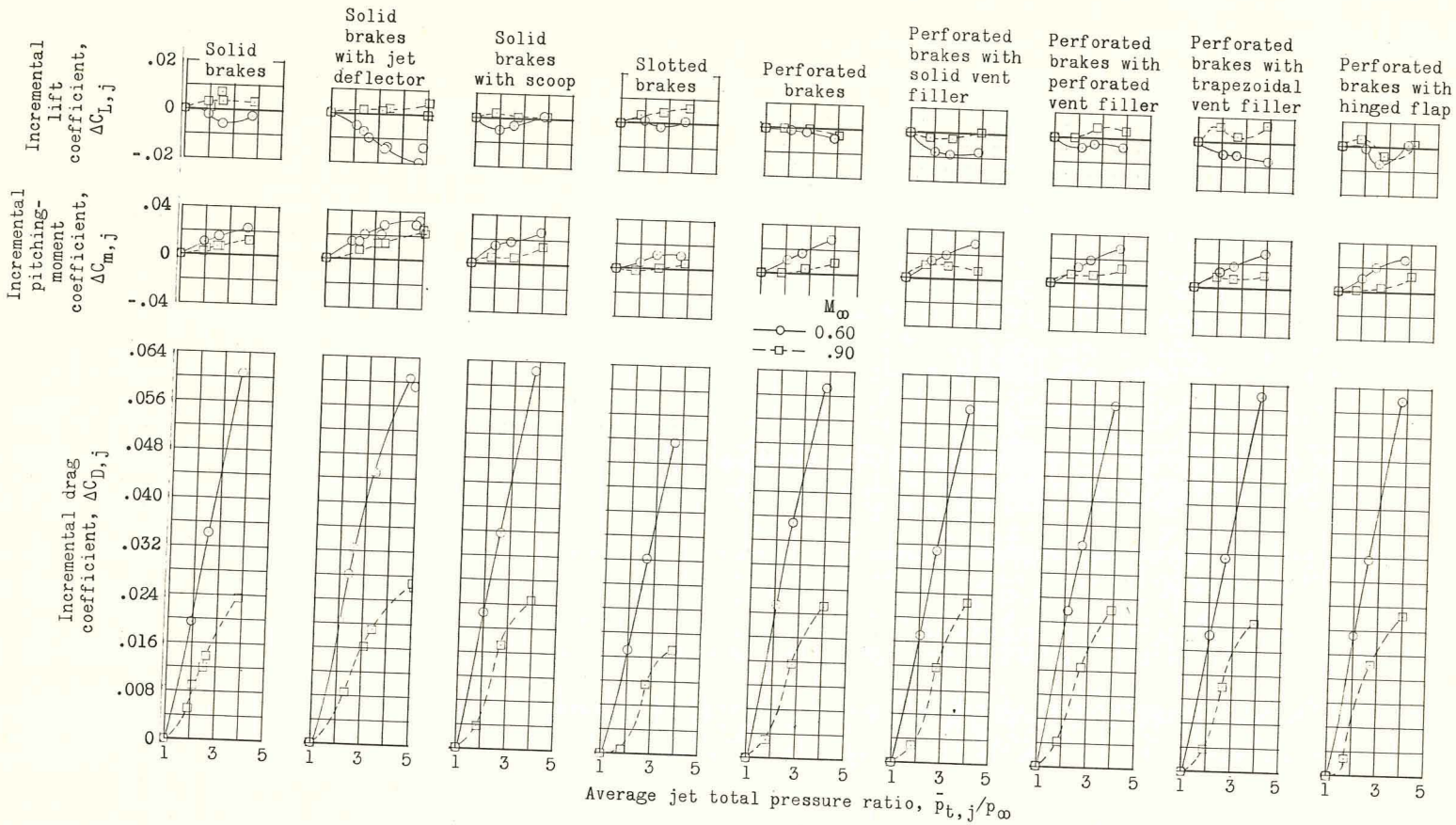

Figure 11.- Jet-induced incremental aerodynamic coefficients for the different speed-brake configurations. All brakes deflected 60°; basic nozzle position; $\alpha = 0°$; $\beta = 0°$; $\delta_h = 0°$.

CONFIDENTIAL

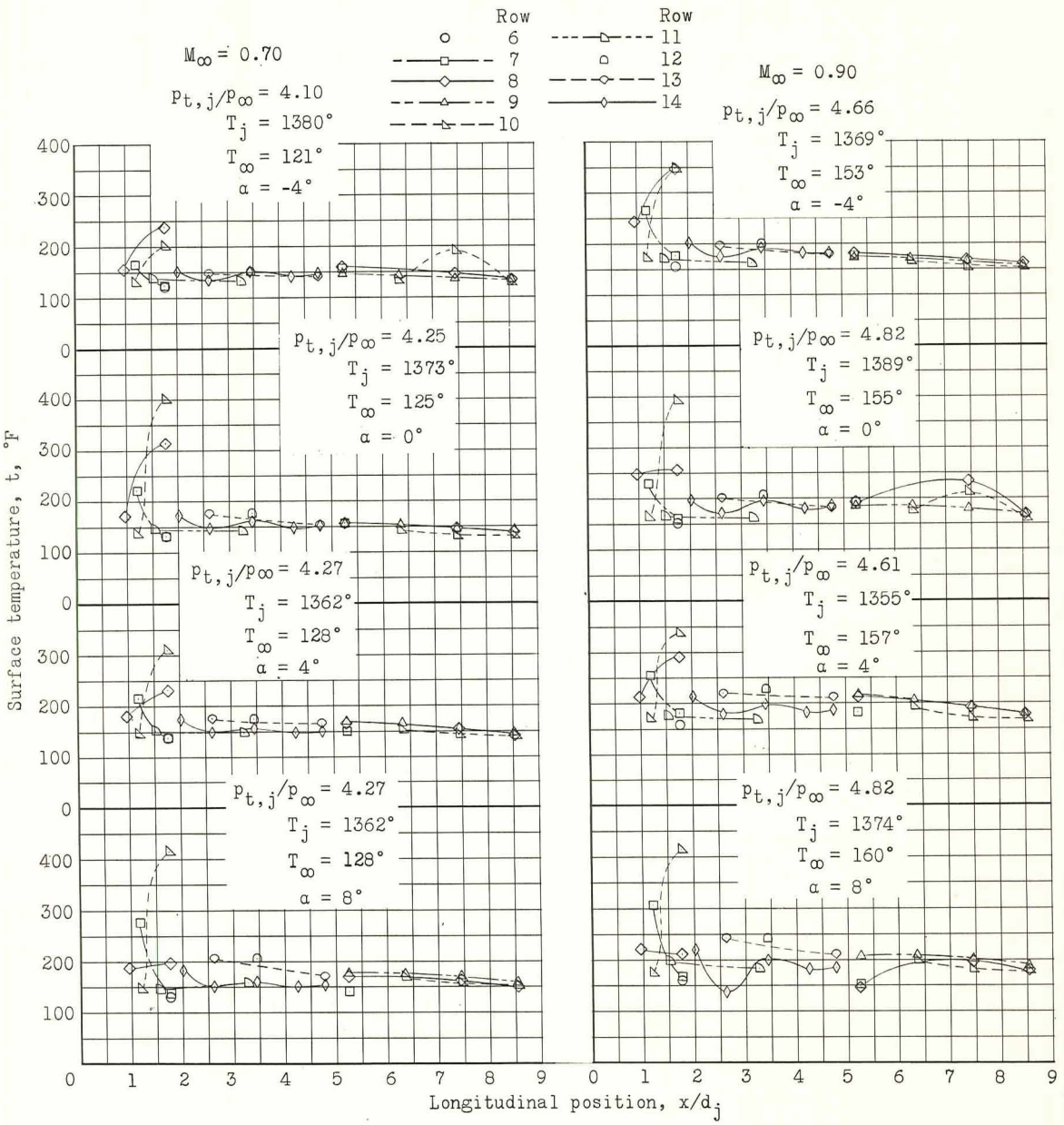

Figure 12.- Variation of fuselage temperatures with angle of attack and Mach number at maximum jet pressure ratio for the 60° perforated brake. Basic nozzle position; $\beta = 0°$; $\delta_h = 0°$.

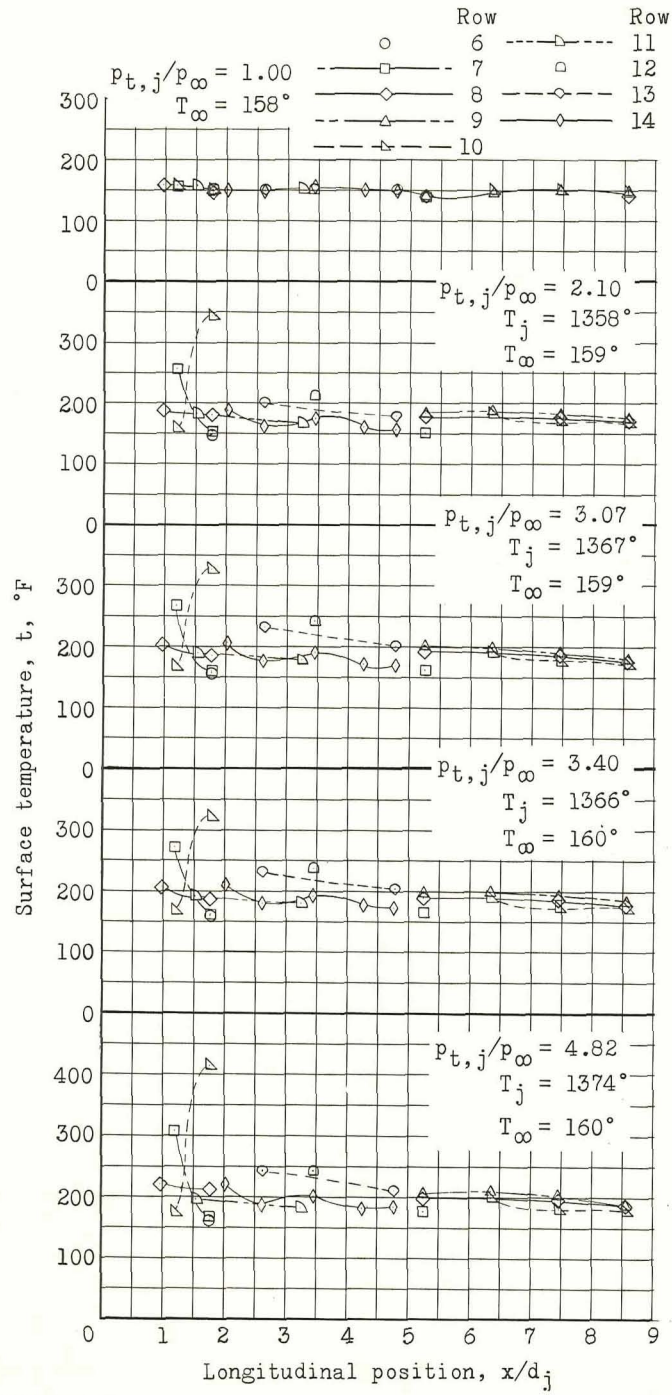

Figure 13.- Fuselage surface temperatures at various jet pressure ratios with 60° perforated brakes installed. Basic nozzle position; $M_\infty = 0.90$; $\alpha = 8°$; $\beta = 0°$; $\delta_h = 0°$.

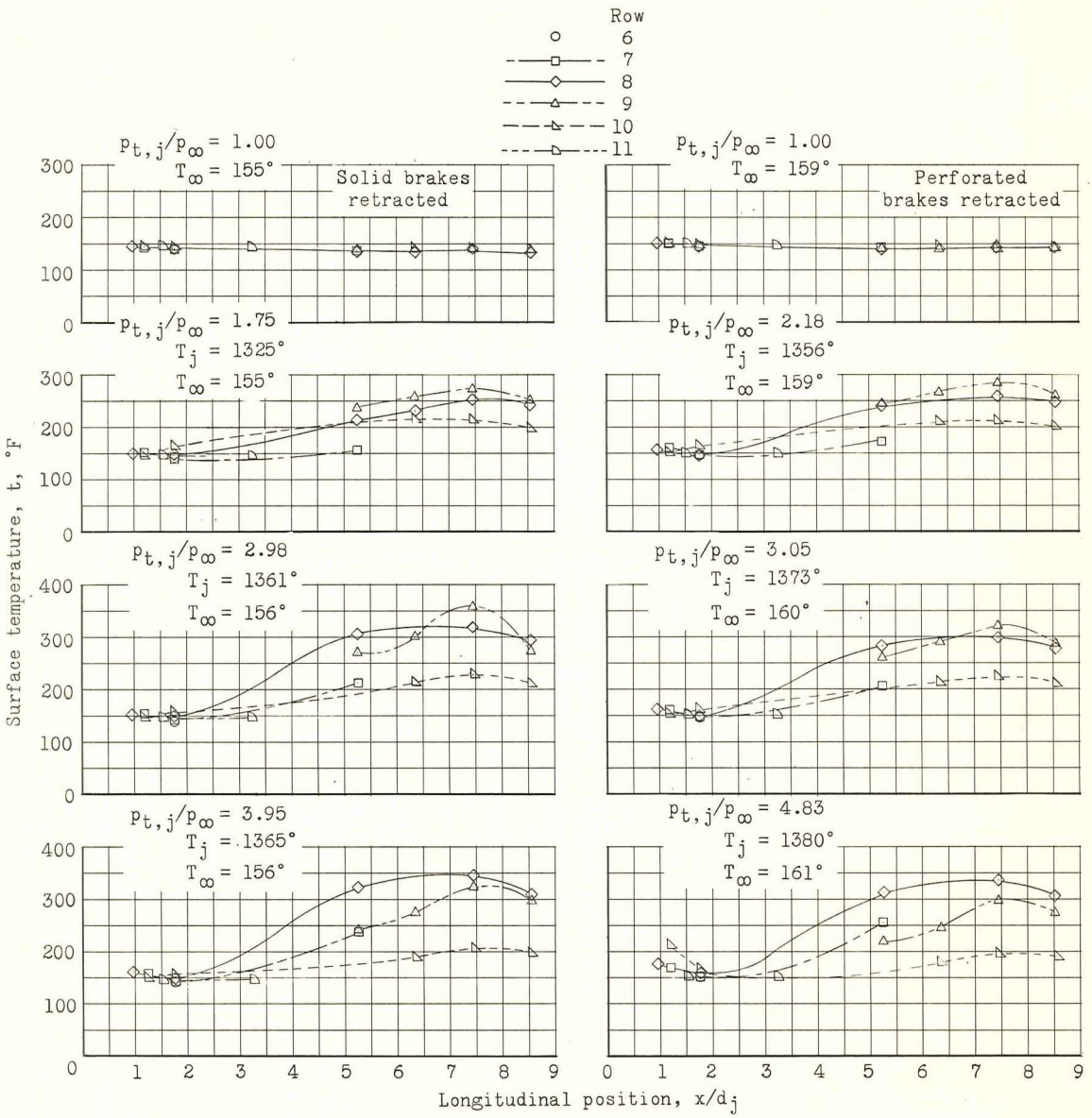

Figure 14.- Influence of jet pressure ratio on fuselage temperatures with solid and perforated brakes retracted. Basic nozzle position; $M_\infty = 0.90$; $\alpha = 8^\circ$; $\beta = 0^\circ$; $\delta_h = 0^\circ$.

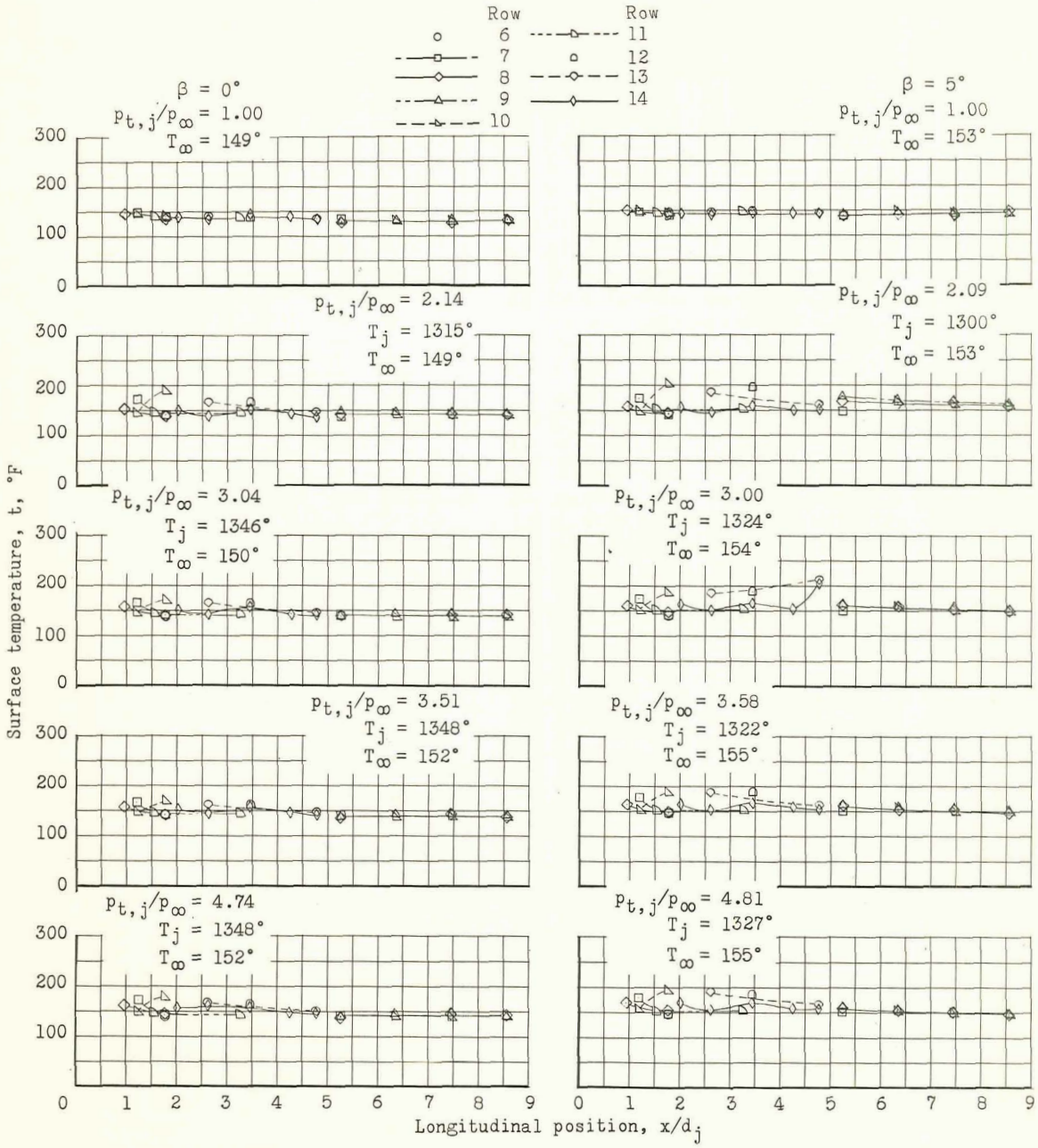

(a) $\tau = 30^\circ$.

Figure 15.- Effect of sideslip angle on fuselage temperatures at various jet pressure ratios for 30° and 60° deflections of the perforated speed brake. Basic nozzle position; $M_\infty = 0.90$; $\alpha = 8^\circ$; $\delta_h = 0^\circ$.

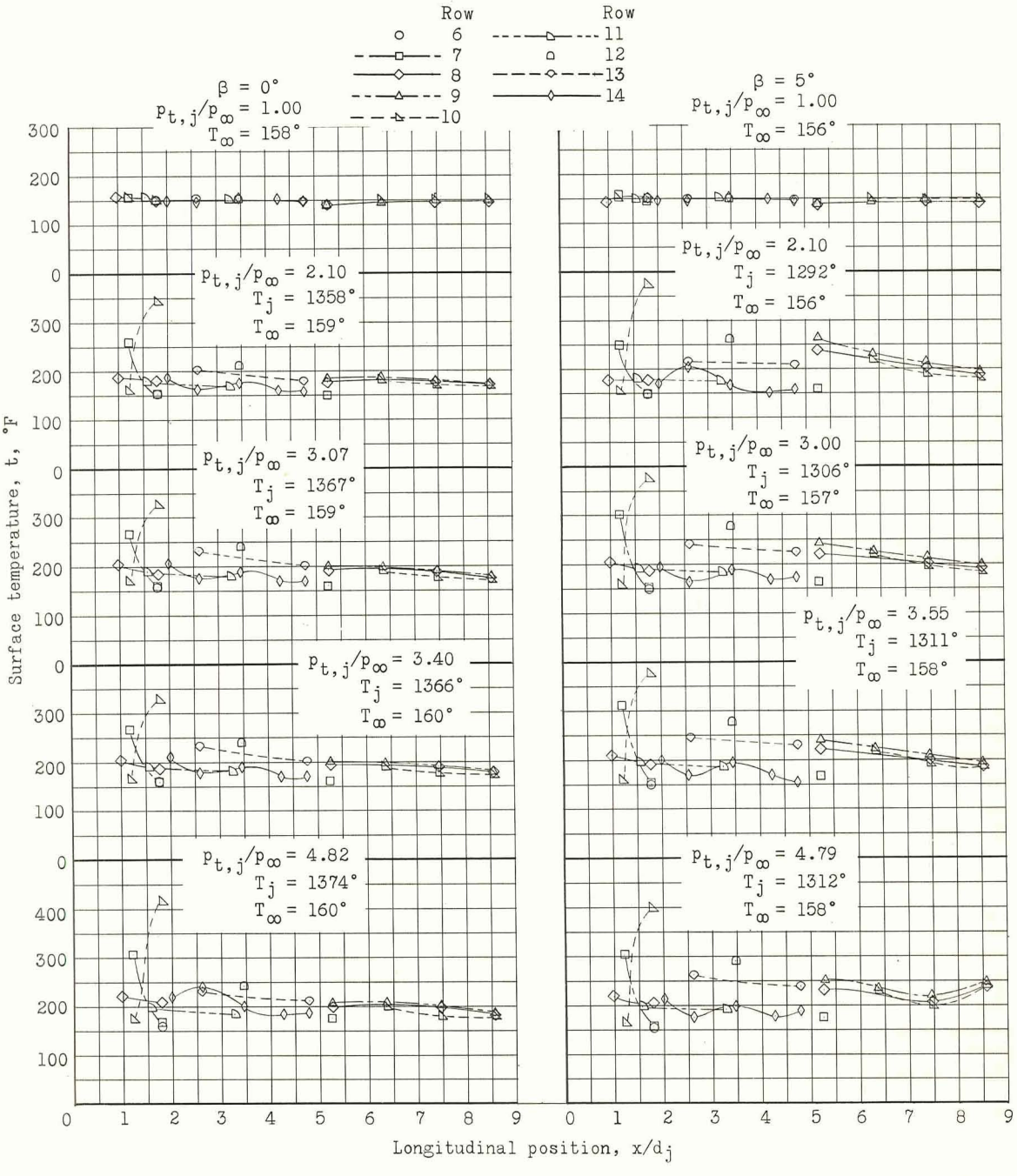

(b) $\tau = 60^\circ$.

Figure 15.- Concluded.

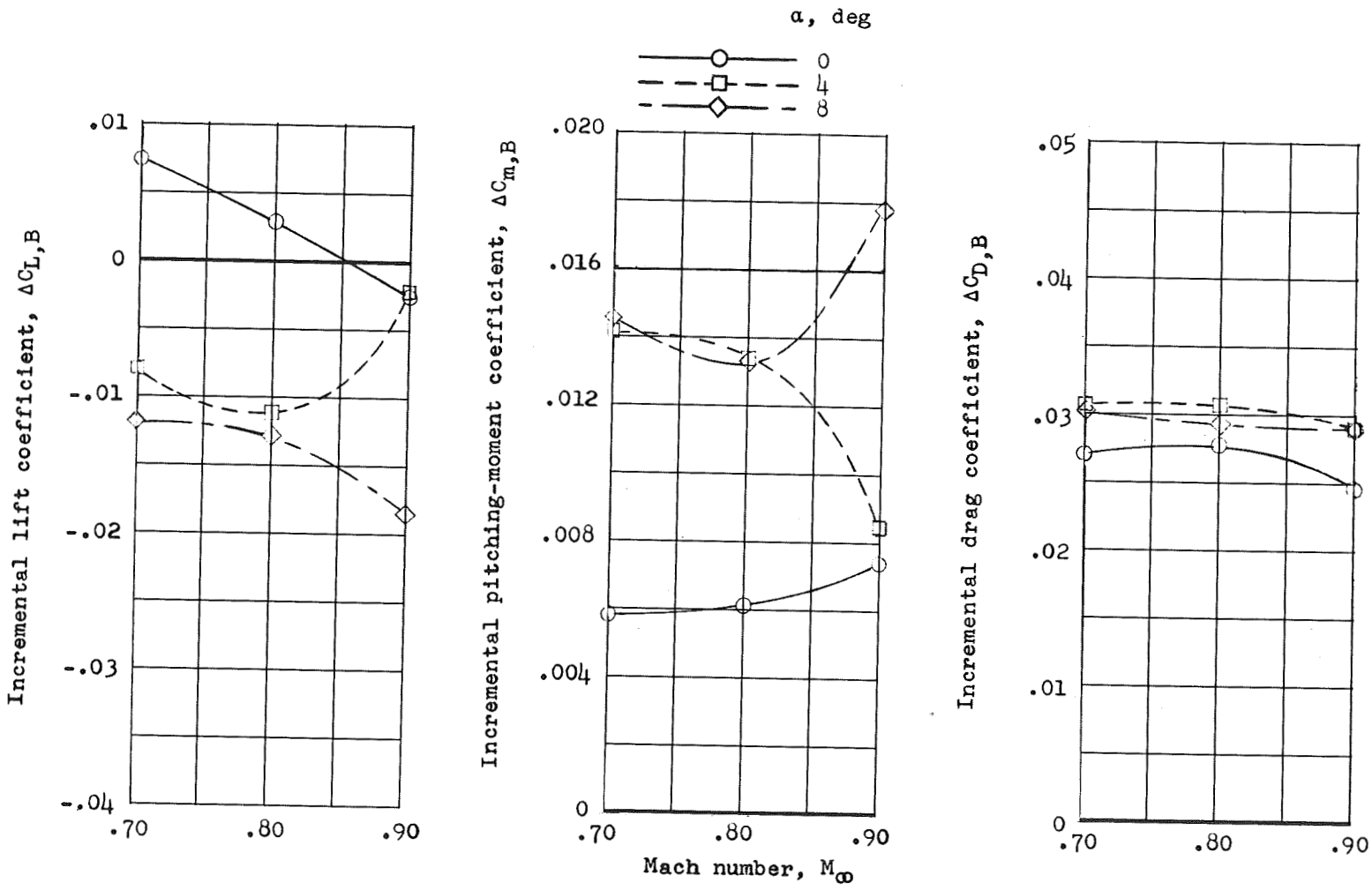

Figure 16.- Power-off aerodynamic contribution of the 60° perforated brakes. Basic nozzle position; $\beta = 0^\circ$; $\delta_h = 0^\circ$.

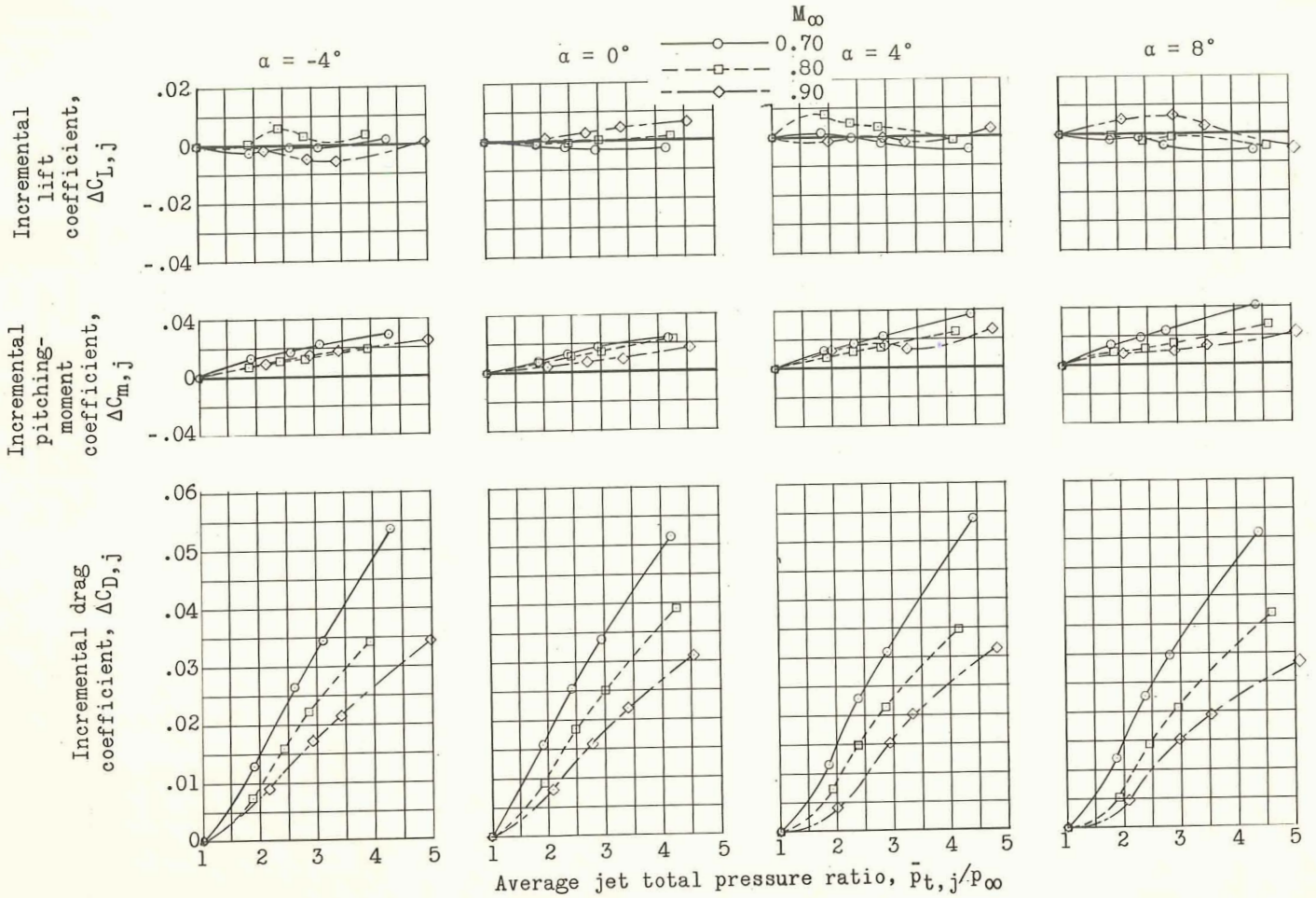

(a) $\delta_h = 0^\circ$.

Figure 17.- Jet interference effects on the model with 60° perforated brakes for horizontal-tail settings of 0° and -5°. Basic nozzle position; $\beta = 0^\circ$.

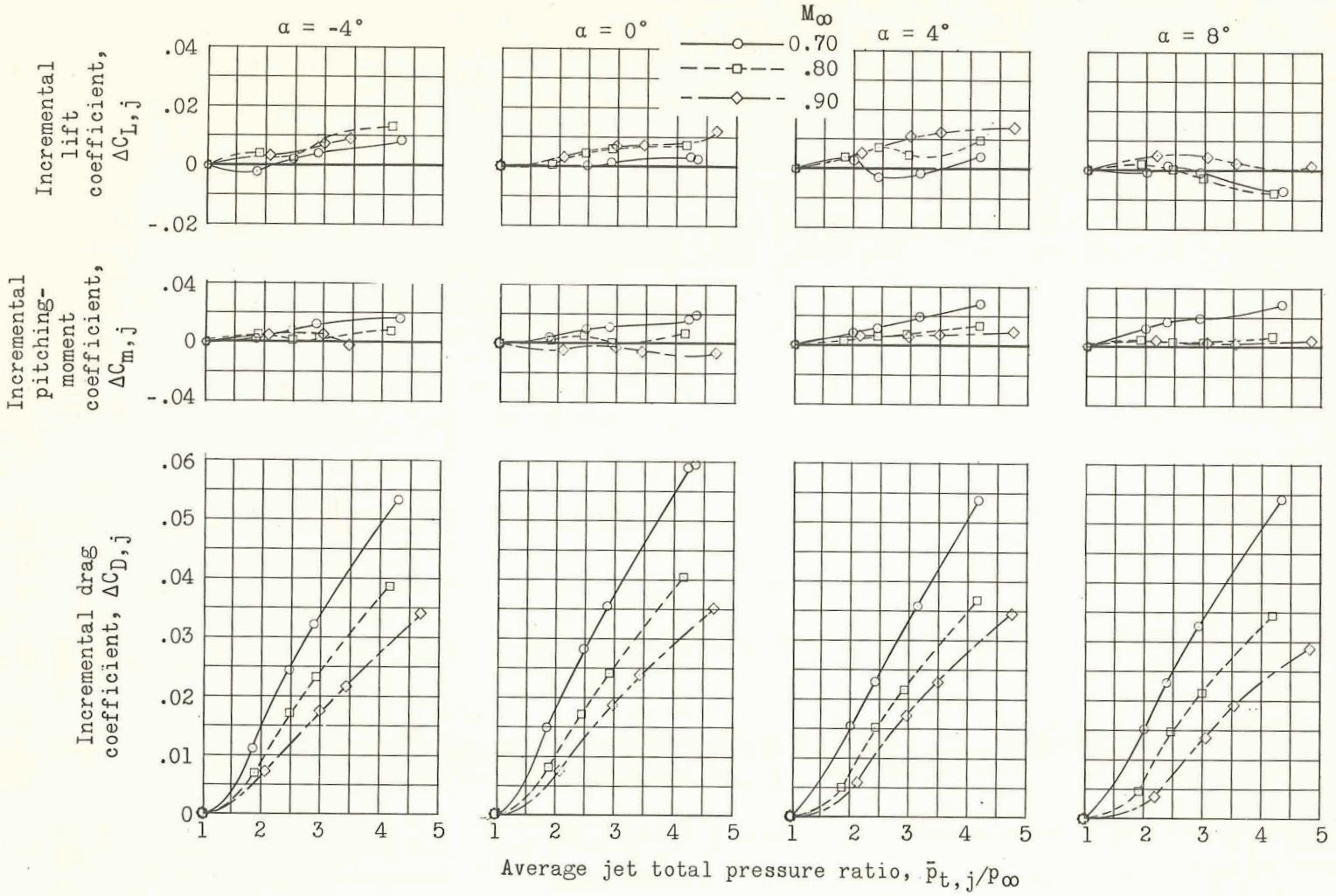

(b) $\delta_h = -5^\circ$.

Figure 17.- Concluded.

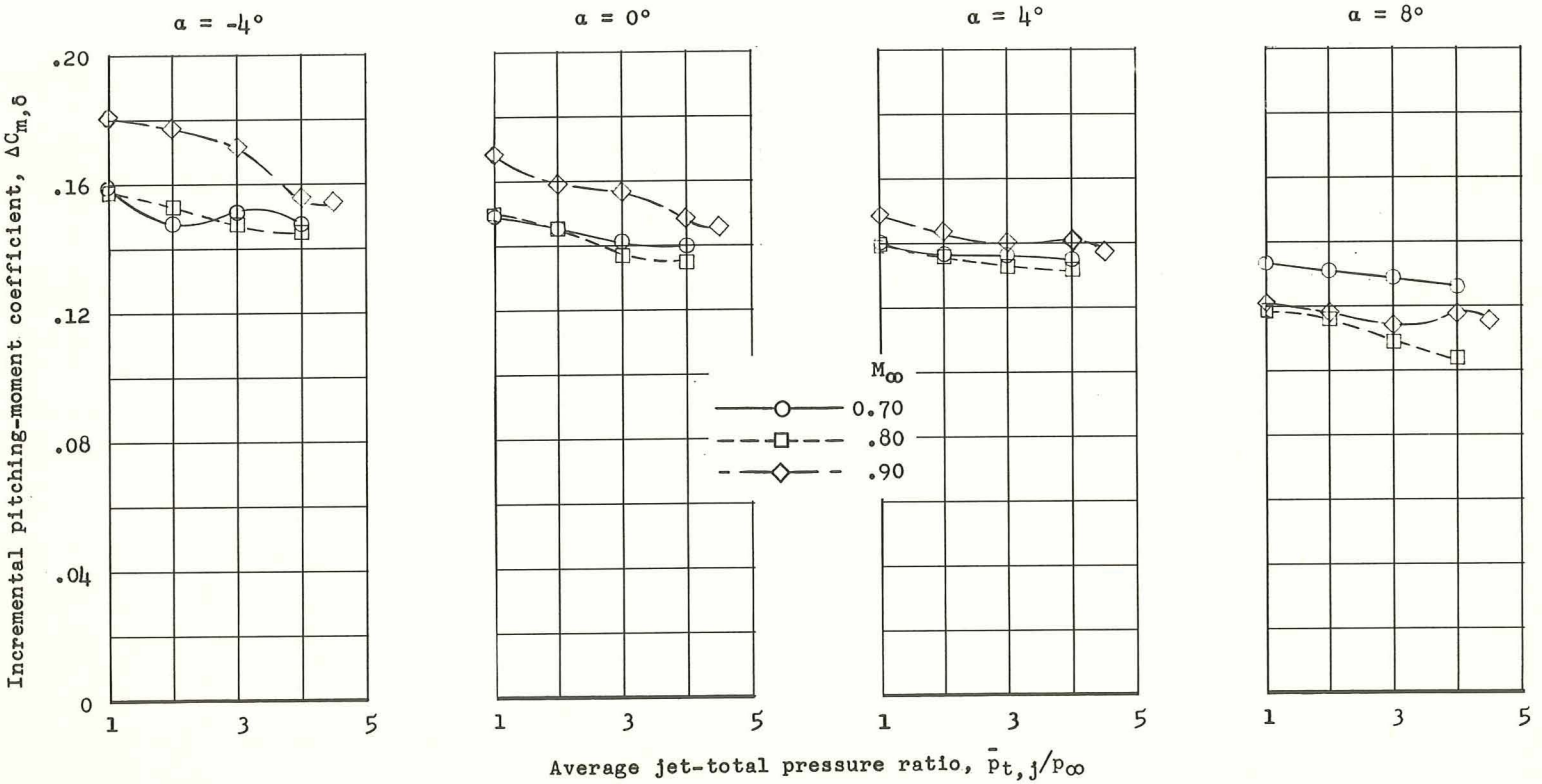

Figure 18.- Effect of jet total-pressure ratio on horizontal-tail effectiveness with 60° perforated brakes installed. Incremental-moment values were determined from tail settings of 0° and -5°. Basic nozzle position; $\beta = 0°$.

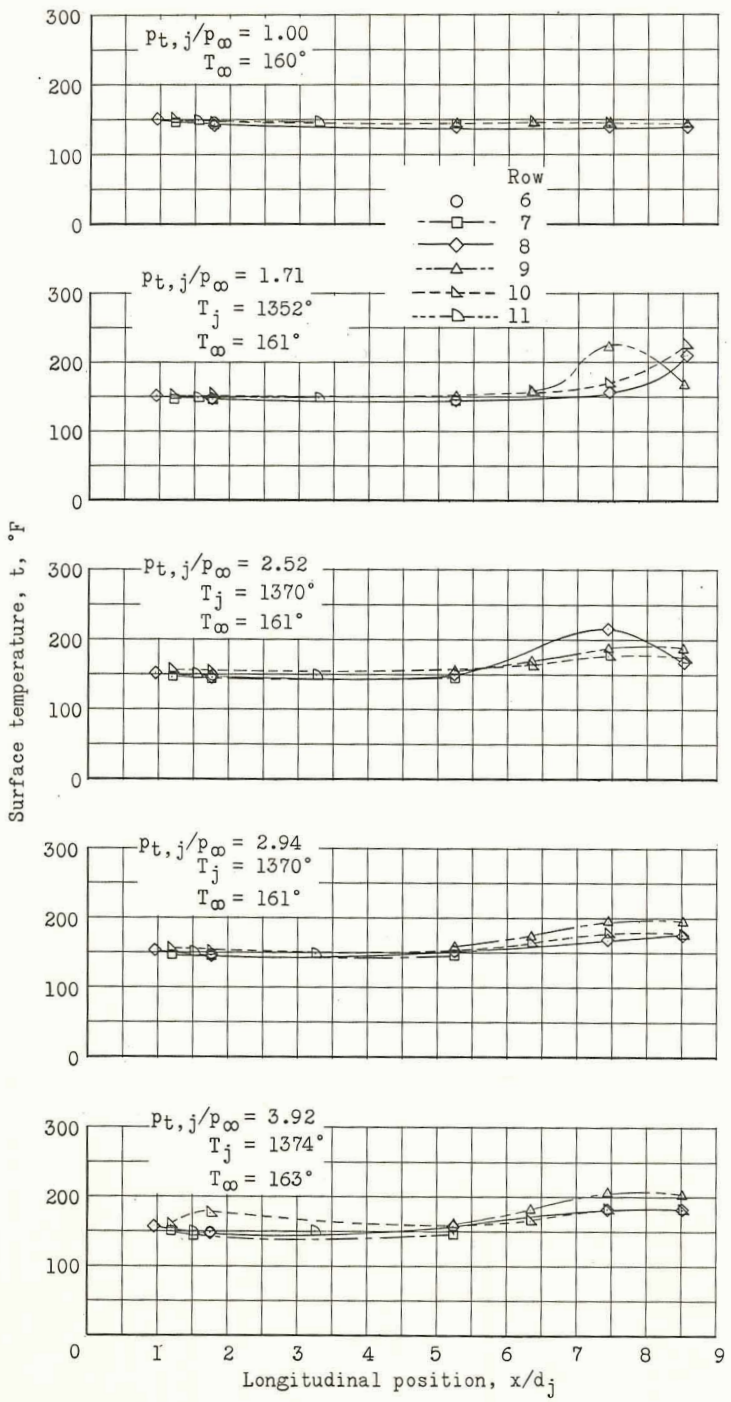

Figure 19.- Effect of jet pressure ratio on fuselage temperatures with the nozzles in the outboard position and solid brakes retracted; $M_\infty = 0.90$; $\alpha = 8^\circ$; $\beta = 0^\circ$; $\delta_h = 0^\circ$.

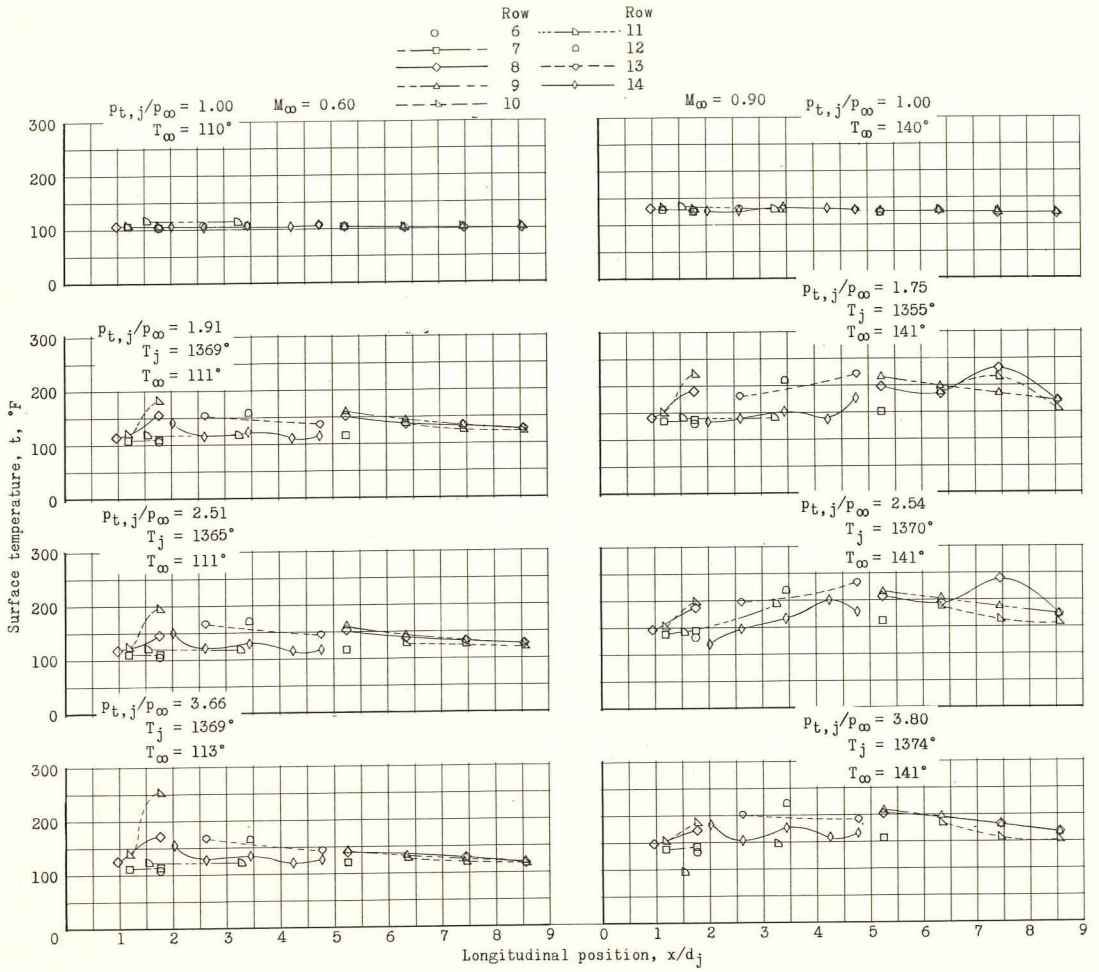

(a) Solid brakes.

Figure 20.- Fuselage surface temperatures at various jet pressure ratios for models with outboard nozzles and 60° solid or perforated brakes; $\alpha = 0°$; $\beta = 0°$; $\delta_h = 0°$.

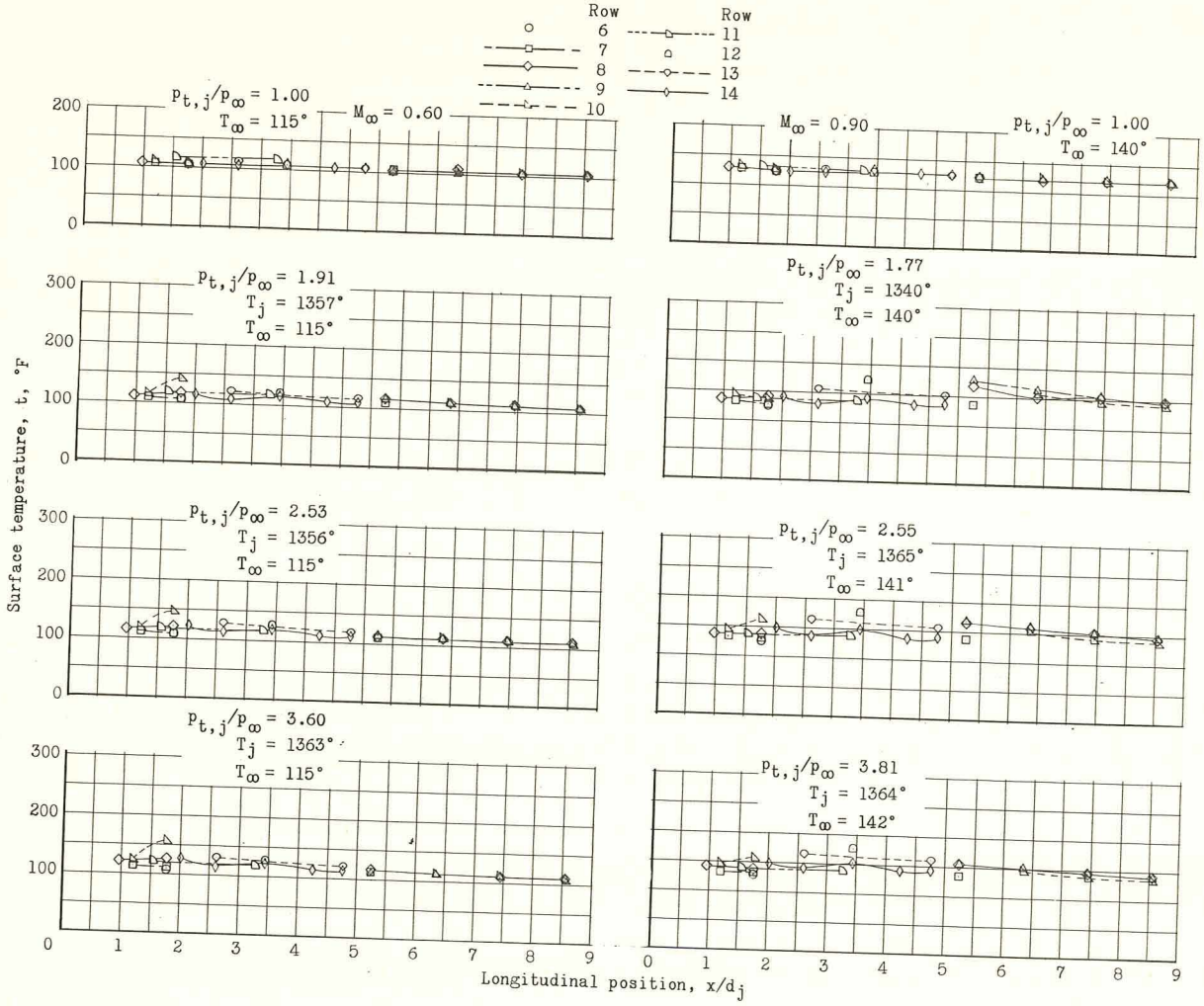

(b) Perforated brakes.

Figure 20.- Concluded.

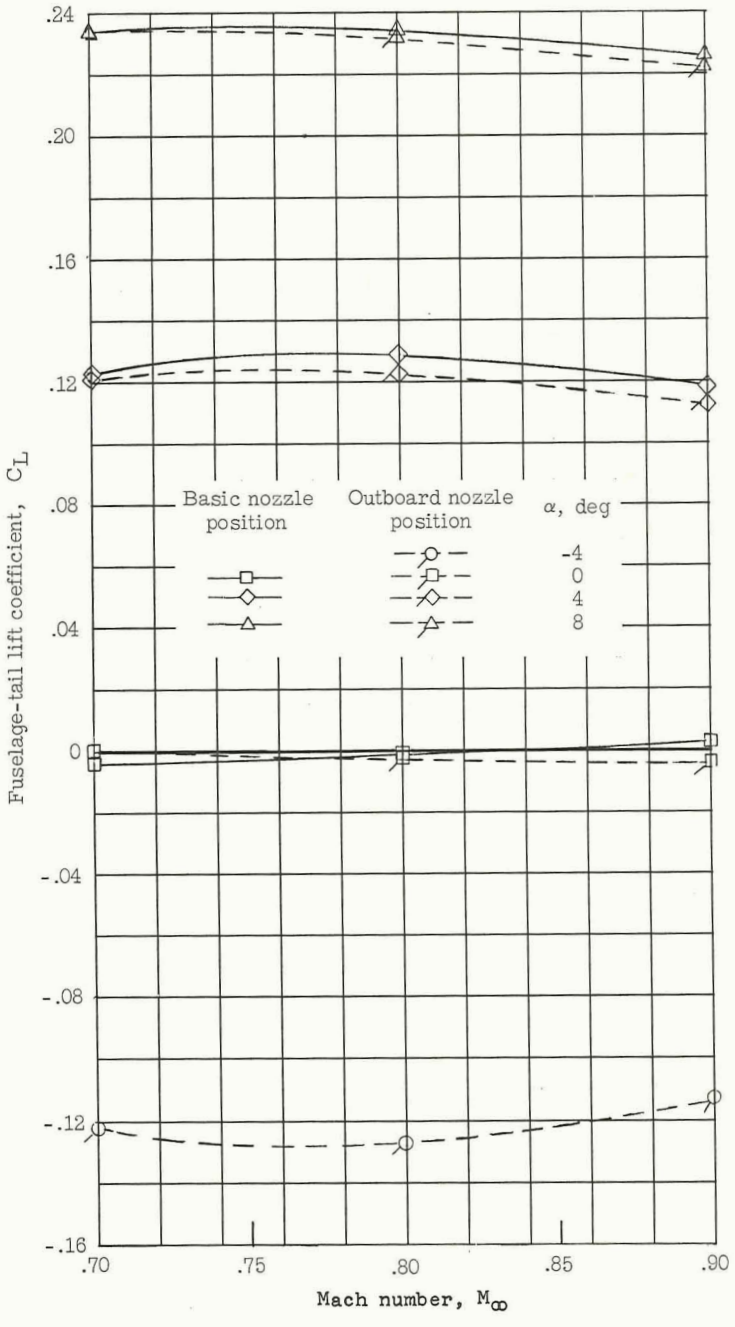

(a) Lift coefficient.

Figure 21.- Influence of nozzle lateral position on the power-off fuselage-tail lift, pitching-moment, and drag coefficients with solid brakes retracted. $\beta = 0^\circ$; $\delta_h = 0^\circ$.

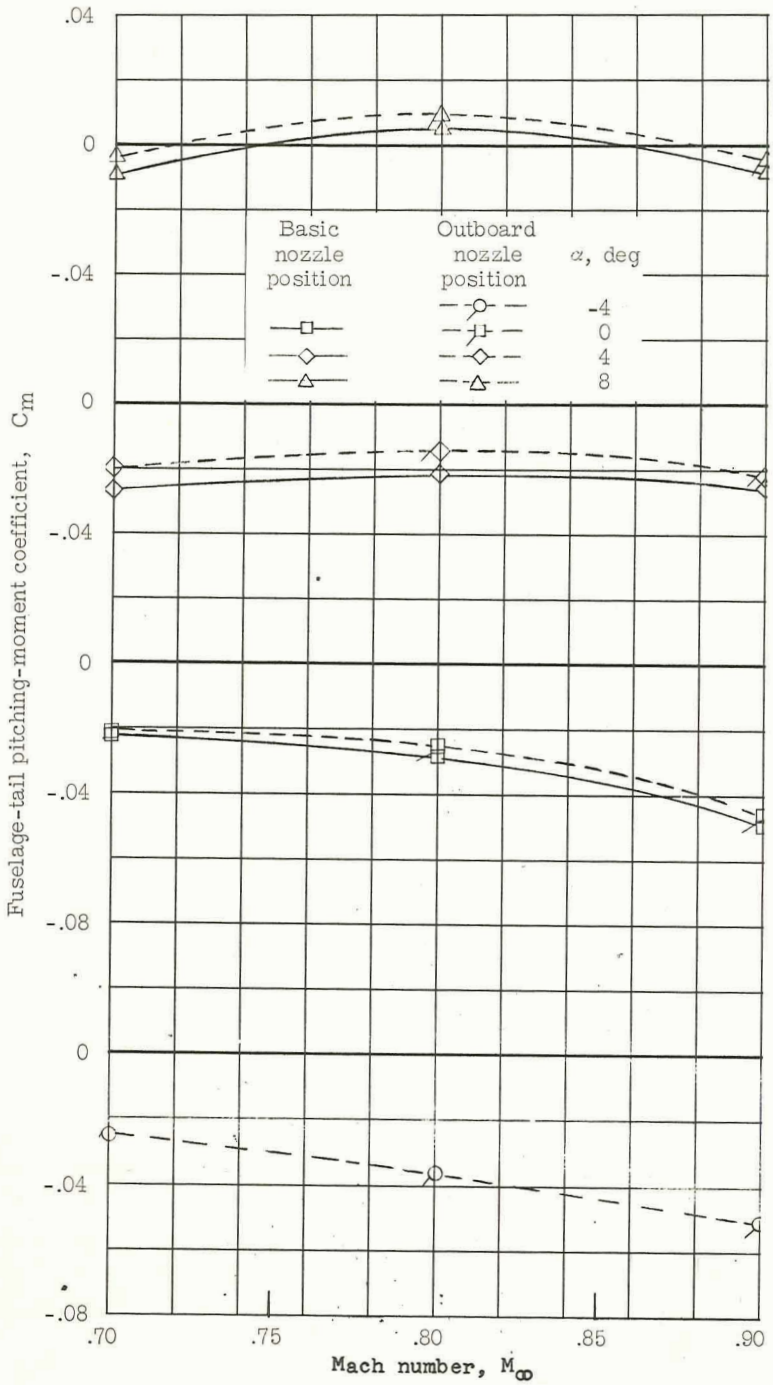

(b) Pitching-moment coefficient.

Figure 21.- Continued.

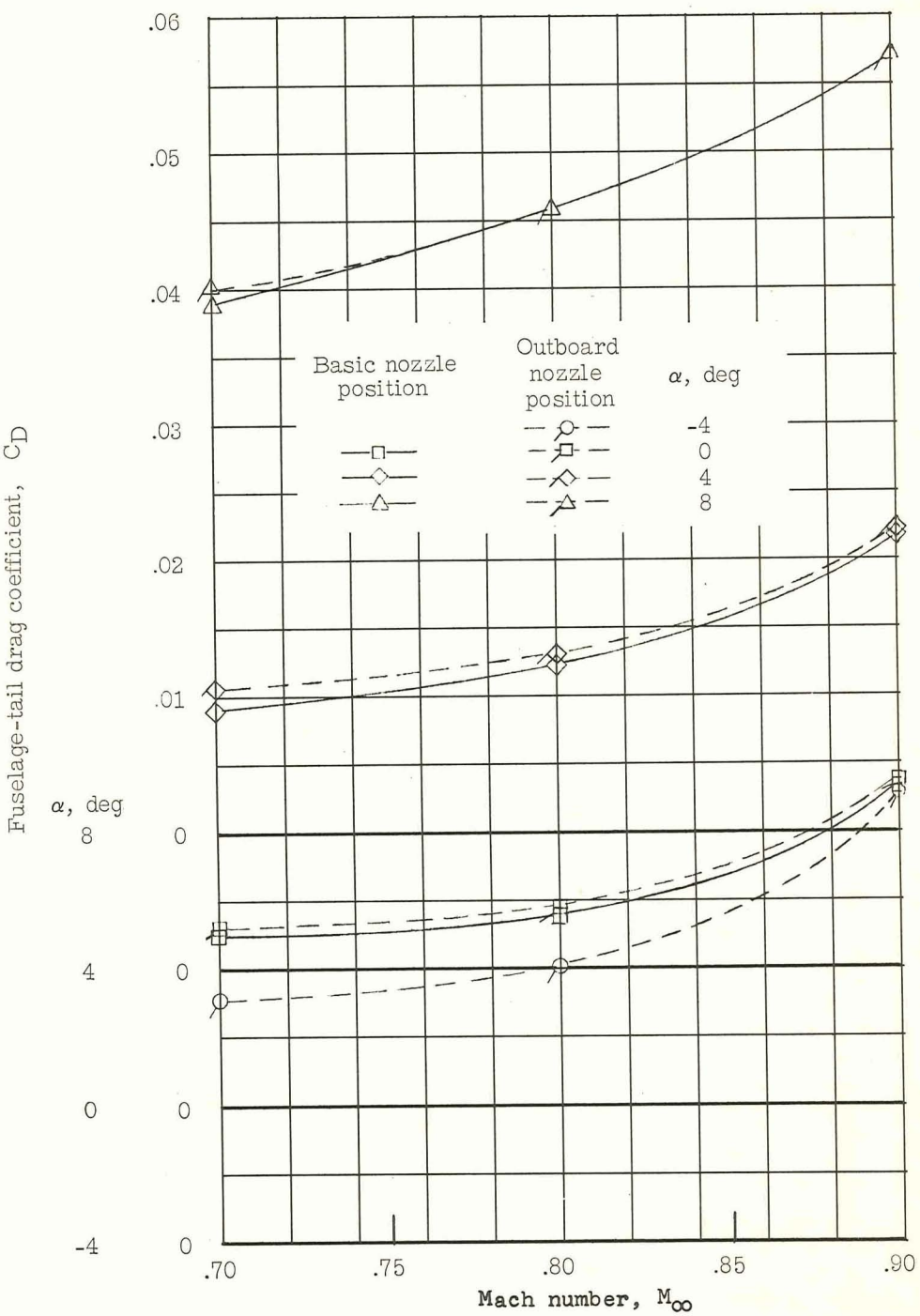

(c) Drag coefficient.

Figure 21.- Concluded.

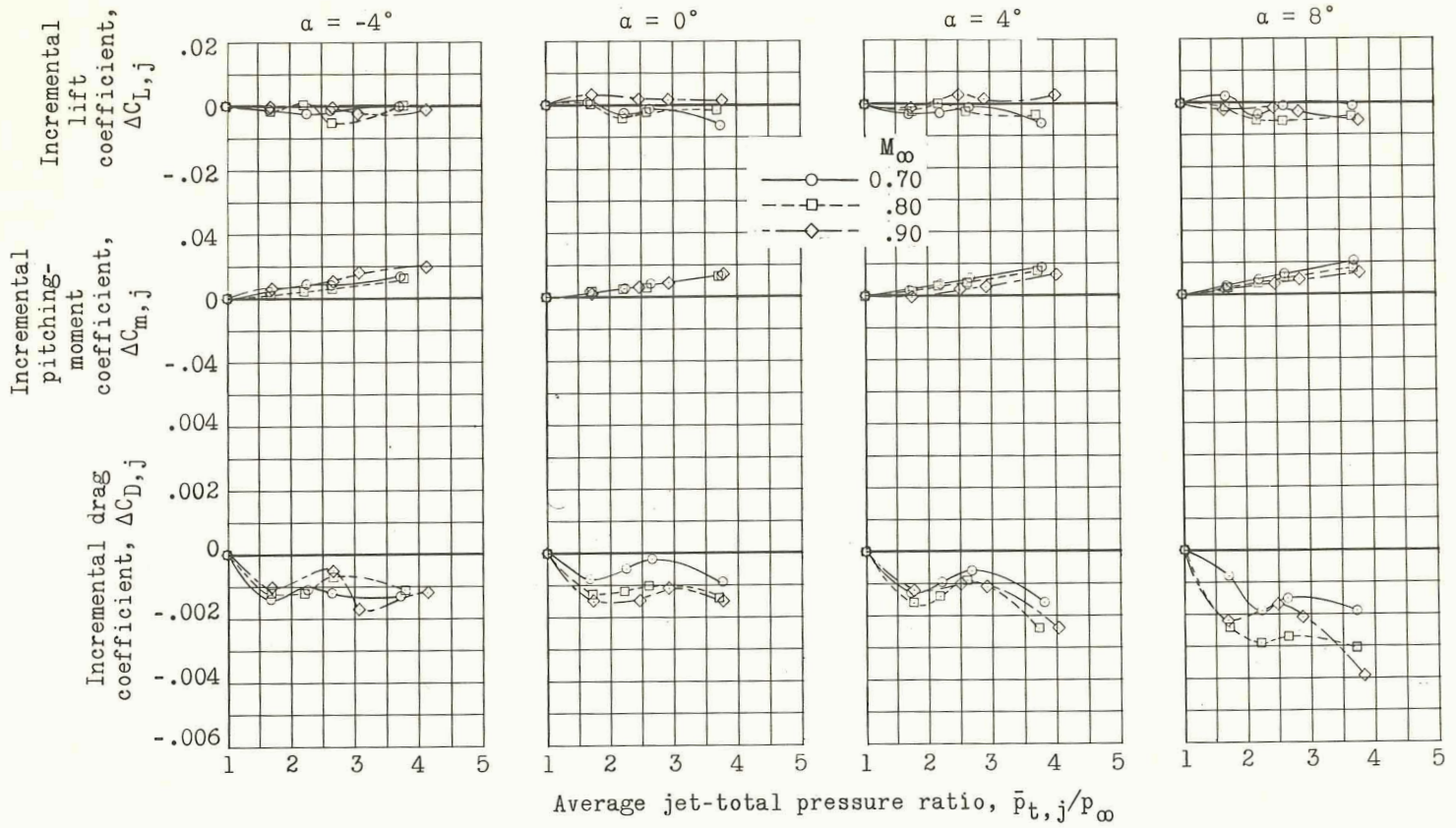

Figure 22.- Jet-induced aerodynamic effects on the model with outboard nozzles and solid brakes retracted; $\beta = 0^\circ$; $\delta_h = 0^\circ$.

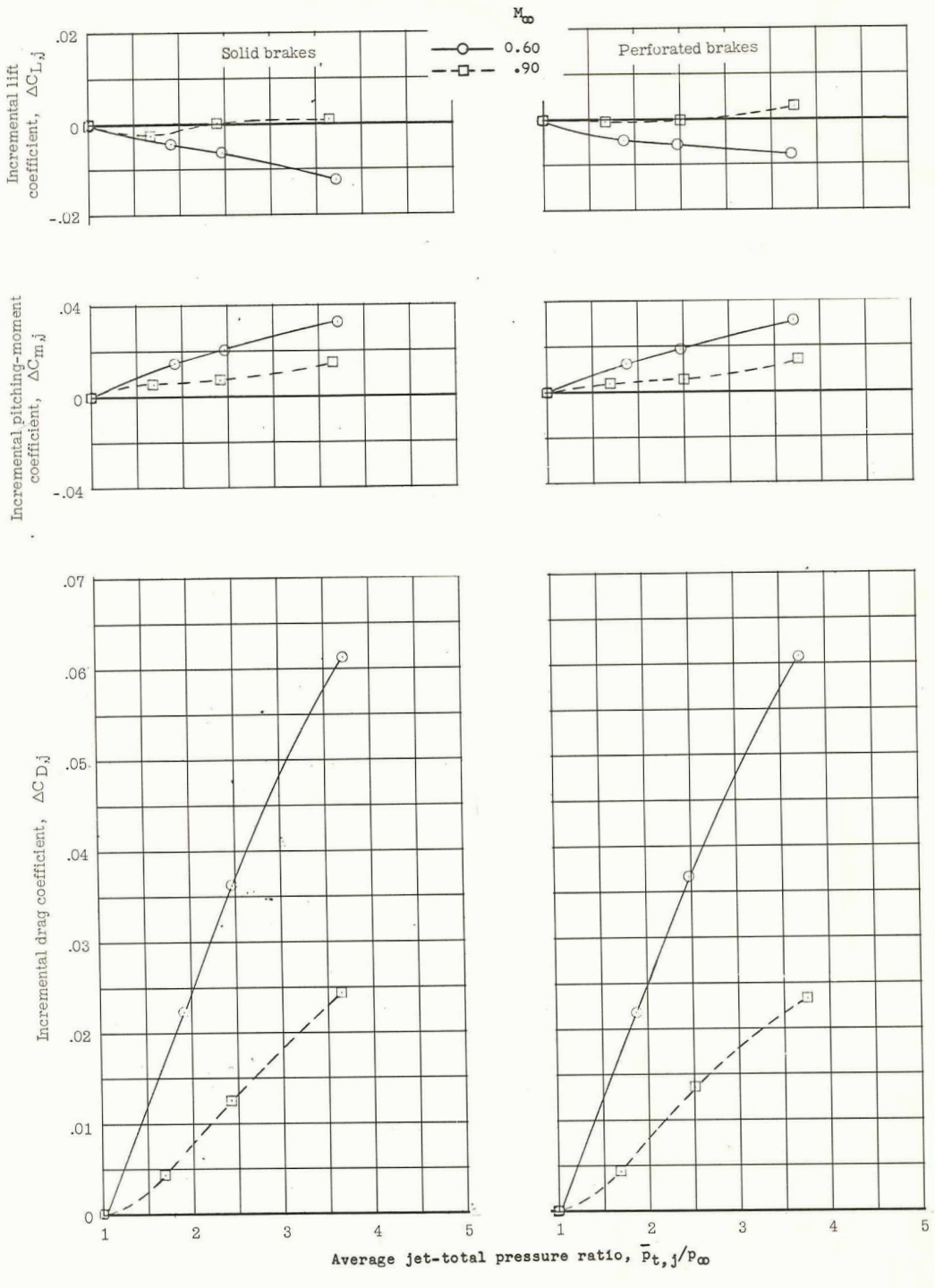

Figure 23.- Aerodynamic jet effects with nozzles in the outboard position and solid or perforated brakes extended 60°; $\alpha = 0°$; $\beta = 0°$; $\delta_h = 0°$.